

ONLINE IN-SITU ESTIMATION OF NETWORK PARAMETERS UNDER INTERMITTENT
EXCITATION CONDITIONS

Except where reference is made to the work of others, the work described in this dissertation is my own or was done in collaboration with my advisory committee. This dissertation does not include proprietary or classified information.

Jason Ashley Taylor

Certificate of Approval:

Charles A. Gross
Professor
Electrical and Computer Engineering

S. Mark Halpin, Chair
Professor
Electrical and Computer Engineering

R. M. Nelms
Professor
Electrical and Computer Engineering

George Flowers
Interim Dean
Graduate School

ONLINE IN-SITU ESTIMATION OF NETWORK PARAMETERS UNDER INTERMITTENT
EXCITATION CONDITIONS

Jason Ashley Taylor

A Dissertation

Submitted to

the Graduate Faculty of

Auburn University

in Partial Fulfillment of the

Requirements for the

Degree of

Doctor of Philosophy

Auburn, Alabama
August 9, 2008

ONLINE IN-SITU ESTIMATION OF NETWORK PARAMETERS UNDER INTERMITTENT
EXCITATION CONDITIONS

Jason Ashley Taylor

Permission is granted to Auburn University to make copies of this dissertation at its discretion, upon request of individuals or institutions at their expense. The author reserves all publication rights.

Signature of Author

Date of Graduation

VITA

Jason Ashley Taylor, son of Charles and Virginia Taylor, was born November 25, 1975 in Biloxi, Mississippi. He received B.S. and M.S. degrees in Electrical Engineering from Mississippi State University in 2000 and 2002. He worked as a Power Systems Engineer at Electrotek Concepts from 2002 to 2004 before pursuing a Ph.D. in Electrical Engineering. While at Auburn University, he worked as an Assistant Instructor, Teaching Assistant, and Graduate Research Assistant.

DISSERTATION ABSTRACT
ONLINE IN-SITU ESTIMATION OF NETWORK PARAMETERS UNDER INTERMITTENT
EXCITATION CONDITIONS

Jason Taylor

Doctor of Philosophy, August 9, 2008
(M.S. Mississippi State University, 2002)
(B.S. Mississippi State University, 2000)

176 Typed Pages

Directed by S. Mark Halpin

Online in-situ estimation of network parameters is a potential tool to evaluate electrical network and conductor health. The integration of the physics-based models with stochastic models can provide important diagnostic and prognostic information. Correct diagnoses and prognoses using the model-based techniques therefore depend on accurate estimations of the physical parameters. As artificial excitation of the modeled dynamics is not always possible for in-situ applications, the information necessary to make accurate estimations can be intermittent over time. Continuous online estimation and tracking of physics-based parameters using recursive least-squares with directional forgetting is proposed to account for the intermittency in the

excitation. This method makes optimal use of the available information while still allowing the solution to following time-varying parameter changes. Computationally efficient statistical inference measures are also provided to gauge the confidence of each parameter estimate. Additionally, identification requirements of the methods and multiple network and conductor models are determined. Finally, the method is shown to be effective in estimating and tracking parameter changes in both the DC and AC networks as well as both time and frequency domain models.

ACKNOWLEDGEMENTS

I wish to express my appreciation to my advisor, Dr. Mark Halpin, for his shared experience, guidance, and patience. I would also like to acknowledge the significant contributions from my committee members, Dr. Mark Nelms and Dr. Charles Gross, whose instruction and advice proved invaluable throughout my academic endeavors. Additionally, I thank my family and friends for their support and encouragement in completing this work. Most importantly, the author wishes to recognize the contributions of his best friend and wife Robin. Her never ending encouragement and support provided both foundation and motivation to accomplish such an undertaking. Thank you.

Style manual:

IEEE Editorial Style Manual

The Chicago Manual of Style, University of Chicago Press

Computer software:

Microsoft Word

Microsoft Excel

MATLAB

PSPICE

TABLE OF CONTENTS

LIST OF FIGURES	xii
LIST OF TABLES	xv
NOMENCLATURE.....	xvi
CHAPTER 1 Introduction.....	1
CHAPTER 2 Literature Review	6
2.1. Electrical Machine and Transformer Condition Monitoring.....	9
2.2. Cable Diagnostic Methods.....	12
2.3. Cable Parameter Estimations Methods.....	16
CHAPTER 3 Recursive Parameter Estimation.....	19
3.1. Identifiability	20
3.2. Recursive Least-Squares.....	24
3.2.1. Directional Forgetting	34
3.2.2. Variable Directional Forgetting.....	37
3.2.3. Covariance Resetting.....	39
3.2.4. Multivariable Solutions	41
3.3. Model and Parameter Validation.....	42
3.3.1. Margins of Error.....	43
3.3.2. Multicollinearity Tests	46
3.3.3. Residual Analysis.....	48

3.4. Measurement Noise	50
3.4.1. Quantization and Sampling Rate	51
3.4.2. Filtering	52
3.5. Normalization	53
CHAPTER 4 Two-Conductor Models.....	55
4.1. Short Transmission Line Model	58
4.2. Nominal Pi Circuit Model	61
4.2.1. SISO Model.....	64
4.2.2. MISO Model.....	66
4.2.3. SISO/MISO Model.....	68
4.2.4. Shunt Conductance.....	69
4.3. Model Evaluations	70
4.4. Summary.....	92
CHAPTER 5 Multiple Conductor Models.....	93
5.1. Identifiability	101
5.2. Model Evaluations	106
5.2.1. Series Element Model	110
5.2.2. Shunt Element Model.....	121
5.2.3. Full Parameter Model.....	122
5.3. Summary.....	126
CHAPTER 6 Frequency-Domain Models	128
6.1. Line Models	128
6.2. Thevenin Equivalent.....	130
6.2.1. Time-Domain	131
6.2.2. Frequency-Domain.....	133
6.3. Parameter Estimate Accuracy.....	136
6.4. Model Evaluations	138
6.5. Summary.....	145

CHAPTER 7 Conclusions.....	146
7.1. Summary.....	146
7.2. Future Work.....	148
Bibliography	150

LIST OF FIGURES

Figure 1-1. Continuous Online Diagnostic and Prognostic Monitor	4
Figure 2-1. Model Reference Approach	7
Figure 2-2. Prognosis Technical Approaches [5]	8
Figure 3-1. Condition Monitor Parameter Estimation and Validation Block.....	43
Figure 4-1. Distributed Parameter Line	56
Figure 4-2. Short Transmission Line Circuit Model.....	58
Figure 4-3. Two-Conductor Mutually Coupled Circuit.....	62
Figure 4-4. Nominal Pi Equivalent Circuit.....	64
Figure 4-5. Single-Phase Test Circuit.....	71
Figure 4-6. Test Case Voltages and Currents	73
Figure 4-8. SISO/MISO Model Parameter Estimates during a Load Change.	74
Figure 4-9. Parameter Estimates with 32-Bit Quantization Error.....	75
Figure 4-10. Parameter Estimates with 16-Bit Quantization Error and $\lambda_c = 0.999$	76
Figure 4-11. Parameter Estimates for Step Change in R	77
Figure 4-12. Parameter Estimates for Step Change in C	77
Figure 4-13. MIMO Model Parameter Estimates	79
Figure 4-14. 95% Confidence Margins of Error.....	79
Figure 4-15. MISO Model Parameter Estimates using RLS/DF	80

Figure 4-16. 95% Confidence Margins of Error	81
Figure 4-17. Prediction Error Autocorrelation.....	81
Figure 4-18. Sending End Voltage and Current Waveforms.....	82
Figure 4-19. Parameter Estimates using RLS	83
Figure 4-20. Parameter Estimates using RLS/DF.....	83
Figure 4-21. Parameter Estimates using RLS/DF	84
Figure 4-22. Parameter Estimates using RLS	85
Figure 4-23. Parameter Estimates using RLS/VDF.....	86
Figure 4-24. DC Signals for a Switching DC Load.....	89
Figure 4-25. Parameter Estimates using RLS/DF	91
Figure 4-26. Parameter Estimates using RLS	91
Figure 5-1. Multiple Conductor Line Model	94
Figure 5-2. Four-Conductor Line Model	99
Figure 5-3. Single Line Diagram of the Three-Phase Test System	108
Figure 5-4. Test System Voltage and Current Waveforms.....	111
Figure 5-5. Multi-conductor Parameter Estimates.....	113
Figure 5-6. 95% Confidence Margins of Error.....	113
Figure 5-7. A-Phase Correlation Matrices	114
Figure 5-8. Multi-conductor Parameter Estimates.....	115
Figure 5-9. B-Phase Correlation Matrix	116
Figure 5-10. Multi-conductor Parameter Estimates.....	117
Figure 5-11. 95% Confidence Margins of Error.....	117
Figure 5-12. Parameter Estimates using RLS/DF.....	118

Figure 5-13. Correlation Matrix for A-phase Estimations.....	119
Figure 5-14. 95% Margins of Error	119
Figure 5-15. Parameter Estimates using RLS	120
Figure 5-16. Parameter Estimates using RLS (Upper) and 95% Confidence Margins of Error (Lower).....	122
Figure 5-17. Parameter Estimates using RLS/DF.....	124
Figure 5-18. 95% Confidence Margins of Error.....	125
Figure 5-19. Parameter Estimates using RLS/DF.....	126
Figure 6-1. Thevenin Equivalent Circuit for h^{th} Order Harmonic Frequency	134
Figure 6-2. Frequency-Domain Thevenin Equivalent Estimation Method	136
Figure 6-3. Single-Phase Test Network	139
Figure 6-4. Network Transfer Impedances Seen at Bus 3	140
Figure 6-5. Input-Output Phasor Components at 60 Hz	141
Figure 6-6. 60 Hz Thevenin Equivalent Parameter Estimates.....	143
Figure 6-7. Covariance Matrix Diagonals	143
Figure 6-8. Input-Output Phasor Components at 300 Hz	144
Figure 6-9. 300 Hz Thevenin Equivalent Parameter Estimates.....	145

LIST OF TABLES

Table 3-1. Recursive Least-Squares Methods	40
Table 3-2. Time Domain Per-Unit Base Relationships	54
Table 4-1. Test System Per-Unit Bases	72
Table 4-2. 95% Univariate Confidence Intervals	88
Table 5-1. Four-Conductor Example Parameters	107
Table 5-2. Test System Per-Unit Bases	108
Table 5-3. Voltage Fourier Components for Balanced Conditions	111
Table 5-4. Current Fourier Components for Balanced Conditions.....	111
Table 5-5. Voltage Fourier Components for Unbalanced Conditions	112
Table 5-6. Current Fourier Components for Unbalanced Conditions.....	112
Table 6-1. Thevenin Equivalent Circuit Data.....	140
Table 6-2. Test System Events.....	141

NOMENCLATURE

Vector-Matrix Notation

a :	Scalar
A :	Matrix
\tilde{a} :	Vector
\bar{a} :	Complex Scalar
\bar{A} :	Matrix of complex values
$\tilde{\bar{a}}$:	Vector of complex values
A_R :	Real component of a complex number
A_I :	Imaginary component of a complex number

Solution Variables

$\text{cov}(\theta)$:	Matrix of parameter estimate covariances
C :	Correlation matrix
e :	Residual error
I :	Identity matrix
$J(\theta)$:	Sum of the squared residuals
k :	Discrete time index

\tilde{L} :	Parameter update gain vector
n :	Number of measurements over time
p :	Number of unknown parameters
\mathbf{P} :	Covariance matrix
P_{jj} :	J^{th} diagonal of the covariance matrix
q :	Quantization step size
\mathbf{R} :	Information matrix
R_{jj} :	J^{th} diagonal of the information matrix
SIF :	Standard deviation influence factor
T_0 :	Exponential delay time constant
VIF :	Variance inflation factor
ε :	Prediction error
$\tilde{\theta}$:	Unknown parameter vector
λ :	Exponential forgetting factor
ρ :	Differential operator d/dt
$\tilde{\varphi}$:	Regressor vector
Φ :	Regressor matrix
σ^2 :	Residual error variance

Model Variables

C :	Capacitance
G :	Shunt conductance

i :	Instantaneous current
\bar{I} :	Frequency-domain phasor current
L :	Inductance
R :	Resistance
s :	Laplacian operator
t :	Instantaneous time
T :	Sampling period
u :	Input regressor
v :	Instantaneous voltage
\bar{V} :	Frequency-domain phasor voltage
y :	Dependent variable / Output variable

Abbreviations and Acronyms

CI:	Confidence Interval
DF:	Directional forgetting
FFT:	Fast Fourier transform
MIMO:	Multiple-input multiple-output models
MISO:	Multiple-input single-output models
PE:	Persistence of excitation
RLS:	Recursive least-squares
RLS/DF:	Recursive least-squares with directional forgetting
RLS/VDF:	Recursive least-squares with variable directional forgetting

SISO: Single-input single-output models

TF: Transfer function method

CHAPTER 1

INTRODUCTION

Recent trends in large vehicular design indicate an increased reliance on electrical networks for power delivery. Whether the vehicle is a naval ship, space shuttle, or space station, networks are typically characterized by low to medium voltages and known system configurations. Poor performance, undesired operation, or faults in these networks can severely degrade or even damage the system. In many networks, little indication of a potentially harmful disturbance or failure is given until an event actually occurs. Furthermore, disturbances such as weak connections, temporary faults, and changing environmental conditions are difficult to diagnose using offline tests. As a result, continuous in-situ monitoring of the network provides better information from which to evaluate the network's health.

Assuming continuous in-situ monitoring (evaluation in the normal operating environment), online diagnostic evaluation can be achieved through direct analysis of measured waveforms and through estimation of characteristic parameters. In the first approach, measured voltage and current waveforms are compared to known "good" waveforms or metrics to evaluate network conditions such as open and short-circuits. In the second approach, parameters characterizing the network's physical properties can be

estimated from measured “input-output” data. By defining model structures in terms of known physical relationships, also known as “gray box” models, the estimated parameters can be compared to known acceptable ranges. As the monitoring is continuous, trending of estimates can distinguish normal changes from problematic conditions. Therefore, parameter identification and tracking provides an approach from which to evaluate both diagnostic and prognostic health.

Many online and offline diagnostic methods apply known external stimuli in order to excite particular dynamic responses [1]. These stimuli are typically tailored to a particular application and require some physical means by which to induce or inject the signals. However, controlling the input stimuli artificially is an unappealing option for a vehicle electrical network. The required stimulus is either too harmful for online applications, as with over-voltage tests, or too specific to be easily implemented for a wide variety of equipment and network configurations. Furthermore, the extra space and weight required to generate and inject the stimuli is prohibitive in mobile applications. For these reasons, passive monitoring of the network will be evaluated. The term passive is used here to indicate that no control or influence is exerted over the system inputs.

Still, without actively controlling the input stimuli there is no guarantee that the measured waveforms contain sufficiently “rich” information to base the parameter estimates. As richness of the information depends upon the system’s normal and abnormal operation, sufficient excitation of the modeled dynamics will potentially vary over time. Under the assumption of passive monitoring, accurate estimation of the

characteristic network parameters requires a method that efficiently utilizes intermittently available information.

The goal of this research is to identify and develop parameter estimation techniques which are suitable to the estimation of network parameters given passive monitoring of network elements in their operating environment. Once the approximations of the characteristic parameters are available, statistical analysis of these values over time provides diagnostic and prognostic measures of network health. The parameter estimates are therefore the foundation of the network health monitoring device illustrated in Figure 1-1. Accuracy of the parameter estimates will obviously have a profound influence over the performance of the diagnostic and prognostic measures. Recursive least-squares techniques are selected to fit the parameter estimates to the measured data as these algorithms are numerically efficient and provide fast accurate estimates. Given their importance to the condition monitoring method, the criteria and conditions under which the algorithms provide accurate estimations are examined in detail in Chapter 3. Additionally, statistical inference measures are provided to gauge the level of confidence in the estimates.

In order to be effective, the method represented in Figure 1-1 requires monitoring the network conditions over extended periods to ensure sufficient information concerning the dynamics is observed. Intuitively, the more information a data set contains about a modeled dynamic, the better the parameter estimate and consequently the diagnostic and prognostic measures. While system disturbances impact the estimates by increasing the dynamic content, the system is not intended as a fast acting protection device. In other

words, the monitoring system's purpose is to observe the slow time varying parameter changes in an attempt to predict future disturbances. Additionally, the observations provide for prognostic evaluation via resulting parameter estimates as well as examination of the measurements themselves. However, the parameter identification procedures are not intended to be quick enough to provide fast acting protection from faults and other disturbances.

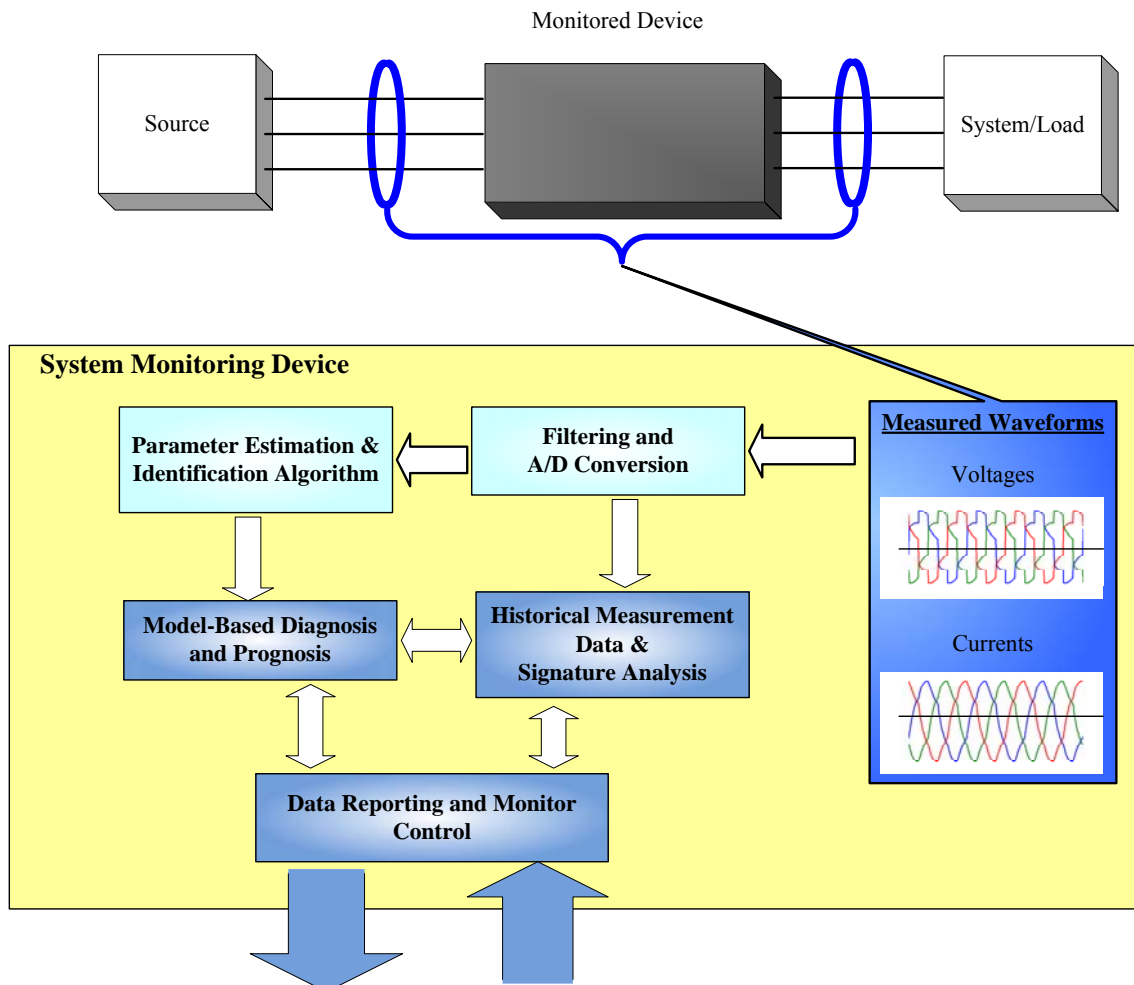


Figure 1-1. Continuous Online Diagnostic and Prognostic Monitor

As indicated in Figure 1-1, the estimations are reliant upon measurement type and location, accurate measurement and quantization, in addition to the parameter identification algorithm. However, another key factor is the model selected to represent the monitored element's physical characteristics. It is assumed that the physical characteristics of the monitored network elements (single conductor and multiple conductor cables, etc.) are describable by linear differential equations. The identifiability requirements of potential two-conductor line models are examined in Chapter 4 along with the ability of the identification algorithms. These findings are then extrapolated further to branches with multiple conductors in Chapter 5. Additionally, the identifiability requirements of the network connected elements using frequency-domain measurement are examined in Chapter 6. While the derived models mostly consider wiring or cables, other networked equipment can be approached in the same manner as long as an accurate linear model can be specified. The parameter estimation algorithms and statistical inference measures were implemented in MATLAB and validated using test data generated in PSPICE.

CHAPTER 2

LITERATURE REVIEW

Condition monitoring is the use of advanced technologies in order to determine equipment condition and potentially predict failure. Methods of conditioning monitoring have been researched and successfully implemented in areas such as industrial applications and transportation. Regardless of the application, these methods share a common goal of detection and diagnosis of unacceptable changes in system parameters, also known as process faults. Accurate assessment of the monitored device's health is therefore dependent on the ability to correctly detect and interpret characteristic parameters changes.

In general, fault detection and diagnosis approaches are divided into two categories: direct analysis methods and model-based methods. Direct analysis methods apply techniques such as logic reasoning, reflectometry, and signature analysis directly to the monitored or observed values. In contrast, model-based methods use the observations in combination with mathematical models to generate quantitative values which can also be analytically evaluated [2]. As Simani et al. stated in [3], "If a fault occurs, the residual signal (*i.e.* the difference between the real system and model behavior) can be used to diagnose and isolate the malfunction." The generation of the residual signal using a

model reference formulation is illustrated in Figure 2-1. Additionally, model-based approaches allow for fault detection through trending and limit checking of the estimated parameters as well as the monitored values. Previously known fault data can also be stored in historical databases to reference observed parameter changes to known fault conditions [4].

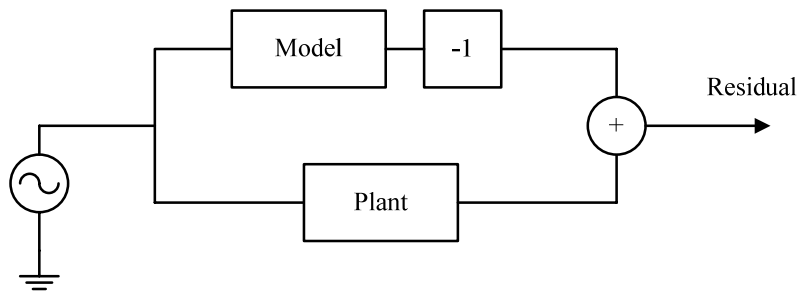


Figure 2-1. Model Reference Approach

Model-based techniques do introduce additional complexity in the form of model selection and parameter identification requirements. Benefits and costs of the model-based techniques is highlighted in Figure 2-2 from a popular text on fault diagnosis and prognosis [5]. As illustrated, model-based prognostics provide better accuracy than other methods but are more application specific and require higher implementation costs. It should also be noted that in Figure 2-2 the methods which do not use a model are further subdivided into data-driven techniques, which rely on measurements, and experience-based prognostics based on simple time-to-failure statistics.

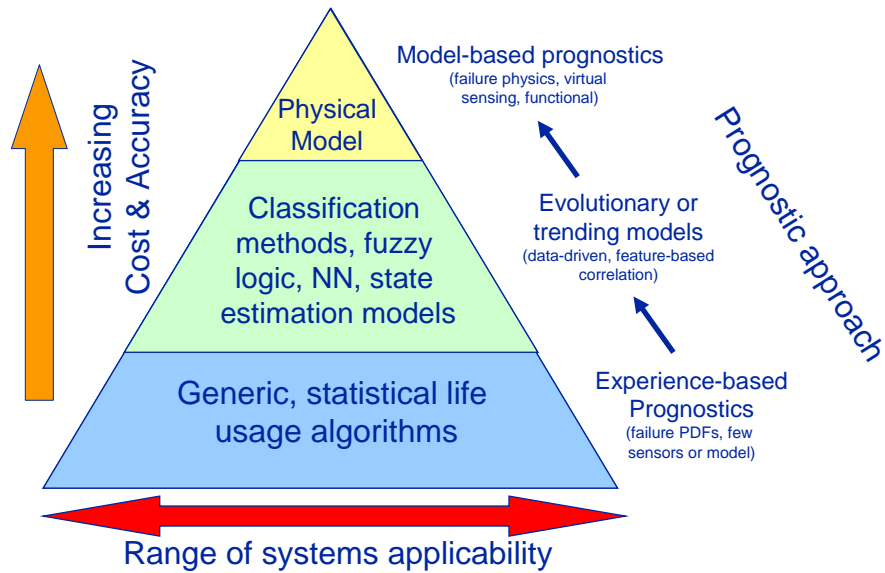


Figure 2-2. Prognosis Technical Approaches [5]

While model-based diagnostics have been successfully applied to a wide range of areas, very little research had investigated the use of model-based diagnostics for condition monitoring of low voltage electric cables or networks. Therefore, it may be instructive to first examine applications with similar diagnostic and prognostic concerns, but where model-based fault detection methods have been successfully applied. Specifically, the literature for diagnostic methods as applied to electric rotating machines and transformers is examined. Afterwards, the recent literature on the cable diagnostics is reviewed followed by a review of the current literature on cable parameter estimation.

2.1. ELECTRICAL MACHINE AND TRANSFORMER CONDITION MONITORING

A large body of research has focused on condition monitoring of rotating electric machines due to the high mechanical and electrical stress involved and the potential for catastrophic failure. Given their importance in industry, much of the literature has been directed towards induction motors. A comprehensive bibliography of induction motor condition monitoring methods was given in [6] and a good overview of fault detection in induction motors using signature analysis was provided in [7]. Background of implemented model-based methods can be found in [8, 9]. Additionally, a comparison between signature analysis methods and model-based methods for induction motor fault diagnostics was recently examined by Harihara et al. in [10]. For the given methods and selected models, Harihara et al. were able to show that the probability of false alarms was reduced by 40% when using the model-based solution. Furthermore, in a study performed by Nasiri et al. [11], tracking of modeled parameter estimates was shown to be a useful indicator of rotor fault conditions.

Model-based condition monitoring has been proposed for other machine types as well, for example [7, 12, 13]. In [12], a method was introduced for the offline diagnostic testing of electromechanical actuators to replace current hydraulic/pneumatic actuators in aircraft. The method represented the actuator's brushless DC motor using a set of physically based discrete time transfer functions. Through perturbations introduced into the control signal, system identification techniques were used to estimate the physical parameters from the observed voltage, current, and rotor speed changes. Test bed evaluations demonstrated the method to be capable of accurately estimating key physical

parameters including resistance, inductance, and rotor inertia. A supervisory system using fuzzy logic was then shown to be successful at diagnosing potential faults from the estimated parameter changes.

In recent decades, significant research into electrical-based diagnostics of power transformers has also been conducted. A technique which received a great deal of attention is the transfer function (TF) method which derived multiple transfer function models from input-output measurements. Malewski and Poulin first proposed the use of transfer functions in 1988 to account for difficulties in obtaining comparable historic voltage and current waveform data [14]. As transfer functions are independent of the applied impulse, the historical transfer functions could be generated without requiring the a consistent input stimuli. Mechanical deformations in the winding arising from short-circuits and mechanical stresses during installation could then be detected by comparing measured TF models to accepted reference models [15].

Initially transfer functions were generated through the application of broadband pulses and time-domain measurements. The transfer functions were then determined as the ratio of the Fourier transformed input-output measurements. A second method determined the transfer function directly in the frequency domain by using a variable frequency sinusoid. At each frequency, phasor input and output measurements describe the transfer function at that particular frequency. Hence, the transfer function was measured by sweeping the frequency of the sinusoidal input across the desired bandwidth and recording the quotient between the phasor input and output at each frequency. The frequency-domain approach has gained prominence in offline tests because it eliminates

signal-to-noise ratio, frequency resolution, and aliasing issues associated with the time-domain approach [15]. However, the time-domain approach was often utilized as the default method for online applications where the input stimuli could not be controlled.

Leibfried and Feser examined both online and offline tests for in service power transformers in [16]. On-site “offline” test inputs were applied by switching the high voltage side of the transformer in and out of service to create impulses. In contrast, “online” tests used transients induced by some external network event. Some of the difficulties expressed by Leibfried and Feser for the on-site tests were the requirements of identical tap-changer settings and similar temperatures in order to produce comparable transfer functions. In addition, reflected traveling waves from the interconnected network could potentially bias the transfer function estimation. In principle, reflected waveforms observed in input will not change the model estimate; however, reflections in the observed outputs may be misinterpreted as changes in the transformer. Wimmer and Feser revisited this issue and proposed limiting the calculation of the transfer function from single waveform peaks [17].

The simplest use of the TF method is a pass-fail test. If the measured transfer function is in agreement with the reference model, typically generated directly after it is manufactured, then no defect can be detected. However, if the measured TF deviates substantially from the reference, the transformer is deemed faulty and removed from service. This simple comparison, however, does not provide any information about what specific defect may have occurred. This limitation was pointed out by Leibfried and Feser who noted at the time that, “there is no reliable information about the relationship

between changes – mechanical or dielectric – of the winding assembly and their effect on the transfer function” [16].

Transfer functions are black-box models or models which do not contain a-priori knowledge of the underlying physical relationships. Recent endeavors have concentrated on correlating physical relationships with the transfer function in an effort to provide detailed fault diagnostics. A sensitivity test of the transfer function was performed by Mikkelsen et al. in [18] which showed that physical changes in the oil, core, and winding insulation influenced the overall shape of the transfer function. A similar study was performed by Rahimpour et al. [19] that showed correlation between transfer function changes and a model of physical displacement in the transformer windings. In Rahimpour’s model, the parameters were determined analytically based on known physical relationships not through monitored conditions and parameter estimation techniques. While research in this area is ongoing, the lack of technical articles using parameter estimation techniques to determine physics-based parameters is demonstrative of the difficulties involved with proper model selection and subsequent estimation of characteristic parameters.

2.2. CABLE DIAGNOSTIC METHODS

One of the simplest electrical cable tests is to measure the resistance of the cable. If the measured resistance is too high it is an indication that the wire is not connected or open circuited. Measurement of the capacitance or inductance can also be used to determine the length of the wire by comparing the cable’s known distributed capacitance

and inductance with the calculated values. As the lumped capacitance and inductance increase with the length of the wire, smaller than expected values can be used to approximate location of the open or short circuit fault. However, errors can occur in these fault locations estimation whenever the distributed parameter values are not constant over the length of the wire. Additionally, these tests cannot be performed while the wire is in use.

In electrical networks, identification and protection of large abrupt faults is generally well understood. Slowly occurring or incipient faults are more difficult to detect and diagnose given the many factors involved. Experiences with incipient faults in cable splices led to the development of the fault specific relay detector described in [20]. The incipient faults resulted from accumulation of water in cable splices which eventually lead to an arcing event. The arc caused the water to evaporate but the resulting combination of pressure and moisture also cleared the fault. The whole process of arcing and self-clearing occurred within less than a quarter-cycle (4.16ms) which was insufficient to cause the overcurrent protection to operate. Due to the continued degradation of the splice, the frequency of these events tends to increase over time. The developed relay operation depends on a known relationship between the disturbance and its symptoms. In particular, the disturbance is characterized by flashovers at the voltage peaks, quarter-cycle overcurrents, and an increasing frequency of occurrence. Once these characteristics are observed, the relay acts by operating protection equipment or signaling an operator. Detection of other types of incipient faults in this manner would require similar a-priori knowledge. While most research utilizing signature analysis techniques

tends to concentrate on the diagnostic of medium and high voltage cables, reflectometry techniques have recently been investigated for the detection and location of faults in aircraft wiring [21-25]. However, these methods do not use model-based techniques and currently can only detect existing faulted conditions.

A few recent studies have focused on incipient fault location in distribution networks in the United Kingdom. In [26] the transient voltage and current waveforms are recorded by a digital disturbance recorder. Assuming known cable impedance characteristics, the fault location was either extrapolated from measurements at multiple locations or through measured transient impedances. Experiences and common causes of incipient faults in underground low voltage networks were also explored by Walton in [27]. While Walton indicated that waveform analysis was used successfully to identify incipient fault locations, he also pointed out the need for online condition assessment.

Another application where cable condition assessment has received strong interest is within nuclear power plants. Exposure of cables to harsh environmental conditions in these plants raised interest in condition monitoring of low voltage cable insulation. Concerns over how to assess the aging and degradation of insulation have led to the requirement of long-term studies of cable materials in nuclear power plants by IEEE/ANSI Standard 383 [28]. Additionally, a detailed summary of aging factors and tests for electrical cables was published by the U.S. Office of Nuclear Regulatory Research in 1996 [29]. Non-electrical tests receiving recent attention include ultrasonic impulse, nuclear magnetic resonance, and optical techniques [30-32]. While new electrical-based tests have not been introduced, recent work has restated the effectiveness

of traditional electrical tests in diagnosing aging and degradation in insulation material. Sun et al. showed insulation resistive changes are correlated with changes in the mechanical and physical properties of ethylene propylene rubber (EPR) due to thermal aging [33]. Hsu et al. went further to show that EPR resistance changes were also correlated with moisture-related degradation [34]. This was a key finding as the lower dielectric stresses associated with low voltage cables could not provide the same indicators of moisture degradation as higher voltage conductor tests.

For 4 kV to 500 kV voltage levels, small discharges known as partial discharges (PD) can occur in small gas voids or cavities between the insulation and conductor. These voids result from manufacturing imperfections or insulation deterioration and are a useful indicator of the insulation's integrity. Numerous studies and methods have been proposed for both offline and online detection of partial discharges in medium and high voltage cables [35-46]. For low voltage cables, partial discharge, also known as corona resistance, is not expected to be significant due to the low dielectric stress. According to IEEE Standard 141-1993, "Although corona resistance is a property associated with cables over 600 V, in a properly designed and manufactured cable, damaging corona is not expected to be present at operating voltage." Nonetheless, an offline PD test was proposed by Steiner and Martzloff [47] for low-voltage cables. In their paper, Steiner and Martzloff recognized that low voltage cable insulation was not designed to limit PD, and discharges would occur along the entire length of the cable during over voltage conditions. They used statistical analyses to identify the increased partial discharge activity associated with the damaged portions of the insulation. While successful at

identifying the damaged locations, test voltages an order of magnitude higher than rated were required to achieve sufficient PD. Offline partial discharge tests for motors and other low voltage equipment were also investigated in [48, 49]. Once more, potentially damaging voltage levels were required by these tests in order to initiate the occurrence of partial discharges.

2.3. CABLE PARAMETER ESTIMATIONS METHODS

Typically, estimation of cable or line parameters is performed deductively. Identified physical relationships in the form of tables or mathematical equations are used to relate known characteristics to modeled equivalents. That is to say, a cable's parameters are deduced from assumed characteristics such as conductor and dielectric material, conductor configuration, and length. Deductive reasoning, however, is only as good as the accuracy of assumed characteristics. In most cases the assumed characteristics are sufficient. However, when considering changes over time, such as environmental conditions, faults, and insulation degradation, general assumptions concerning the cable properties may not be sufficient. Additionally, every factor influencing a cable's parameters may not be known or accounted for by deductive reasoning. Experimental evaluations performed by Yu et al., for instance, recently showed that the metallic chassis' influence on vehicular power cables parameters was not accounted for in most lab tests or models [50]. Inductively determining the parameters from in-situ measurements may be a more viable alternative.

Parameters can be estimated using either steady-state or dynamic measurements. However, the information provided by particular measurements types may not be sufficient to identify the desired characteristics. For instance, in a DC network inductive and capacitive values cannot be estimated from steady-state measurements, but these values can be estimated if dynamic measurements are available for the same network. Thus, effective condition monitoring requires agreement between the available information and modeled parameters.

Modern energy management systems utilize telemetered measurements at a large number of locations in the network. The majority of recorded information consists of steady-state magnitudes. As the complete description of a sinusoidal waveform requires both the magnitude and phase angle, the estimation of AC line parameters from magnitude only measurements is generally not possible. However, new measurement techniques utilizing global positioning systems (GPS) provides the ability to measure the phase angles of the steady-state measurement as well [51]. Calculation of the line parameters using synchronized measurements is examined in [52, 53].

Estimation of the cable parameters using actual waveforms or dynamic measurements has typically been done in offline tests. Harmonic impedance measurements of building distribution cables, for example, was performed by Du and Yuan in [54] by injecting harmonic currents into shorted cables. Using the measurements generated in the lab, transfer functions illustrating changes in resistance and inductance as a function of harmonic order were created. Yet, the application of these test measurements to diagnostic measures was not discussed.

Applying model-based techniques to cable diagnostics provides a potential avenue to increase the accuracy of the condition monitoring. Additionally, model-based techniques can be implemented online which is an advantage over many traditional cable diagnostic methods. While model-based diagnostics have been successfully applied to electric machines and transformers, little research has applied the techniques to cables and other network elements. Effective condition monitoring using model-based techniques, however, hinges upon accurate estimation of the desired parameters which can be heavily influenced by the availability of relevant information. The ability to accurately estimate characteristics parameters when the necessary excitation is intermittent over time provides a key first step in implementing a condition monitoring method using passive monitoring.

CHAPTER 3

RECURSIVE PARAMETER ESTIMATION

The recursive least-squares (RLS) solution is a popular and effective means of estimating linear model parameters in online applications. RLS has all the statistical properties of a least-squares solution, but its recursive formulation also efficiently updates the solution when provided new measurements. By exponentially forgetting or discounting past information, the recursive least-squares formulation can track time-varying solutions by placing less weight on past measurements. However, exponential forgetting also means the retained information, or excitation, can vary with time as well. When the excitation is not artificially regulated, the solution accuracy is completely dependent on the system providing necessary levels of excitation.

In this chapter, the ability of recursive least-squares methods to estimate and track parameters under intermittent excitation conditions is investigated. Multiple methods are presented and evaluated for their abilities to estimate and track time-varying parameters. Recognizing the accuracy of the solution depends on the uncontrolled excitation, statistical measures that indicate the level of confidence in the estimates is also presented. Finally, other factors that will influence the accuracy of the solution such as measurement noise are addressed.

3.1. IDENTIFIABILITY

Identifiability addresses the question of whether modeled parameters can be accurately identified (estimated) given an infinite amount of noise-free data. It can be shown that model identifiability is dependent on the solution method, the model structure, and the measured input-output data [55]. It is assumed that the modeled element's dynamics can be represented by linear regression shown in (3.1); where the unknown parameter vector, $\tilde{\theta}$, is related to the current model output, y , and past input-output measurements contained in the regressor vector, $\tilde{\varphi}(k)$. The variable k is used as a discrete time index where k indicates the most recent sample, $k-1$ the previous measurement set, and so on. Measurement noise and other sources of errors are represented by residual error, e , which is assumed to be white noise with zero mean and a defined variance, σ^2 .

$$y(k) = \tilde{\varphi}(k)^T \tilde{\theta} + e(k) \quad (3.1)$$

The vector-matrix form of (3.1) is given in (3.2); where \tilde{y} is the vector of observed output variables, Φ contains past input-output vectors, and $\tilde{\theta}$ is a vector containing the unknown parameters. If there are n measurements and p unknown parameters, the $n \times p$ matrix Φ contains n vectors as shown in (3.3) with each vector $\tilde{\varphi}$ containing p regressors or past input-output measurements for that particular instant in time.

$$\tilde{y} = \Phi \tilde{\theta} + e \quad (3.2)$$

$$\Phi = \begin{bmatrix} \tilde{\varphi}^T(k) \\ \tilde{\varphi}^T(k-1) \\ \vdots \\ \tilde{\varphi}^T(k-n+1) \end{bmatrix} \quad (3.3)$$

A model is termed identifiable provided the estimate for the unknown parameter vector, $\tilde{\theta}$, always converges to a single solution. In this case the estimate is said to be consistent and the solution is unique. Provided a large enough sample set, the over-determined set of equations in (3.2) can be used to formulate parameter estimates which predict the system output. Hence, the goal is to find a solution which minimizes the residuals or the difference between the estimated and measured outputs. One such approach is to minimize the sum of the squared residuals shown in the cost function (3.4) using the classic least-squares method provided in (3.5).

$$J(\theta) = \frac{1}{2} \sum_{i=k-n+1}^k (\tilde{\varphi}(i)^T \tilde{\theta} - y(i))^2 \quad (3.4)$$

$$\tilde{\theta} = \{\Phi^T \Phi\}^{-1} \Phi^T \tilde{y} \quad (3.5)$$

However, in cases where the matrix $\Phi^T \Phi$ is singular, a unique solution for the parameter estimates cannot be determined. Therefore, identifiability of the linear model is coupled to the non-singularity of the least-squares solution or more specifically the matrix $\Phi^T \Phi$. The matrix $\Phi^T \Phi$ becomes singular whenever the modeled dynamics are not contained in the measurements. Depending on the viewpoint, singularity is the result of

the particular measurements not containing sufficient information about the modeled dynamics, or the selected model contains more dynamics than the system is capable of generating.

Assuming a regression model where the regressors are composed purely of past inputs, a finite impulse response (FIR) model can be defined completely in terms of past inputs as shown in (3.6). The dimensions of Φ are determined by the total number of equations used in the least squares solution, n , and the number of unknown parameters to be estimated, p .

$$\Phi = \begin{bmatrix} u(k-1) & u(k-2) & \cdots & u(k-p) \\ u(k-2) & u(k-3) & & \vdots \\ \vdots & & \ddots & \vdots \\ u(k-n) & \cdots & \cdots & u(k-n-p+1) \end{bmatrix} \quad (3.6)$$

$\Phi^T \Phi$ is then simply the sum of the products of the inputs as shown in (3.7) which is a square $p \times p$ matrix. Therefore, the inputs must contain sufficient excitation to guarantee $\Phi^T \Phi$ will be of full rank, also known as the excitation condition [56].

$$\Phi^T \Phi = \begin{bmatrix} \sum_{i=1}^n u^2(k-i) & \sum_{i=1}^n u(k-i)u(k-i-1) & \cdots & \sum_{i=1}^n u(k-i)u(k-i-p) \\ \sum_{i=1}^n u(k-i)u(k-i-1) & \sum_{i=1}^n u^2(k-i-1) & & \vdots \\ \vdots & & \ddots & \vdots \\ \sum_{i=1}^n u(k-i)u(k-i-p) & \cdots & \cdots & \sum_{i=1}^n u^2(k-i-p+1) \end{bmatrix} \quad (3.7)$$

Let us assume a simple case where the input, u , is a constant nonzero value for all instances of time. For this input, all the entries in (3.6) are identical and (3.7) is rank one. Thus, a constant nonzero input provides enough information to derive the DC gain but not enough excitation to determine higher order dynamics.

Conversely, singularity of $\Phi^T \Phi$ can result when the model is over-parameterized or contains more independent parameters than the actual system. In this case, some of the modeled parameters cannot be excited and subsequently estimated. For example, assume the plant in (3.8) represents the true plant dynamics [57].

$$y(k) = -a_1 y(k-1) + b_0 u(k) + b_1 u(k-1) \quad (3.8)$$

Now assume that a higher order model (3.9) is selected to determine the parameters from the input and output. The “^” is used here to distinguish estimates from true values.

$$y(k) = -\hat{a}_1 y(k-1) - \hat{a}_2 y(k-2) + \hat{b}_0 u(k) + \hat{b}_1 u(k-1) + \hat{b}_2 u(k-2) \quad (3.9)$$

The regressor vector for the model is then

$$\tilde{\varphi}(k)^T = [-y(k-1) \quad -y(k-2) \quad u(k) \quad u(k-1) \quad u(k-2)] \quad (3.10)$$

Examination of (3.8) indicates that the regressors in (3.10) will be linearly related as defined by $\tilde{\alpha}^T \tilde{\varphi}(k+1) = 0$ where $\tilde{\alpha} = [-1 \quad a_1 \quad 0 \quad b_0 \quad b_1]$.

This linear relationship between the regressors means that at least one column in (3.6) can be expressed as a linear combination of the other columns. Consequently, both Φ and $\Phi^T \Phi$ are rank deficient or singular. The singularity of (3.7) again results in a non-

unique minimum solution to the least-squares method. Informally, the dynamics of the system do not warrant the over complexity of the model, and multiple solutions can be found which provide an identical output response to the given set of data.

Conversely, it should be noted that a model which does not represent all the parameters cannot be expected to converge to the unique or “true” parameters. Obviously, a model which does not include all of the dynamics cannot accurately predict the output, and a converged solution cannot guarantee correspondence of $\tilde{\theta}$ with the “true” values. In this case, the unmodeled dynamics will show up in the residuals violating the assumption that the residuals error is white noise. In fact, residual whiteness tests are commonly employed to check for unmodeled characteristics and potential bias in the estimates. Additionally, the excitation conditions discussed here are not limited to FIR models. The regressors can be defined by any combination of past inputs and outputs without alteration to the overall conclusions.

3.2. RECURSIVE LEAST-SQUARES

For online applications, the standard least-squares solution is not the most efficient method for updating the solution as new measurements become available. In fact, updating the least-squares solution for each new measurement would require solving (3.5) using all the available past data. As time goes to infinity, the computational and storage burdens become unacceptable. Additionally, tracking parameters as they slowly change over time requires newer data to be more heavily weighted in the solution than older data. While weighted least-squares could be used, it would also increase the

computation times required. Fortunately, the least-squares estimate can be expressed in a recursive form, thus reducing computation time and allowing for efficient weighting of the past data.

The least-squares solution shown in (3.5) can be examined in two parts shown in (3.11) and (3.12). In much of the literature, \mathbf{P} is termed the covariance matrix as the solution's covariances are defined by scaling \mathbf{P} by the residual error variance, σ^2 . Therefore, the diagonals of \mathbf{P} represent the unscaled variances of the individual parameter estimates.

$$\mathbf{P}(k) = \{\boldsymbol{\Phi}^T \boldsymbol{\Phi}\}^{-1} \quad (3.11)$$

$$\boldsymbol{\Phi}^T \tilde{\mathbf{y}} = [\tilde{\varphi}(k) \quad \tilde{\varphi}(k-1) \quad \dots \quad \tilde{\varphi}(1)] \begin{bmatrix} y(k) \\ y(k-1) \\ \vdots \\ y(1) \end{bmatrix} \quad (3.12)$$

Expressing (3.12) as an update given the most recently observed output and regressors, as illustrated in (3.13), the solution update is shown in (3.14).

$$\boldsymbol{\Phi}^T \tilde{\mathbf{y}} = [\tilde{\varphi}(k-1) \quad \dots \quad \tilde{\varphi}(1)] \begin{bmatrix} y(k-1) \\ \vdots \\ y(1) \end{bmatrix} + \tilde{\varphi}(k)y(k) = \boldsymbol{\Phi}(k-1)^T \tilde{\mathbf{y}}(k-1) + \tilde{\varphi}(k)y(k) \quad (3.13)$$

$$\tilde{\boldsymbol{\theta}}(k) = \mathbf{P}(k) * [\boldsymbol{\Phi}(k-1)^T \tilde{\mathbf{y}}(k-1) + \varphi(k)y(k)] \quad (3.14)$$

The previous output can also be defined in terms of the previous regressor matrix and parameter estimates, (3.15), allowing the solution update to be expressed as shown in (3.16).

$$\tilde{y}(k-1) = \Phi(k-1) * \tilde{\theta}(k-1) \quad (3.15)$$

$$\tilde{\theta}(k) = \mathbf{P}(k) * [\Phi(k-1)^T \Phi(k-1) \tilde{\theta}(k-1) + \tilde{\varphi}(k)y(k)] \quad (3.16)$$

Recognizing the covariance matrix of the previous update, $\mathbf{P}(k-1)$, gives

$$\tilde{\theta}(k) = \mathbf{P}(k) * [\mathbf{P}(k-1)^{-1} \tilde{\theta}(k-1) + \tilde{\varphi}(k)y(k)] \quad (3.17)$$

Examination of $\mathbf{P}(k)^{-1}$ shows that the covariance matrix formulation can be also expressed as a matrix update as shown in (3.18). Equation (3.18) illustrates how the current information contained in the current regressor vector $\tilde{\varphi}(k)$ is used to update the covariance matrix. Given this relationship, the inverse of the covariance matrix, $\Phi^T \Phi$, is called the information matrix and denoted by \mathbf{R} . Therefore, the update in (3.18) can also be restated in terms of the information matrix as shown in (3.19).

$$\mathbf{P}(k)^{-1} = \mathbf{P}(k-1)^{-1} + \tilde{\varphi}(k) \tilde{\varphi}(k)^T \quad (3.18)$$

$$\mathbf{R}(k) = \mathbf{R}(k-1) + \tilde{\varphi}(k) \tilde{\varphi}(k)^T \quad (3.19)$$

Substituting (3.18) for $\mathbf{P}(k-1)^{-1}$, the solution updated in (3.17) is restated as

$$\tilde{\theta}(k) = \mathbf{P}(k) * [\mathbf{P}(k)^{-1} \tilde{\theta}(k-1) - \tilde{\varphi}(k) \tilde{\varphi}(k)^T \tilde{\theta}(k-1) + \tilde{\varphi}(k) y(k)]. \quad (3.20)$$

Multiplying (3.20) by $\mathbf{P}(k)$ and manipulating the expression yields

$$\tilde{\theta}(k) = \tilde{\theta}(k-1) + \mathbf{P}(k) \tilde{\varphi}(k) \{y(k) - \tilde{\varphi}(k)^T \tilde{\theta}(k-1)\}. \quad (3.21)$$

In (3.21), it is shown that the previous estimates are updated by scaling the step-ahead prediction error by the updated covariance matrix.

Using the matrix inversion lemma (3.22) and defining the corresponding values in (3.18) as $\mathbf{A} = \mathbf{P}(k-1)^{-1}$, $\mathbf{B} = \tilde{\varphi}(k)$, $\mathbf{C} = \mathbf{I}$, and $\mathbf{D} = \tilde{\varphi}(k)^T$, a new expression for $\mathbf{P}(k)$ is shown in (3.23).

$$[\mathbf{A} + \mathbf{BCD}]^{-1} = \mathbf{A}^{-1} + \mathbf{A}^{-1} \mathbf{B} [\mathbf{C}^{-1} + \mathbf{DA}^{-1} \mathbf{B}]^{-1} \mathbf{DA}^{-1} \quad (3.22)$$

$$\mathbf{P}(k) = \mathbf{P}(k-1) - \frac{\mathbf{P}(k-1) \tilde{\varphi}(k) \tilde{\varphi}(k)^T \mathbf{P}(k-1)}{1 + \tilde{\varphi}(k)^T \mathbf{P}(k-1) \tilde{\varphi}(k)} \quad (3.23)$$

Reducing the expression algebraically, (3.24), and replacing $\mathbf{P}(k) \tilde{\varphi}(k)$ in (3.21) gives the recursive least-squares algorithm shown in (3.25). Each new sample set requires updates to both the solution in (3.25) and covariance matrix using (3.23). While both updates contain a matrix inversion, the inverted matrix will always be a scalar value as long as the selected model has a single output $y(k)$.

$$\mathbf{P}(k) \tilde{\varphi}(k) = \frac{\mathbf{P}(k-1) \tilde{\varphi}(k)}{1 + \tilde{\varphi}(k)^T \mathbf{P}(k-1) \tilde{\varphi}(k)} \quad (3.24)$$

$$\tilde{\theta}(k) = \tilde{\theta}(k-1) + \frac{\mathbf{P}(k-1)\tilde{\varphi}(k)}{1 + \tilde{\varphi}(k)^T \mathbf{P}(k-1)\tilde{\varphi}(k)} \left[y(k) - \tilde{\varphi}(k)^T \tilde{\theta}(k-1) \right] \quad (3.25)$$

The recursive least-squares solution is commonly expressed as three update calculations as presented in (3.26) through (3.28). The matrix \mathbf{I} in (3.28) is the $p \times p$ identity matrix. As the vector $\tilde{\mathbf{L}}(k)$ is used to scale the prediction error before updating the estimates, as shown in (3.26), it is commonly termed the parameter update gain.

$$\tilde{\mathbf{L}}(k) = \mathbf{P}(k-1)\tilde{\varphi}(k) \left\{ 1 + \tilde{\varphi}^T(k)\mathbf{P}(k-1)\tilde{\varphi}(k) \right\}^{-1} \quad (3.26)$$

$$\tilde{\theta}(k) = \tilde{\theta}(k-1) + \tilde{\mathbf{L}}(k) \left(y(k) - \tilde{\varphi}^T(k)\tilde{\theta}(k-1) \right) \quad (3.27)$$

$$\mathbf{P}(k) = \left(\mathbf{I} - \tilde{\mathbf{L}}(k)\tilde{\varphi}^T(k) \right) \mathbf{P}(k-1) \quad (3.28)$$

Before the first iteration, both the covariance matrix and unknown parameter guesses in $\tilde{\theta}$ must be set to initial values. If prior knowledge concerning the parameters is not available, the initial values of $\tilde{\theta}$ can be set to zero. As magnitudes in $\mathbf{P}(0)$ reflect the level of confidence of the current solution, $\mathbf{P}(0)$ is typically initialized with large diagonal values. The large covariance matrix results in large prediction errors gains as defined by (3.26) and large step changes in the solution. Provided sufficiently exciting data is available, the prediction error scaling will decrease along with the covariance matrix as the estimates converge to a solution.

It is important to note that as the number of sample measurements goes to infinity, the uncertainty in the parameter estimates will decrease as long as sufficiently exciting

measurements are available. This decrease in uncertainty is governed by the dyadic product used to update the information matrix shown in (3.19). Therefore, both $\mathbf{P}(k)$ and $\tilde{\mathbf{L}}(k)$ will either trend towards zero or remain unchanged depending on the level of information contained in $\tilde{\varphi}(k)$. Furthermore, the covariance matrix will tend towards zero even in the presence of Gaussian noise. However, the decreasing gain also means the method will become increasingly less sensitive to prediction errors. As a consequence the RLS method will eventually be unable to follow or track parameter changes. This is easily demonstrated by introducing a zero matrix for $\mathbf{P}(k)$ in (3.21). Clearly in this case, updates to the parameter estimates will not occur regardless of the prediction errors.

To permit tracking parameter changes it is necessary to discount or forget past data. This can be done through an exponential forgetting factor λ [56], where $0 < \lambda \leq 1$ and $\lambda=1$ corresponds to recursive least-squares without any discounting. The effect of including the forgetting factor in the solution is shown through the updated cost function in (3.29). For values of λ less than 1, the past residuals are exponentially decreased by a rate determined by λ until their influence is negligible, thus emphasis is placed on recent measurements. Therefore, inclusion of the forgetting factor in the least-squares solution is equivalent to a weighted least-squares formulation.

$$J(\theta) = \frac{1}{2} \sum_{i=m-k+1}^k \lambda^{k-i} (\tilde{\varphi}(i)^T \tilde{\theta} - y(i))^2 \quad (3.29)$$

The discounting of past information can also be expressed in terms of the information matrix update given in (3.30). During each update of the information matrix,

the previous information matrix is scaled by λ before it is updated by the current information contained in $\tilde{\varphi}(k)$. Therefore, the information at a given instant in time is exponentially reduced during each subsequent update.

$$\mathbf{R}(k) = \lambda * \mathbf{R}(k-1) + \tilde{\varphi}(k) \tilde{\varphi}(k)^T \quad (3.30)$$

The new RLS formulation is shown in (3.31) through (3.33). Fortunately, inclusion of the forgetting factor in the RLS formulation does not represent a significant increase to the overall computational effort.

$$\tilde{\theta}(k) = \tilde{\theta}(k-1) + \tilde{L}(k) \left(y(k) - \tilde{\varphi}^T(k) \tilde{\theta}(k-1) \right) \quad (3.31)$$

$$\tilde{L}(k) = \mathbf{P}(k-1) \tilde{\varphi}(k) \left\{ \lambda I + \tilde{\varphi}^T(k) \mathbf{P}(k-1) \tilde{\varphi}(k) \right\}^{-1} \quad (3.32)$$

$$\mathbf{P}(k) = \left(I - \tilde{L}(k) \tilde{\varphi}^T(k) \right) \mathbf{P}(k-1) / \lambda \quad (3.33)$$

Assuming constant excitation in $\tilde{\varphi}(k)$ and $\lambda < 1$, the information matrix is bounded and cannot become infinite. Accordingly, \mathbf{P} can no longer trend fully to zero which is a necessary condition for tracking parameter changes. As shown in (3.33), the solution's sensitivity to prediction errors is determined by the size of λ . The higher the sensitivity the faster the solution will track changes in the parameters. However, increased sensitivity also means the influence of measurement errors is increased as well. Consequently, a trade-off exists between parameter tracking and sensitivity to noise. The

selection of λ will therefore need to be performed on an ad-hoc basis to ensure necessary tracking capabilities are provided without undue sensitivity to noise.

The discounting rate can be selected based on the desired exponential-decay time constant, T_o , and the time between measurements, T , using the relationship shown in (3.34). This approach requires prior knowledge about the nature of the parameter changes and acceptable tracking rates. For instance, approximately four to five time constants are required to converge to the new solution after an abrupt step change in a parameter. Therefore, lower values of λ should be expected. However, in the case of slowly varying parameter changes, larger values of λ will provide less sensitivity to measurement noise while retaining the ability to track the parameter changes. As model-based diagnostic and prognostic evaluations are not meant to facilitate fast acting protection, selecting λ as 0.99 or higher is expected to provide sufficient tracking capabilities.

$$T_o = \frac{T}{-\ln(\lambda)} \quad (3.34)$$

It can be shown the time constant in terms of the number of samples N is approximated by (3.35) for values of λ close to one. One study states that (3.35) represents the rectangular sliding window size necessary to approximate the solution provided by the exponentially discounted window [58]. However, a common rule of thumb is to approximate the “memory” of the estimator as twice the time constant given in (3.35) [56].

$$N = \frac{1}{1 - \lambda} \quad (3.35)$$

In cases where the observed measurements are not sufficiently exciting, the inclusion of the forgetting factor has a marked effect on the covariance matrix $\mathbf{P}(k)$. Without the forgetting factor the covariance matrix would either remain constant or decrease depending on the information contained in the regressors. However, when the excitation is insufficient and $\lambda < 1$, the covariance matrix can increase without bound. This is commonly termed estimator windup or estimator blowup. For instance examine the simple case of $\tilde{\varphi} = 0$ for all values of k ; the update relationship given in (3.33) shows that the covariance matrix will grow exponentially or “blow up” by a rate defined by λ . The larger the covariance matrix becomes the more sensitive the estimates are to measurement noise. Hence, if information contained in the regressors is completely discounted without being replaced, the increased sensitivity will cause the estimations to “drift” from their previously converged values.

Exponentially discounting past information also allows the rank of $\Phi^T \Phi$ to change dynamically along with changes in the excitation. If the exponential discounting is considered an exponentially decaying sliding window, information can be completely discounted before any additional information is observed. Furthermore, $\Phi^T \Phi$ is not actually inverted in during the RLS solution. Instead, the covariance matrix P is updated via (3.33) with each new sample set. Therefore, a solution is always provided when using RLS. All the same, the solution will only be unique under the same conditions in which

the covariance matrix is non-singular. Obviously, these excitation properties of RLS with exponential forgetting are a concern when the excitation is intermittent.

When applying recursive solutions the excitation condition is known as the persistence of excitation. Persistence of excitation simply means that the signal contains sufficient excitation to keep the information matrix from becoming singular over infinite time. A signal u is termed persistently exciting (PE) of order n if it results in the $n \times n$ $\Phi^T \Phi$ matrix being full rank. As the information matrix's dimension equals the number of unknown parameters, a unique solution is only determined when the signal's PE equals the number unknown parameters. It is important to note that the number of unknown parameters directly determines the required level of excitation.

Excitation in the regressors can be examined by the dynamic content contained in the observed waveforms. For example, it can be shown that a step function is PE order of 1 while a signal containing k sinusoids is PE of order $2k$ [56]. Therefore, a possible test for sufficient excitation might be to use Fourier analysis to determine the number of nonzero sinusoids in the measurements and compare this to the number of parameters to be estimated. Another test would be to determine the rank of the information matrix. Parameters could then be updated only if the excitation is sufficient to estimate all the modeled parameters. Such methods are known in the controls literature as conditional updating methods.

A rank deficient covariance matrix indicates that incoming information is not equally distributed among the parameter space. While some dimensions of the parameter space may be excited, or contain new data, other dimensions may not. Conditional updating

methods do not take advantage of the available information as they only update the covariance matrix when information exists in all dimensions of the parameter space. If the covariance matrix is not bounded, however, estimator windup will occur in the unexcited region of the parameter space. A method which bounds the covariance matrix in all dimensions while still updating the excited regions represents a more efficient use of the available information.

3.2.1. DIRECTIONAL FORGETTING

Numerous methods have been proposed to address covariance windup, typically through enforcement of some type of upper bound on the covariance matrix. One of the earliest solutions varies the forgetting factor as a function of the prediction error and the excitation [59]. During periods of low excitation, when limited information is being received, the forgetting factor is forced towards unity to limit the loss of past information and bound the covariance matrix. In [60] resetting of the covariance matrix during low periods of excitation was proposed. However, both variable forgetting (VF) and resetting methods are applied equally in all directions of the parameter space regardless of the distribution of information.

In contrast, directional forgetting (DF) methods only discount past data in those directions in which newer data is available. This means the parameters associated with newer information can be updated without causing estimator windup to occur in the other parameters. Initial methods of direction forgetting were given in [61, 62]. However, these methods did not bound the covariance matrix from below [63-65]. Consequently, the

originally proposed directional forgetting method's covariance matrix could trend fully to zero causing in the method to lose its ability to track parameter changes.

Analogous to directional forgetting, a method was proposed in [66] which uses the eigenvectors of the information matrix to determine the directional distribution of the information. Individual forgetting factors were then assigned to the eigenvalues to ensure upper and lower bounds were enforced upon the covariance matrix. As individual forgetting factors were allocated to each eigenvector (dimension), discounting of the past information was performed selectively in each direction of the parameter space. Accordingly, this method was termed "selective" forgetting (SF) and was shown to be effective when estimating time-varying parameters which vary at different rates [67]. As the eigen-structure must be calculated for every new sample, a good deal of computation effort was required by the method.

A new directional forgetting algorithm was proposed in [68, 69] that determines what dimensions of the parameter space can be safely discounted through decomposition of the information matrix. This method has been shown to have the benefit of bounding the covariance matrix from above (preventing estimator windup) and below (preventing loss of tracking). Additionally, the algorithm does not require calculation of the eigenvalues and eigenvectors as performed by the SF method. The algorithm decomposes the information matrix into two parts as shown in (3.36), $\mathbf{R}_1(k-1)$ which contains the information orthogonal to the new information and $\mathbf{R}_2(k-1)$ which contains the information projected onto the parameter space of the current excitation. Exponential forgetting is only applied to the portion of the information matrix in the same parameter

space as the current excitation. Consequently, information associated with a particular parameter is only discounted when newer information is available. This is highly advantageous as relevant information about each parameter can be retained even when it is obtained at different rates. The algorithm's equations are provided below in (3.37) through (3.42) and detailed derivations can be found in [68, 69].

$$\mathbf{R}(k) = \mathbf{R}_1(k-1) + \lambda * \mathbf{R}_2(k-1) + \tilde{\varphi}(k)\tilde{\varphi}^T(k) \quad (3.36)$$

$$\mathbf{M}(k) = (1-\lambda) \frac{\mathbf{R}(k-1)\tilde{\varphi}(k)\tilde{\varphi}^T(k)}{\tilde{\varphi}^T(k)\mathbf{R}(k-1)\tilde{\varphi}(k)} \quad (3.37)$$

$$\mathbf{R}(k) = [\mathbf{I} - \mathbf{M}(k)]\mathbf{R}(k-1) + \tilde{\varphi}(k)\tilde{\varphi}^T(k) \quad (3.38)$$

$$\mathbf{P}^*(k-1) = \mathbf{P}(k-1) + \frac{1-\lambda}{\lambda} \frac{\tilde{\varphi}(k)\tilde{\varphi}^T(k)}{\tilde{\varphi}^T(k)\mathbf{R}(k-1)\tilde{\varphi}(k)} \quad (3.39)$$

$$\mathbf{P}(k) = \mathbf{P}^*(k-1) - \frac{\mathbf{P}^*(k-1)\tilde{\varphi}(k)\tilde{\varphi}^T(k)\mathbf{P}^*(k-1)}{1 + \tilde{\varphi}^T(k)\mathbf{P}^*(k-1)\tilde{\varphi}(k)} \quad (3.40)$$

$$\tilde{\mathbf{L}}(k) = \mathbf{P}^*(k-1)\tilde{\varphi}(k) \left\{ \mathbf{I} + \tilde{\varphi}^T(k)\mathbf{P}^*(k-1)\tilde{\varphi}(k) \right\}^{-1} \quad (3.41)$$

$$\tilde{\theta}(k) = \tilde{\theta}(k-1) + \tilde{\mathbf{L}}(k) \left(y(k) - \tilde{\varphi}^T(k)\tilde{\theta}(k-1) \right) \quad (3.42)$$

Note that (3.37) and (3.40) will be undefined when the regressor vector is zero ($\tilde{\varphi}(k)=0$). A dead zone is applied through (3.43) to keep the algorithm from being activated unless the regressor vector contains some amount of information greater than an

assumed noise level α . When the test in (3.43) is satisfied, the DF method is altered by (3.44) and (3.45). Therefore, discounting will not occur when the measurements contain only noise.

$$|\tilde{\varphi}(k)| \leq \alpha \quad (3.43)$$

$$M(k) = 0 \quad (3.44)$$

$$P^*(k-1) = P(k-1) \quad (3.45)$$

3.2.2. VARIABLE DIRECTIONAL FORGETTING

An interesting design consideration arises when considering long-term passive monitoring requirements. Specifically, how much weight should be applied to older data when significant gaps exist between periods of sufficient excitation or when significantly abrupt parameter changes occur? Suppose that after converging to the “true” solution, new information about a parameter is unavailable for a long period of time. During this time the actual value of the parameter varies slowly but significantly from the last parameter estimate. When the excitation returns to that parameter space the change will appear as an abrupt step change in the estimation and the estimates will be biased until the past information is replaced.

As past information is discounted only as new information becomes available, the actual rate at which past data is discounted is a function of λ as well as a function of the rate at which newer information becomes available. Therefore, it is more convenient to

consider the retained information in terms of the equivalent memory size as defined (3.35) versus a time constant. For example, an equivalent memory size of 200 data points results when λ is 0.99. When an abrupt parameter change occurs, 200 new relevant data points will need to be observed before the all past information is discounted. As a result, directional forgetting may exhibit slower parameter tracking capabilities compared to standard exponential forgetting. However, this assumes the excitation is sufficient to overcome estimator windup and the influence of measurement errors when using standard exponential forgetting.

One option to account for abrupt parameter changes is to dynamically alter the memory size by adjusting λ . The amount of past data retained in the calculations is then determined by how well the model predicts current observations. When the prediction error (3.46) is larger than a set tolerance, λ is set to a low value then exponentially increased. As the information which triggered the high prediction error may not exist in subsequent observation, λ is exponentially increased back to its original set-point. This allows increased discounting to occur in any parameter space associated with incoming information.

$$\varepsilon(k) = \{y(k) - \tilde{\varphi}(k)^T \tilde{\theta}(k-1)\} \quad (3.46)$$

3.2.3. COVARIANCE RESETTING

Another option is to simply remove all the past data when a large abrupt step-change occurs. Given indications that the model is inadequately predicting the observations (i.e. the error in (3.46) is larger than a set tolerance) the covariance matrix \mathbf{P} could be reset to its initial value $\mathbf{P}=\alpha*\mathbf{I}$; where α is a large scalar value and \mathbf{I} is the identity matrix. Resetting the covariance matrix indicates that there is little confidence in the current estimations and essentially restarts the estimation process using the current parameter estimates as the initial starting point. When \mathbf{P} (and consequently \mathbf{R}) is reset the past information for every parameter is lost, and all of the parameters estimates will deviate from their previously converged values until sufficient excitation for each parameter is again obtained. Obviously, covariance resetting represents a drastic response. In cases where the excitation is extremely intermittent, resetting the covariance matrix will keep past data from biasing the estimates over longer periods of time.

Other system identification methods and methods to prevent estimator windup exist and a detailed examination of these methods can be found in [55]. Determination of which method to use should be based on the complexity of the model and the expected excitation. A summary of the various recursive estimation variations discussed here are presented in Table 3-1 along with a brief discussion of potential applications as well as pros and cons.

Table 3-1. Recursive Least-Squares Methods

Method	Potential Applications	Advantages	Disadvantages
Least-squares	Situations containing high signal to noise ratios but constant parameter values.	The estimate variance approaches zero as the number of observations increases to infinity.	Unable to track parameter changes.
Recursive least-squares with exponential forgetting (RLS)	Situations where the normal operation of the system is expected to provide persistent excitation.	Discounts past information at a fixed rate allowing for parameter tracking.	Requires persistently exciting information to keep estimator windup from occurring.
Recursive least-squares with directional forgetting (RLS/DF)	Situations where the excitation is only sufficient during intermittent system operations.	Past information for each parameter is discounted only if newer information is available thereby preventing estimator windup.	Potentially slower tracking response than recursive least-squares with exponential forgetting.
Recursive least-squares with variable directional forgetting (RLS /VDF)	Situations where significant individual parameter changes are expected between periods of sufficient excitation.	Allows faster discounting of past data in a given parameter space when the prediction error is high.	Requires the ad-hoc selection of two additional parameters and can be overwhelmed by noise.
Recursive least-squares with covariance resetting	Situations where significant changes in all parameter are expected between periods of sufficient excitation.	Discounts all past information to remove any bias in the estimates from past information.	Sufficient excitation is required after resetting to obtain convergence

3.2.4. MULTIVARIABLE SOLUTIONS

The presented recursive formulations are applicable to models where a single output is specified. However, the formulations are also applicable to models with multiple inputs and multiple outputs (MIMO models). One approach is to divide the model into individual multiple input single output (MISO) models which are fitted to the data separately using the previously derived techniques. Conversely, it can be recognized that the multiple inputs are shared by each MISO model signifying that the regressors are shared by each model. If each model is weighted equally in the overall cost function, only (3.31) must be updated to account for the increased dimensions as denoted in (3.47) where $\boldsymbol{\theta}(k)$ contains multiple parameter vectors. For m outputs, $\boldsymbol{\theta}(k)$ is a $p \times m$ matrix and $\tilde{\mathbf{y}}(k)$ is a $1 \times m$ vector containing the output variables.

$$\boldsymbol{\theta}(k) = \boldsymbol{\theta}(k-1) + \tilde{\mathbf{L}}(k) (\tilde{\mathbf{y}}(k) - \tilde{\boldsymbol{\varphi}}^T(k) \boldsymbol{\theta}(k-1)) \quad (3.47)$$

While the multivariable formulation appears more efficient than solving the individual MISO models, the parameter vectors composing $\boldsymbol{\theta}(k)$ are still independent from each other. The same unknown modeled in multiple locations of $\boldsymbol{\theta}(k)$ will have multiple independent solutions. Additionally, the multivariable solution requires that each of the MISO models share the same regressors. Consequently, the MIMO model may not represent the most optimal form to estimate the desired parameters. However, the multivariable models should be considered in cases where these limitations are not a significant factor.

3.3. MODEL AND PARAMETER VALIDATION

As previously noted, the RLS algorithm always provides a solution regardless of the current or past level of excitation. Because the excitation is not artificially regulated, there is no assurance that the current estimation set is representative of the true parameters. More specifically, without sufficient past excitation the collected information may not be adequate for satisfactory convergence. In response, statistical inference measures were implemented to validate or judge the level of confidence in the parameter estimates. Additional tests are also introduced to quantify the regressors' linear independence. Finally, model validation through residual analysis is discussed.

The statistical measures will be useful in the diagnosis and prognosis sections of the condition monitor and will be stored along with the estimates, $\tilde{\theta}$, as shown in Figure 3-1. Both the unknown estimates and the statistical measures are determined using the sampled measurements ($v_1(k), i_1(k), \dots$) which are filtered and normalized ($v_1(k)^*$, $i_1(k)^*$, ...) before applying the solution method. The stored statistical measures include the prediction error, ε , determined by the solution method as well as the variance of the unknown parameter estimates, σ^2 , and the calculated confidence intervals (CI) which are determined from the covariance matrix, \mathbf{P} , and ε . Other forms of expressing the estimates accuracy, such as margins or error, could be stored instead of the confidence intervals.

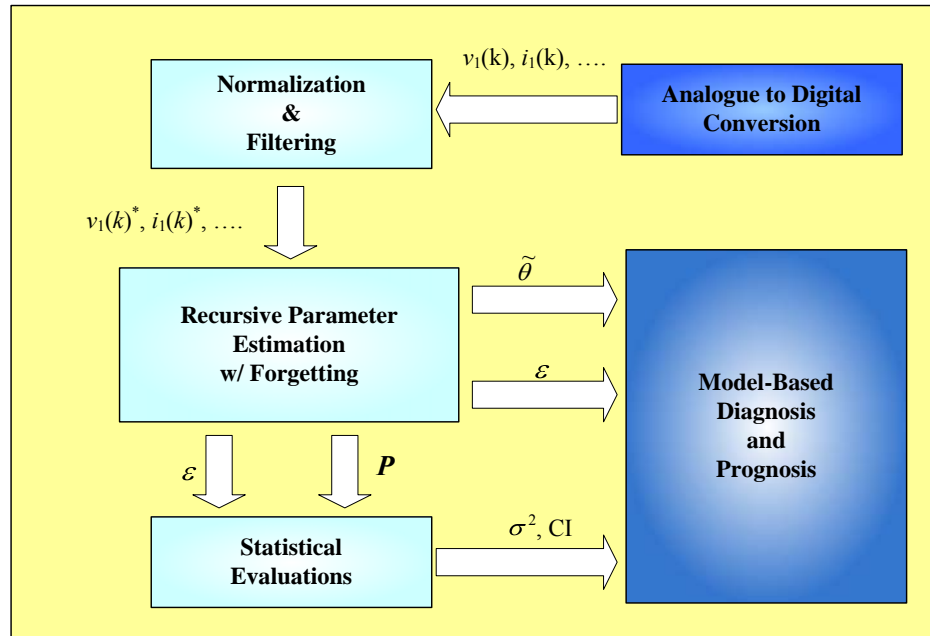


Figure 3-1. Condition Monitor Parameter Estimation and Validation Block

3.3.1. MARGINS OF ERROR

Statistical inference about the parameter estimates requires knowledge about the estimate variance. As previously noted, the actual matrix of covariances for the parameter estimates is found by scaling \mathbf{P} by noise variance as indicated in (3.48).

$$\text{cov}(\theta) = \sigma^2 \mathbf{P} \quad (3.48)$$

While \mathbf{P} is readily available from the recursive least-squares formulations, the error or noise variance, σ^2 , is not. Revisiting (3.1), σ^2 is the variance of the residuals between the true and predicted output values for a particular estimated parameter set. One possible approach is to recalculate the residual errors for each new parameter solution and re-

estimate the variance. This approach represents a large computation burden and requires the storage of a large amount of past regressor data. If the parameters are assumed constant, both the residual and prediction error variances are equal to the noise variance. Thus, σ^2 can be approximated using the prediction error instead.

The sample variance of the prediction error can be estimated using (3.49).

$$\hat{\sigma}^2(N) = \frac{1}{N} \sum_{k=1}^N [y(k) - \tilde{\varphi}(k)^T * \tilde{\theta}(N)]^2 \quad (3.49)$$

Taking into account that the number of samples N used to estimate the parameters is defined by (3.35), the sample variance can be rewritten as shown in (3.50).

$$\hat{\sigma}^2(N) = \sum_{k=1}^{N-1} [y(k) - \tilde{\varphi}(k)^T * \tilde{\theta}(N)]^2 + (1 - \lambda) [\varepsilon^2(N)] \quad (3.50)$$

When the parameter estimates $\theta(N)$ are constant over a sufficient period of time, the prediction errors, ε , over this period are good predictors of the residuals. In this case, (3.50) can be restated in a recursive form with the past estimates discounted in the same manner as the parameter estimates. Therefore, the approximation of σ^2 can change over time in a manner similar to the parameter estimations.

$$\hat{\sigma}^2(N) = \lambda \hat{\sigma}^2(N-1) + (1 - \lambda) [\varepsilon^2(N)] \quad (3.51)$$

Furthermore, it was shown in [70, 71] that the estimations of the residual from the prediction errors could be improved by accounting for the past information contained in

P. The final version of the residual variance estimate is given in (3.52). The forgetting factor used in (3.52) is the same value used to discount the observed information.

$$\hat{\sigma}^2(k) = \lambda \hat{\sigma}^2(k-1) + (1-\lambda) * [1 - \tilde{\varphi}(k)^T \mathbf{P}(k) \tilde{\varphi}(k)] * [y(k) - \tilde{\varphi}(k)^T \tilde{\theta}(k-1)] \quad (3.52)$$

The noise variance estimate of (3.52) can be used in (3.48) to estimate the variance and covariance values necessary to determine the confidence intervals. Assuming the error is zero mean white noise and insignificant correlation between the parameters, the 100(1- α)% confidence interval for each parameter can be estimated using (3.53), where n and p are again the number of observations and unknown parameters respectively and P_{jj} is the j^{th} diagonal term in the covariance matrix. The parameter estimations follow a chi-squared distribution [72] and the Student-t value with $n-p$ degrees of freedom is chosen to scale the interval. Recalling that the number of observations used by the calculations is governed by the forgetting factor, the value of n is approximated as five times the memory size defined in (3.35).

$$\theta_j \pm t(1-\alpha/2; n-p) * \hat{\sigma} \sqrt{P_{jj}} \quad (3.53)$$

However, the univariate confidence interval in (3.53) only addresses the hypothesis that a particular parameter's true value is contained within the interval. A more conservative hypothesis is whether all the intervals simultaneously contain their respective true values. In other words, what confidence space simultaneously contains the model's true parameters for a specified confidence level? Bonferroni confidence intervals

are the simplest simultaneous test to account for the joint evaluation of multiple parameters as this approach divides the confidence level $(1-\alpha)$ by the number of parameters to be estimated, as seen in (3.54). Accordingly, the Bonferroni confidence intervals are easily calculated and provide a conservative interval range. The benefit of the Bonferroni confidence intervals as applied to online synchronous machine parameter estimation was recently examined in [73].

$$\theta_j \pm t \left(\frac{1-\alpha/2}{p}; n-p \right) * \hat{\sigma} \sqrt{P_{jj}} \quad (3.54)$$

The added/subtracted value in (3.54) is termed the margin of error which is often reported in lieu of an actual confidence interval. During the online application, the margins of error could be tested against preset tolerances to decide whether an estimate is sufficiently accurate to warrant action or storage for later evaluation. However, in order for the confidence intervals to accurately reflect upon the accuracy of the estimations, the assumption that the residuals are white noise must still be satisfied.

3.3.2. MULTICOLLINEARITY TESTS

It was previously shown that identifiability is determined by the singularity or non-singularity of the information matrix, $\mathbf{R} = \Phi^T \Phi$. Intrinsically, singularity of the matrix is determined by the linear independence of the regressors which form the columns of Φ . Therefore, the level of excitation is decreased whenever linear dependence or multicollinearity exists between the regressors. A multiple regression statistic known as

the variance inflation factor (VIF) is a commonly used indicator of linear dependence between multiple variables. Typically, the VIF is defined in the form shown in (3.55) where the j^{th} column of Φ is denoted by $\tilde{\Phi}_j$.

$$\text{var}(\theta_j) = VIF_j * \frac{\sigma^2}{\tilde{\Phi}_j^T \tilde{\Phi}_j} \quad (3.55)$$

Revisiting (3.7), it can be seen that $\tilde{\Phi}_j^T \tilde{\Phi}_j$ is the j^{th} diagonal of the information matrix \mathbf{R} . Additionally, a parameter estimate's variance is given by the j^{th} diagonal of (3.48). Therefore, (3.55) can be simplified to the form shown in (3.56). Recalling that \mathbf{P} and \mathbf{R} are inverses, the VIF reflects the degree in which a diagonal in \mathbf{P} is increased due to nonzero off-diagonals in the information matrix. For example when \mathbf{R} is diagonal, R_{jj} and P_{jj} are direct inverses and the value of VIF must be one. Conversely when perfect linear dependence exists between the regressors, both P_{jj} and VIF_j are infinite.

$$P_{jj} = VIF_j * \frac{1}{R_{jj}} \quad (3.56)$$

While the variance inflation factor is a useful diagnostic, the square root of the VIF is more functional because it directly specifies how the standard error, and consequently the confidence interval, is enlarged by the multicollinearity. In [74] this value is termed the standard-error inflation factor (SIF) and its calculation is given in (3.57). An obvious

benefit of the SIF is the required data is already generated by the recursive algorithms. Storage of the SIF will be a valuable offline tool for evaluating a model's effectiveness.

$$SIF_j = \sqrt{P_{jj} R_{jj}} \quad (3.57)$$

While the SIF is a good indicator of multicollinearity, it does not indicate which regressor terms are strongly correlated. While examining the model identifiability requirements, collinearities between the regressors are established through examination of the correlation matrix. The correlation matrix is determined by scaling the entries in \mathbf{P} by the associated standard deviations as indicated in (3.58). The off-diagonal entries of the correlation matrix indicate the level of correlation that exists between the regressors; values close to one indicate a strong positive correlation while values close to negative one indicate a strong negative correlation.

$$\mathbf{C} = \begin{bmatrix} 1/\sqrt{P_{11}} & & & \\ & 1/\sqrt{P_{22}} & & \\ & & \ddots & \\ & & & 1/\sqrt{P_{pp}} \end{bmatrix} * \mathbf{P} * \begin{bmatrix} 1/\sqrt{P_{11}} & & & \\ & 1/\sqrt{P_{22}} & & \\ & & \ddots & \\ & & & 1/\sqrt{P_{pp}} \end{bmatrix} \quad (3.58)$$

3.3.3. RESIDUAL ANALYSIS

Whether the chosen model sufficiently represents the true characteristics of the device is a subjective question of validation. A simple evaluation is whether the estimated parameters are physically viable. For example, a negative resistance model would be a

red flag to revisit the selected model. Another useful validation test is to inspect the confidence intervals to determine if a modeled parameter could be removed from the model. For example, a confidence interval which consistently crosses zero might indicate that a variable could be removed from the model. However, an unmodeled variable could bias the estimates when conditions change. This selection is often described as a trade off between model flexibility and parsimony [55]. Simply put, the model can be flexible and better at explaining more of the dynamics (reducing bias), or the number of parameters can be reduced which typically reduces the variance (fewer parameters reduces the potential for multicollinearity). In fact, large standard deviations may be a sign of an over-defined model.

As previously noted, the confidence intervals proposed in the previous section are dependent on the residuals being zero mean white noise. Otherwise, the residuals contain additional content which could be modeled. Consequently, non-white residuals are a sign of inaccuracy in the model structure. Model validation is a process that is best achieved offline when necessary corrections are easier to recognize and implement. Some general solutions to non-white residuals are:

1. Modify the model structure to account for any unmodeled physical dynamics,
2. Modify the model and/or solution method to include an error model (i.e. extended least squares),
3. Filter the extra dynamic content, or
4. Deem the bias to be at an acceptable level for the given application.

While there are numerous tests which could be applied to evaluate the residuals' whiteness (autocorrelation, Durbin-Watson test, etc.) each test requires significant calculations and data storage to recalculate the residuals at each time step. Moreover, temporary dynamic residual content arising from parameter changes and subsequent tracking could also be interpreted falsely by an automated test. The proposed online model validations are limited to the parameter feasibility and confidence intervals mentioned earlier. However, the historical data portion of Figure 1-1 could be used to periodically generate whiteness test reports if desired.

Assuming that a sufficiently representative model is utilized, analysis of the residuals between the measured and predicted output could provide valuable diagnostic information. For example, a model reference approach as shown in Figure 2-1 could be used to indicate when the device operates in a manner which cannot be accounted for by the model. Therefore, storage and evaluation of the prediction error in (3.46) should be considered along with the parameter estimates.

3.4. MEASUREMENT NOISE

Any parameter estimate cannot be more accurate than the data used in the approximation. Increasing the memory size can reduce the influence of noise but results in slower tracking of time-varying parameters. Measurement noise also influences the confidence interval estimates by increasing the noise variance in (3.48). To some extent, the amount of measurement noise is determined by the method used to collect the sample

data. Hence, common filtering and quantization design criteria which affect the accuracy of the estimates require examination.

3.4.1. QUANTIZATION AND SAMPLING RATE

As shown in Figure 1-1, the proposed parameter online diagnostic monitor requires discrete measurements provided by an analog-to-digital converter. Assuming the analog signal can take on any value, the resulting quantization error is typically considered uniformly distributed white noise with the probability density shown in (3.59). The limits of the uniform distribution are defined by the incremental step size q used by the A/D process while the step size is determined by the number of bits, n , used in the A/D process and the full scale over which the analog values are discretized $|\Delta r| = r_{\max} - r_{\min}$. This relationship is illustrated in (3.60). While the actual noise variance σ^2 is dependent on many factors, in general larger measurement noise will result in larger noise variance. Therefore, the noise variance, and hence the estimate variance, can be improved by increasing the number of bits used in the A/D process.

$$p(e; k) = \begin{cases} -\frac{q}{2} \leq e(k) \leq \frac{q}{2} \\ 0 \quad \text{otherwise} \end{cases} \quad (3.59)$$

$$q = \frac{|\Delta r|}{2^n} \quad (3.60)$$

The sampling rate of the A/D conversion also influences the estimates by determining the content contained in the sample observations. To keep from aliasing the sample data the sampling frequency should be twice the highest expected frequency. As the frequency content cannot be known ahead of time, anti-aliasing filters are necessary to ensure frequency content above the Nyquist frequency is not contained in the sample data. Potentially, any sampling rate could then be implemented as long as sufficient filtering is applied, though sampling at lower frequencies will potentially capture less information. In general, the measurements should be sampled as fast and with as much accuracy as hardware will allow.

3.4.2. FILTERING

As noted in the previous sections, filtering is an important component of the parameter estimation procedure. Proper filter selection prevents aliasing and reduces the noise variance. However, identical filters must be applied to every measurement to keep from artificially biasing the input-output relationship. While filtering can be viewed as biasing estimates toward a particular frequency range, it can be shown that when identical filters are applied to each measurement the input-output relationships are unaltered. Consequently, filter design issues such as ripple in the pass band are not a significant concern. Therefore, filters characterized by sharper transitions between the passband and stopbands, such as high order Chebyshev filters, can be used.

Given some of the gathered information may result from transient events whose frequency content cannot be predicted, sampling at a high rate alone cannot guarantee

aliasing will not occur. Thus, anti-aliasing filters must be implemented by analog devices before the measurements are fed into the A/D device. However, additional digital filtering can be applied as needed. For example, digital filters may be needed to remove unmodeled content from the observations not removed by the anti-aliasing filters. This is an important design consideration as any unmodeled content will bias the parameter and confidence interval estimates. Therefore, filter design must be performed for each monitoring device considering the model's dynamic characteristics.

3.5. NORMALIZATION

Measured input-output data and the parameters estimates themselves will typically exist in different scales. Significantly dissimilar scales are a concern as they can result in numerical errors during the estimation process. One solution is to normalize or per-unitize the input-output data, and consequently the estimations, by scaling the data using carefully chosen bases. Each data type (voltage, current, time, etc.) shares a single base value and any physical relationships between these data types must be enforced.

In the time domain the per-unit bases for the physical or electrical parameters can be expressed in terms of v , i , and t [75]. The relationships between $v-i-t$ bases and the bases representing the physical parameters are provided in Table 3-2. It is necessary that three of the bases shown in Table 3-2 be specified. All unspecified bases will be determined using the relationships given in the fourth column of Table 3-2. However, care must be taken to ensure the selected bases fully span all three dimensions of $v-i-t$. Other bases could be introduced given additional measurement types and model configurations.

Table 3-2. Time Domain Per-Unit Base Relationships

Base	Quantity	Units	<i>v-i-t</i> Relationship
V_{base}	Voltage	Voltage (v)	v
I_{base}	Current	Amperes (A)	i
t_{base}	Time	Seconds (s)	t
S_{base}	Power	Volt-Amperes (VA)	vi
R_{base}	Resistance	Ohms (Ω)	v/i
L_{base}	Inductance	Henries (H)	vt/i
C_{base}	Capacitance	Farads (F)	it/v

Proper base selection is essential when utilizing RLS with directional forgetting. Projecting the information matrix onto a parameter space which is overly skewed will result in numerical errors that influence the convergence and tracking abilities of the method. Specifically, past information associated with the smaller scaled regressors will not accurately be projected onto the space parallel to the incoming information. Hence, discounting of past information associated with these regressors will be limited. As such, base selection can intentionally or inadvertently influence parameter tracking when directional forgetting is used.

CHAPTER 4

TWO-CONDUCTOR MODELS

As mentioned in section 3.1, parameter identifiability is dependent on the solution method, the model structure, and the measured input-output data. Model-based diagnostics of network health is therefore reliant upon the available measurements and selected model as much as the estimation algorithm. In this chapter estimation of two conductor electrical parameters is evaluated using time-domain measurements. The identifiability requirements of multiple conductors using time-domain measurements are subsequently evaluated in Chapter 4. Finally, estimation of network parameters using frequency-domain observations is examined in Chapter 5.

The distributed parameter model or incremental model for a two-conductor line is shown in Figure 4-1. The model represents a single conductor using either a second conductor or a common ground plane as the return. Examples of the common grounds in vehicular applications include military and commercial aircraft which commonly use the metal hull as a return to reduce weight of the aircraft. In either case, the return path is modeled by an equivalent conductor model. As shown, the voltages and currents at the sending and receiving ends are related through incremental values of the resistance and inductance as well as the shunt conductance and capacitance. While a resistance and

inductance is associated with each conductor, these terms are modeled by an equivalent single resistance and inductance as shown in Figure 4-1. As the length of the increment, Δx , increases, the corresponding parameter values also increase. For long spans (or high frequency content), accuracy of the line model can be improved by using multiple sections of the distributed parameter model of Figure 4-1 connected in series. While distributed parameter estimation techniques are available, estimation of distributed parameters is computationally costly making them an undesirable option for an online application.

In many applications a lumped parameter model accurately represents the electrical characteristics of the entire line. In lumped parameter models the distributed parameters are collected or “lumped” together into a finite model represented by an ordinary differential equation. However, line length and frequency content must be considered to ensure that the selected model accurately represents the electrical characteristics.

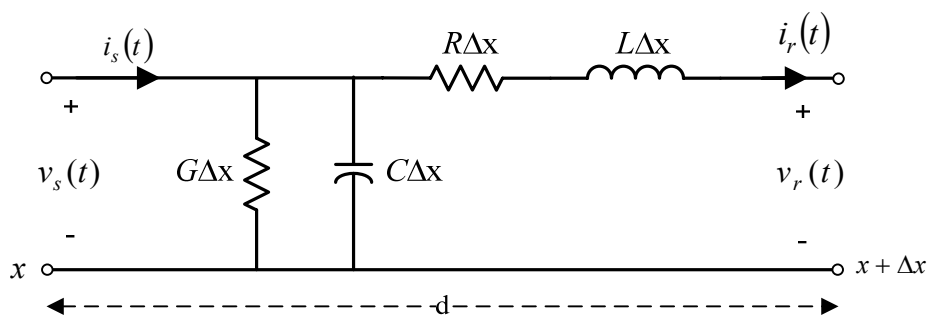


Figure 4-1. Distributed Parameter Line

Specifying the line length by d , hyperbolic functions, (4.1) and (4.2), can be determined which relate the voltage and current relationships defined in Figure 4-1, [76, 77]. As frequency cannot be assumed constant, the equations are given here in terms of the Laplacian operator, s . The presented parameter estimation techniques cannot yet be applied as the equations are nonlinear. However given assumptions about line length and frequency content, equivalent lumped parameter models can be developed which satisfy the linear constraints of the least-squares parameter estimation techniques.

$$V_s(s) = \cosh\left(d^* \sqrt{(R + sL)(G + sC)}\right) V_r(s) + \sqrt{\frac{(R + sL)}{(G + sC)}} \sinh\left(d^* \sqrt{(R + sL)(G + sC)}\right) I_r(s) \quad (4.1)$$

$$I_s(s) = \sqrt{\frac{(G + sC)}{(R + sL)}} \sinh\left(d^* \sqrt{(R + sL)(G + sC)}\right) V_r(s) + \cosh\left(d^* \sqrt{(R + sL)(G + sC)}\right) I_r(s) \quad (4.2)$$

The conductor's electrical parameters are dependent on many factors including conductor size, insulation/jacketing, as well as environmental conditions. Literature and standards relating to electrical parameter models can be found in [1, 78-85]. In the following sections the models are based on specified assumptions concerning equivalent lumped parameter models from (4.1) and (4.2). It is expected that other models can be selected which satisfy specific circumstances based on prior knowledge of the conductors, available measurements, and network operation.

4.1. SHORT TRANSMISSION LINE MODEL

Assuming the length of the line is relatively short with respect to the expected frequencies, (4.1) and (4.2) are reasonably approximated by the circuit in Figure 4-2. This circuit is commonly referred to as the short transmission line model. The differential equation for the circuit is provided in (4.3) where ρ is the differential operator d/dt .

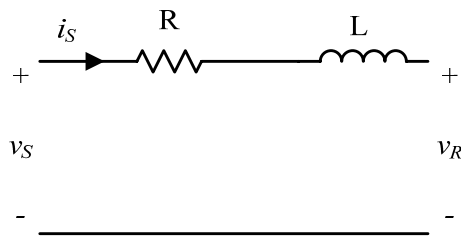


Figure 4-2. Short Transmission Line Circuit Model

$$v_s = i_s(R + \rho L) + v_R \quad (4.3)$$

Considering the potential difference between the two terminal voltages as a single term, the transfer function relating the current and voltages is shown here in (4.4). As there is a single input and output the model is called a single input single output (SISO) system. In contrast, a multiple input single output (MISO) model could be defined simply by considering each voltage as separate inputs.

$$\frac{i_s}{v_s - v_R} = \frac{1}{R + \rho L} \quad (4.4)$$

Because the proposed monitoring method uses sampled data, discrete-time models are required. The bilinear transform (4.5) is used to approximate the continuous-time behavior because it preserves model stability and does not exhibit aliasing in the frequency response. The bilinear approximation can cause warping in the frequencies close to the Nyquist frequency. However, as long as sufficient filtering is imposed and sampling period, T , is small, the approximation of the continuous-time system should be sufficiently accurate. Selecting $y = i_s$ and $u = v_s - v_r$, the resulting difference equation is shown in (4.6), where k is again used to indicate the current sample. In this case, the output is selected to keep the transfer function from being improper, but this is not a requirement for selecting the model's form.

$$s = \frac{2(z-1)}{T(z+1)} \quad (4.5)$$

$$y(k) = \frac{T}{RT+2L}u(k) + \frac{T}{RT+2L}u(k-1) - \frac{RT-2L}{RT+2L}y(k-1) \quad (4.6)$$

The three coefficients in (4.6) can be reduced by collecting the common parameter terms as shown in (4.7). The new regressor vector is composed of two newly defined terms (4.8) and is a function of both the input and output.

$$y(k) = \frac{1}{RT+2L}[Tu(k) + Tu(k-1)] - \frac{RT-2L}{RT+2L}y(k-1) \quad (4.7)$$

$$\tilde{\varphi}^T(k) = \begin{bmatrix} Tu(k) + Tu(k-1) \\ -y(k-1) \end{bmatrix} \quad (4.8)$$

In order to find a solution using linear regression techniques, the model must be considered “linear in the parameters.” Linear in the parameters implies the unknown coefficients are not functions of each other or raised to any power. Clearly, the coefficients are not linear in terms of the R and L parameters but can be redefined or reparameterized with respect to the parameters to be estimated. The reparameterized model is given in (4.9) and (4.10).

$$D_1 = \frac{1}{RT + 2L} \tag{4.9}$$

$$D_2 = \frac{RT - 2L}{RT + 2L}$$

$$y(k) = D_1 [(u(k) + u(k-1))] + D_2 [-y(k-1)] \tag{4.10}$$

There is a penalty for reparameterizing the model. Specifically, the physical relationships designated in (4.9) between R and L are not enforced by the estimation procedure. In other words, the parameters D_1 and D_2 are determined merely on how well the curve fit of (4.10) models the observed input-output data. Nevertheless if the model is a good physical representation of the line and a unique solution is found for the parameters, the estimated parameters provide good approximations of the physics-based parameters. That is, R and L can be approximated from the D_1 and D_2 using the relationships given in (4.11). Reparameterization can lead to unidentifiable parameters if a mapping does not exist between the estimated and physics-based parameters. In these instances, diagnosis and prognosis measures could be based on the estimated coefficients.

$$R = \left(\frac{1}{2T} \right) \frac{D_2 + 1}{D_1} \quad (4.11)$$

$$L = \left(\frac{1}{4} \right) \frac{1 - D_2}{D_1}$$

Reparameterization of this model can be avoided though a different selection of which variable to model as the output as shown in (4.12) and (4.13). While this model contains a derivative in the regressors, the numerical sensitivity to measurement errors is not any better or worse than that associated with the reparameterization. Additionally, models that permit the direct estimation of the physics-based parameters are intuitively easier to analyze. In contrast, the variances of R and L using (4.11) are dependent on nonlinear relationships between the variances of D_1 and D_2 . When possible, direct estimation of the physics-based parameters is preferred.

$$\frac{y}{u} = \frac{v_S - v_R}{i_S} = R + \rho L \quad (4.12)$$

$$y(k) + y(k-1) = R[u(k) + u(k-1)] + L \left[\frac{2}{T} * (u(k) - u(k-1)) \right] \quad (4.13)$$

4.2. NOMINAL PI CIRCUIT MODEL

A two-conductor line model is presented in Figure 4-3 with both conductors retaining their individual resistance and inductance terms. Additionally, the model includes the shunt capacitance (equally divided at the two ends of the line) as well as

mutual coupling between the lines. As a negligible amount of leakage current is assumed, the shunt conductance is not modeled. This circuit is a reasonable approximation of lines with relatively longer lengths compared to the short transmission line model. One analysis estimates that the model is acceptable for power cables less than one mile in length and operating at 60Hz [76]. If significantly higher frequencies are expected, the acceptable line length under which this model is accurate will need to be evaluated accordingly.

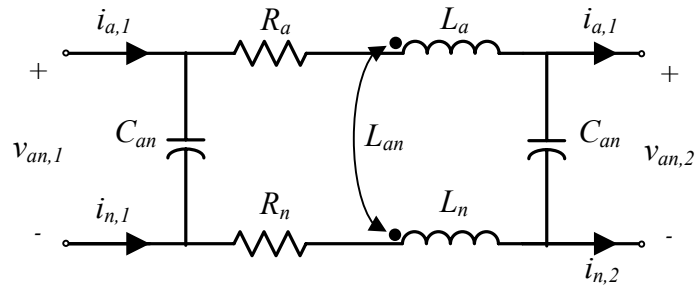


Figure 4-3. Two-Conductor Mutually Coupled Circuit

Applying Kirchoff's voltage law about the inner loop of Figure 4-3, the voltage and current relationships are defined by (4.14).

$$\begin{aligned}
 v_{an,1} - v_{an,2} = & (R_a + \rho L_a) \{ \dot{i}_{a,1} - \rho C_{an} (v_{an,1}) \} + \rho L_{an} \{ \dot{i}_{n,1} + \rho C_{an} (v_{an,1}) \} \\
 & - (R_n + \rho L_n) \{ \dot{i}_{n,1} + \rho C_{an} (v_{an,1}) \} - \rho L_{an} \{ \dot{i}_{a,1} - \rho C_{an} (v_{an,1}) \}
 \end{aligned} \quad (4.14)$$

Collecting the voltage and current terms of (4.14) gives (4.15) with the derivative of the time varying terms denoted by the number of dots above the variables.

$$\begin{aligned}
v_{an,1} - v_{an,2} = & R_a [i_{a,1}] - R_n [i_{n,1}] - C_{an} (R_a + R_n) \left[v_{an,1}^{\bullet} \right] + C_{an} (-L_a - L_n + 2L_{an}) \left[v_{an,1}^{\bullet\bullet} \right] \\
& + (L_a - L_{an}) \left[i_{a,1}^{\bullet} \right] - (L_n - L_{an}) \left[i_{n,1}^{\bullet} \right]
\end{aligned} \quad (4.15)$$

Assuming current injected into either conductor is equal in magnitude but opposite in sign (i.e. $i_{a,1} = -i_{n,1}$), equation (4.15) reduces to (4.16). As indicated in (4.16), the resistance and inductances were lumped together in order to reduce the number of unknowns. While the individual conductor parameters cannot be determined independently, the overall health can still be gauged by estimating of the equivalent parameters. More importantly, by reducing the number of unknown parameters the required excitation is reduced accordingly. The reduced two-conductor model can now be represented by the nominal pi equivalent circuit presented in Figure 4-4; the terminal voltages and currents were renamed to reduce notation. This circuit could also be derived from the distributed parameter model of (4.1) and (4.2).

$$\begin{aligned}
v_{an,1} - v_{an,2} = & \underbrace{(R_a + R_n)}_R [i_{a,1}] + \underbrace{(L_a + L_n - 2L_{an})}_L \left[i_{a,1}^{\bullet} \right] - \underbrace{C_{an} (R_a + R_n)}_{RC} \left[v_{an,1}^{\bullet} \right] \\
& - \underbrace{C_{an} (L_a + L_n - 2L_{an})}_{LC} \left[v_{an,1}^{\bullet\bullet} \right]
\end{aligned} \quad (4.16)$$

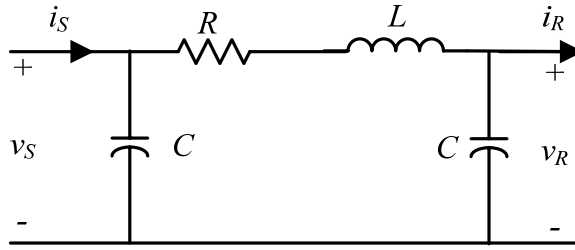


Figure 4-4. Nominal Pi Equivalent Circuit

It is initially assumed that voltage and current measurements on either end of the line are available. The vector matrix relationship between the currents and voltages in the circuit are defined by matrix (4.17). As with the short transmission line model, any of the currents or voltages can be considered as the output or dependent variable.

$$\begin{bmatrix} i_S \\ i_R \end{bmatrix} = \begin{bmatrix} \frac{1}{R + \rho L} + \rho C & -\frac{1}{R + \rho L} \\ \frac{1}{R + \rho L} & -\frac{1}{R + \rho L} - \rho C \end{bmatrix} \begin{bmatrix} v_S \\ v_R \end{bmatrix} \quad (4.17)$$

4.2.1. SISO MODEL

A SISO model was generated by subtracting the two rows of (4.17) and treating the resulting voltage difference and current summation as single measurements. As shown in (4.18), selection of these input-output relations results in the cancellation of the R and L terms. The bilinear transform was again employed to derive the equivalent difference equation presented in (4.20).

$$[i_S - i_R] = \frac{v_S - v_R}{R + \rho L} - \frac{v_S - v_R}{R + \rho L} + \frac{v_S}{1/(\rho C)} + \frac{v_R}{1/(\rho C)} = \rho C [v_S + v_R] \quad (4.18)$$

$$\frac{y}{u} = \frac{i_S - i_R}{v_S + v_R} = \rho C \quad (4.19)$$

$$y(k) + y(k-1) = C \left[\frac{2}{T} (u(k) - u(k-1)) \right] \quad (4.20)$$

Another SISO model can be examined by writing the equations as the difference between the voltage terms (or sum of the currents) as shown in (4.21). While the R and L parameters are contained in the model, evaluation of (4.21) indicates they cannot be directly estimated.

$$\frac{y}{u} = \frac{v_S - v_R}{i_S + i_R} = \frac{R + \rho L}{LC\rho^2 + RC\rho + 2} \quad (4.21)$$

Utilizing the same process used previously to derive the simplified regression model, the regressor model for this SISO model is given in (4.22) and (4.23).

$$y(k) = \begin{bmatrix} \frac{R}{\alpha} & \frac{L}{\alpha} & \frac{1}{\alpha} & \frac{LC}{\alpha} & \frac{RC}{\alpha} \end{bmatrix} \begin{bmatrix} T^2 * \{u(k) + 2u(k-1) + u(k-2)\} \\ T * \{2u(k) - 2u(k-2)\} \\ T^2 \{-4y(k-1) - 2y(k-2)\} \\ 8y(k-1) - 4y(k-2) \\ T * \{2y(k-2)\} \end{bmatrix} \quad (4.22)$$

$$\alpha = 4LC + 2RC + 2T^2 \quad (4.23)$$

In this model, five parameters must be estimated before the three physical quantities can be approximated, but the consequences of the reparameterization are more severe than just increasing the required excitation. That is to say, if the excitation is ever insufficient to determine the third parameter ($1/\alpha$) all the physics-based parameter approximations will be inaccurate. Clearly, this interdependence is unacceptable. The limitations of this model highlight the benefits of selecting a model that permits the physics-based parameters to be directly estimated. Other input-output combinations were investigated but with similar shortcomings.

4.2.2. MISO MODEL

While a MIMO model could be derived from (4.17), the resulting model would not permit direct estimation of R or L . The transfer function relationships in (4.17) are therefore examined as individual MISO models. One possible MISO model is presented in (4.24) which defines relationship between the terminal voltages and sending end current injection shown in Figure 4-4.

$$i_s = \left(\frac{1}{R + \rho L} + \rho C \right) v_s + \left(\frac{-1}{R + \rho L} \right) v_R \quad (4.24)$$

Selecting $y = v_R$, $u_1 = v_s$, and $u_2 = i_s$, the corresponding difference equation is expressed in (4.25). The regressors for the model, (4.26) through (4.29), are expressed in terms of the input-output observations and the reparameterized coefficients are expressed in terms of the physical parameters as shown in (4.30). The receiving end voltage was selected as the

dependent variable, as it provided the least amount of reparameterization of the estimated coefficients. Reparameterization of the coefficients was unavoidable, however, and results in a model requiring a minimum 4th order excitation. While the excitation requirement appears large at first, other forms of the model can be shown to require no less than 5th order excitation.

$$\begin{aligned} & y(k) + 2y(k-1) + y(k-2) - u_1(k) - 2u_1(k-1) - u_1(k-2) \\ & = [D_1 \ D_2 \ D_3 \ D_4] * [\varphi_1(k) \ \varphi_2(k) \ \varphi_3(k) \ \varphi_4(k)]^T \end{aligned} \quad (4.25)$$

$$\varphi_1(k) = \frac{4}{T^2} u_1(k) - \frac{8}{T^2} u_1(k-1) + \frac{4}{T^2} u_1(k-2) \quad (4.26)$$

$$\varphi_2(k) = \frac{2}{T} u_1(k) - \frac{2}{T} u_1(k-2) \quad (4.27)$$

$$\varphi_3(k) = -u_2(k) - 2u_2(k-1) - u_2(k-2) \quad (4.28)$$

$$\varphi_4(k) = -\frac{2}{T} u_2(k) + \frac{2}{T} u_2(k-2) \quad (4.29)$$

$$D_1 = LC \quad D_2 = RC \quad D_3 = R \quad D_4 = L \quad (4.30)$$

The unavoidable reparameterization of the physics-based parameters is not without repercussions. Most importantly, the physical relationships designated in (4.30) are not enforced. As a result, the capacitance is unidentifiable. While a secondary calculation can be performed to approximate C , the accuracy of the approximation depends on the accuracy of the individual parameter estimates. Additionally, there are two potential

approximations of C each requiring separate statistical evaluation. Therefore, the estimates for the RC and LC parameters were treated as the final results required by the proposed monitoring method. Rewriting (4.17) so that the MISO models use the two current measurements results in similar reparameterization issues except, in this case, the resistance and inductance will be unidentifiable.

As the algebraic relationships between the estimated coefficients are known, not enforcing these relationships could be viewed as not taking advantage of all the available information. Constraints could possibly be introduced to enforce the known physical relationships. However, the resulting constraints are nonlinear and would require a nonlinear optimization method.

4.2.3. SISO/MISO MODEL

The number of parameters in (4.25) can be reduced further when voltage and current measurements at both ends of the line are available. In these cases, (4.20) is used to first update the estimate of C which is subsequently used in (4.25) to reduce the unknowns to R and L . The updated MISO model is provided in (4.31) through (4.33) with the most recent update of C shown in the regressors. Given its dependence, the MISO portion of the model requires an accurate estimation of C . In most cases the actual shunt capacitance is relatively small compared to other parameters. As long as the error variance associated with the estimate of C is not too great, its influence on the other estimates should be minimal. If the shunt capacitance is negligible, (4.31) can be shown to be equivalent to the short transmission line model of (4.13).

$$\begin{aligned}
& y(k) + 2y(k-1) + y(k-2) - u_1(k) - 2u_1(k-1) - u_1(k-2) \\
& = [R \ L]^* [\varphi_1(k) \ \varphi_2(k)]^T
\end{aligned} \tag{4.31}$$

$$\begin{aligned}
\varphi_1(k) = C(k) * \left\{ \frac{2}{T} u_1(k) - \frac{2}{T} u_1(k-2) \right\} \\
- u_2(k) - 2u_2(k-1) - u_2(k-2)
\end{aligned} \tag{4.32}$$

$$\begin{aligned}
\varphi_2(k) = C(k) * \left\{ \frac{4}{T^2} u_1(k) - \frac{8}{T^2} u_1(k-1) + \frac{4}{T^2} u_1(k-2) \right\} \\
- \frac{2}{T} u_2(k) + \frac{2}{T} u_2(k-2)
\end{aligned} \tag{4.33}$$

Not only does this two-tier method directly estimate the physics-based parameters, it also reduces the minimum excitation to 2nd order. Therefore if both voltages and currents are available, the parameters can be estimated given only the fundamental frequency. However, when one of the currents is unavailable, the loss of information supplied from the measurement must be offset by doubling the minimum required excitation.

4.2.4. SHUNT CONDUCTANCE

Shunt conductance can be included in the nominal pi circuit model if leakage currents through the dielectric material are expected, or if it is a key measure of the cable's health. Inclusion of this parameter does not significantly influence the general form of the models previously developed. However, it does introduce an additional parameter which increases the excitation requirement in some models. For instance, the SISO model difference equation is easily updated to include the shunt conductance as

shown in (4.34). Comparison with (4.20) shows that the only significant change is an increase of the required persistence of excitation to 2nd order.

$$y(k) + y(k-1) = G[(u(k) + u(k-1))] + C \left[\frac{2}{T} (u(k) - u(k-1)) \right] \quad (4.34)$$

Similarly, the MISO model can be updated to include the shunt conductance. However, this update does not alter the regressor portion of the model. Therefore, equations (4.25) through (4.29) will remain the same. However, the redefined parameters are now given by (4.35). Note that an accurate approximation of the shunt conductance using this model not only relies on an accurate estimation of D_2 but the accuracy of the other three parameters as well.

$$D_1 = LC \quad D_2 = RC + GL \quad D_3 = R \quad D_4 = L \quad (4.35)$$

4.3. MODEL EVALUATIONS

In order to evaluate the estimation techniques and derived models, test data was generated in PSPICE using the single-phase two bus system shown in Figure 4-5. The nominal pi circuit model, connecting bus 1 and bus 2, represents one hundred feet of two conductor 14-AWG cable characterized by $R = 505 \text{ m}\Omega$, $L = 33.47 \text{ }\mu\text{H}$, and $C = 0.895 \text{ pF}$. The load is represented by a constant impedance and the source is modeled by a 120 V 60 Hz voltage source with an internal impedance of $1 \text{ }\Omega$. It should be noted that while the fundamental frequency was chosen as 60 Hz, other fundamental frequencies would provide the same order of excitation and therefore similar results. However, different

operating frequencies necessitate different sampling criteria and possibly model structures.

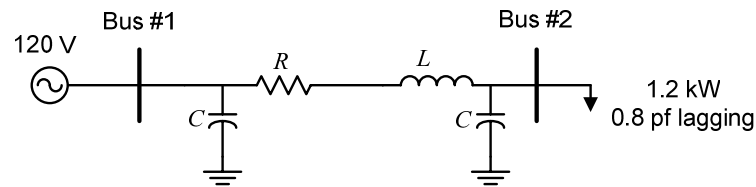


Figure 4-5. Single-Phase Test Circuit

Gaussian white noise with variance $\sigma^2 = 50 \times 10^{-6}$ was introduced into the recorded values to signify noise induced into the measurements before quantization. The values were then quantized based on equivalent 16-bit data acquisition (DAQ) hardware set to quantize the voltage and current on $[-200, 200]$ V and $[-20, 20]$ A ranges. While these factors were chosen arbitrarily, changes to either are expected to influence the estimates accordingly. It is recognized that steps to reduce both factors are key design criteria when implementing the monitoring method.

Finally, before it is used by the solution algorithm, the measurement data is per-unitized using the bases given in Table 4-1. The voltage, current, and time bases were chosen to provide relatively uniform regressors values, while the parameter bases were subsequently determined using the relationships defined in Table 3-2. While the voltage base was selected to match the rated fundamental voltage, the current base is not as easily selected given load variations. Therefore, a base of 10 A was heuristically selected to emphasize the regressors associated with the resistance and inductance parameters of the

MISO model. The selection was made based on experience which indicated that during low periods of excitation the R and L parameters show more signs of convergence than the RC and LC estimates. Finally, the time base was selected to counter the radian frequency scaling which occurs in the derivative terms. While the per-unit base values were chosen based on the expected content in the fundamental frequency, varying loading conditions, harmonics, and other system conditions will all influence the size of the parameter space spanned by the regressors. Therefore, selection of the base values must be done on an ad-hoc basis. Dynamic adjustments of the bases can be implemented by the monitoring controller, but would require re-initializing the estimation algorithm.

Table 4-1. Test System Per-Unit Bases

Base	Units
V_{base}	120 (V)
I_{base}	10 (A)
t_{base}	2.653 (ms)
S_{base}	120 (VA)
R_{base}	120 (Ω)
L_{base}	318.3 (mH)
C_{base}	22.10 (μF)

In each of the following cases, the sampling period was fixed at $T = 100 \mu\text{s}$ and a forgetting factor of $\lambda = 0.99$ were specified in the MATLAB code implementing the parameter estimation techniques. Additionally, the unknown parameter vector $\tilde{\theta}$ was set to zero and the diagonals in \mathbf{P} set to large values (1×10^4) to indicate little confidence in the initial values in $\tilde{\theta}$. The SISO/MISO model combination was examined first to

illustrate the influence of measurement noise and λ . As the normal operation of the test system was sufficient to meet the model's excitation requirements, RLS with standard exponential forgetting was used.

In order to evaluate the performance of the proposed method during abrupt changes in the observations, a significant step change in the load was examined. The observed voltage and current waveforms, during the load change, are illustrated in Figure 4-6. As shown in Figure 4-7, the parameter estimates, using (4.20) and (4.31), quickly converge to the true solutions, indicated by the dashed lines, but are not significantly influenced by the load change. As the network change did not represent a change to the modeled parameters, the extra excitation slightly improves the estimates.

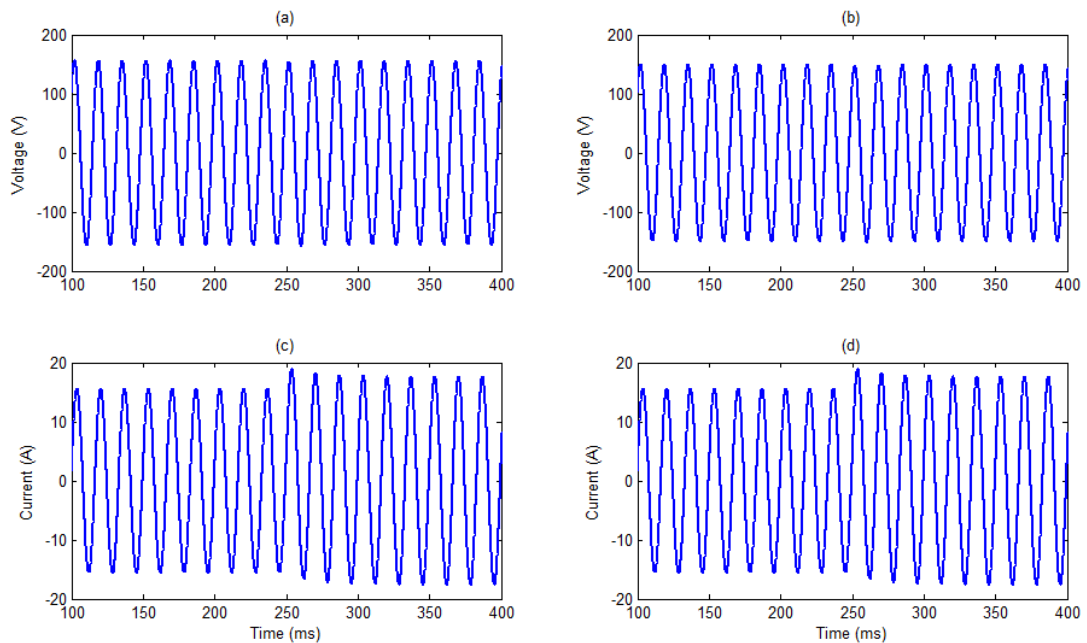


Figure 4-6. Test Case Voltages and Currents
(a) Sending End and (b) Receiving End

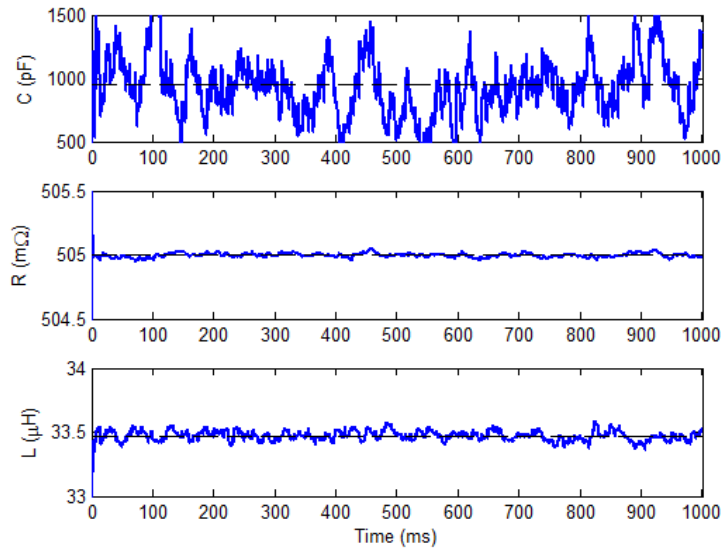


Figure 4-7. SISO/MISO Model Parameter Estimates during a Load Change.

As previously noted, parameter estimate accuracy is dependent on the measurement noise. To illustrate the sensitivity, the test was performed again but with a 32-bit quantization. The lower quantization error decreased the variance in each parameter estimate as shown in Figure 4-8. However, the capacitance estimation is especially sensitive to the noise given its dependence on the current differential between the line terminals. This current is small by nature (as is the capacitance) which can be easily overwhelmed by the noise contained in the two measurements. This is an inherent difficulty when estimating the capacitance in general indicating the level of accuracy required.

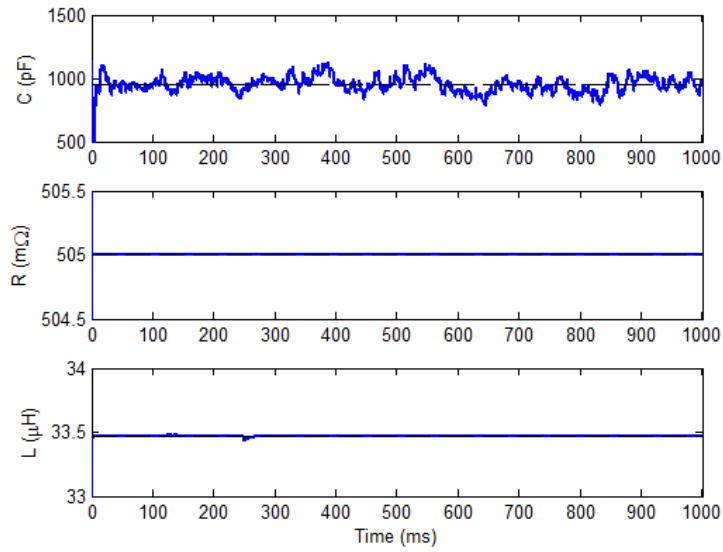


Figure 4-8. Parameter Estimates with 32-Bit Quantization Error.

The sensitivity to measurement errors is also influenced by the equivalent memory size determined by the forgetting factor. When the forgetting factor of the SISO model was increased to 0.999, representing an order of magnitude increase to the equivalent memory size, the variance was reduced significantly, as shown in Figure 4-9. As R and L are estimated by a model with the original setting for λ , their potential tracking ability was not altered but their variance was still reduced through their dependence on the estimate of C .

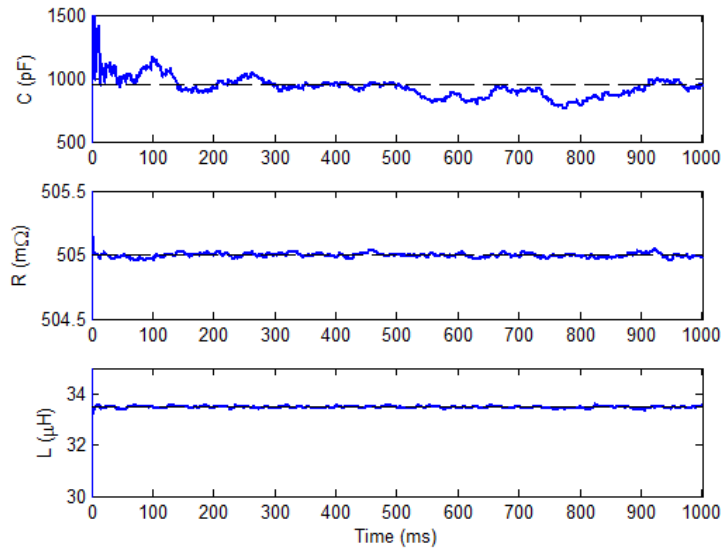


Figure 4-9. Parameter Estimates with 16-Bit Quantization Error and $\lambda_c = 0.999$.

The chosen algorithm must also be capable of tracking parameter changes. Still utilizing the SISO/MISO model combination, the resulting estimates for a step change in R are shown in Figure 4-10. The estimate of R exponentially converges to the new solution in approximately 50 ms, or five times the time constant associated. A similar step change in C was evaluated and the resulting estimations are given in Figure 4-11.

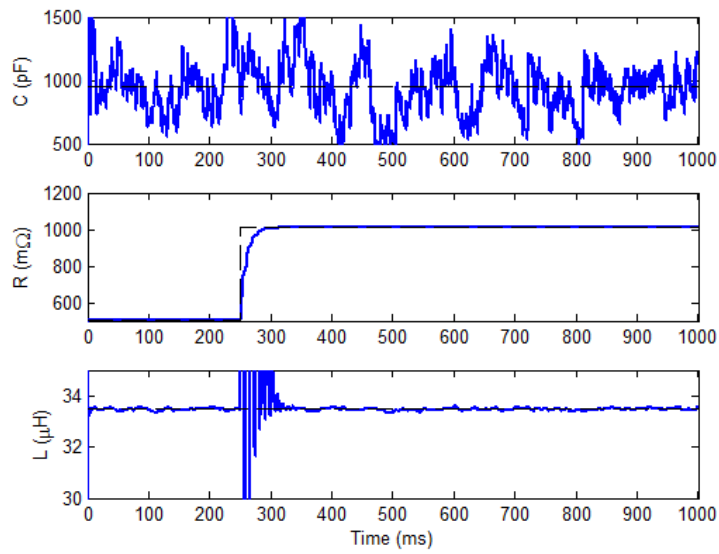


Figure 4-10. Parameter Estimates for Step Change in R .

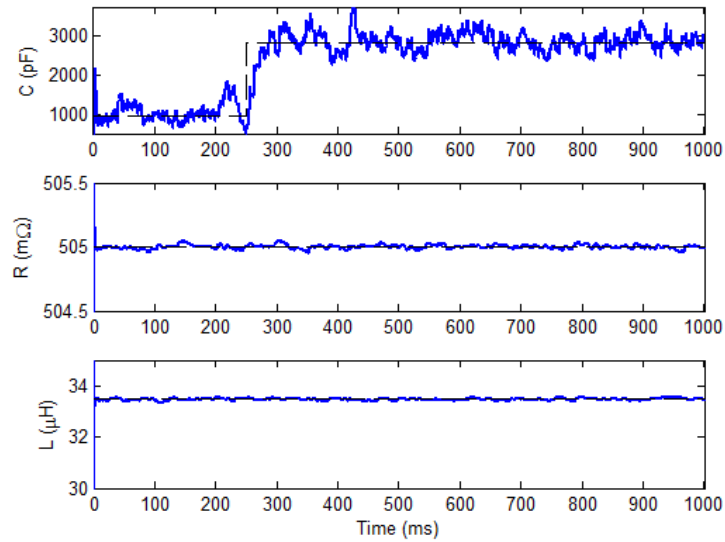


Figure 4-11. Parameter Estimates for Step Change in C .

Recursive parameter estimation using the MISO model is evaluated in the same manner as with the SISO/MISO evaluations. The model contains four parameters which increases the required excitation to a minimum 4th order. To stress the MISO model's increased identifiability requirements, the parameters were first estimated using RLS with standard exponential forgetting and the same load change used before. The estimated parameters are provided in Figure 4-12. Until the transient from the load change occurs, the 60Hz signal alone does not provide sufficient excitation for convergence of the estimates to occur. However during the transient, the excitation temporarily increases and the solution converges to the true values. Nonetheless, after the transient decays the exciting information is eventually discounted and the parameters drift from the converged solution. Note that both the mean and variance of the parameter estimates are affected.

The loss of information was also indicated by the 95% confidence margins or error shown in Figure 4-13. The values in Figure 4-13 represent the margin or error which contains the true solution with confidence level of 95%. During the transient, the confidence interval decreased significantly but increases once the information was discounted. The principle factors in the changing confidence intervals were similar trends in the covariance matrix diagonals. As P increased, the increased sensitivity to noise gave rise to increased estimate variance as seen in Figure 4-12. Given the lack of constant excitation in this scenario, some form of estimator windup prevention is clearly desirable.

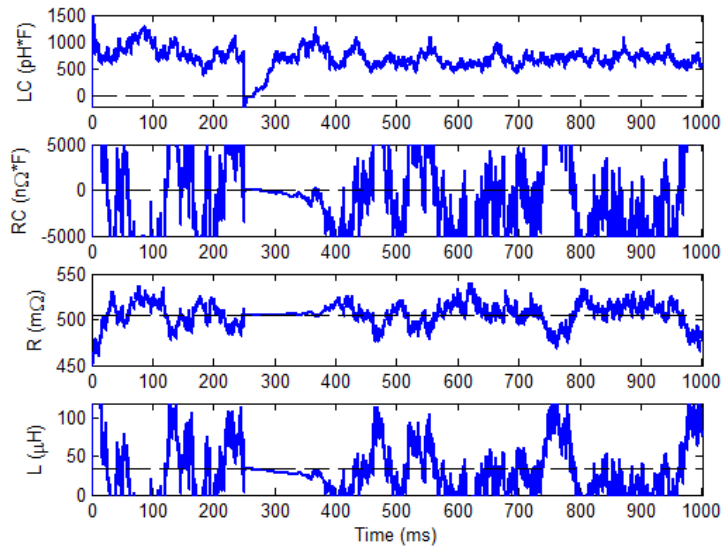


Figure 4-12. MIMO Model Parameter Estimates

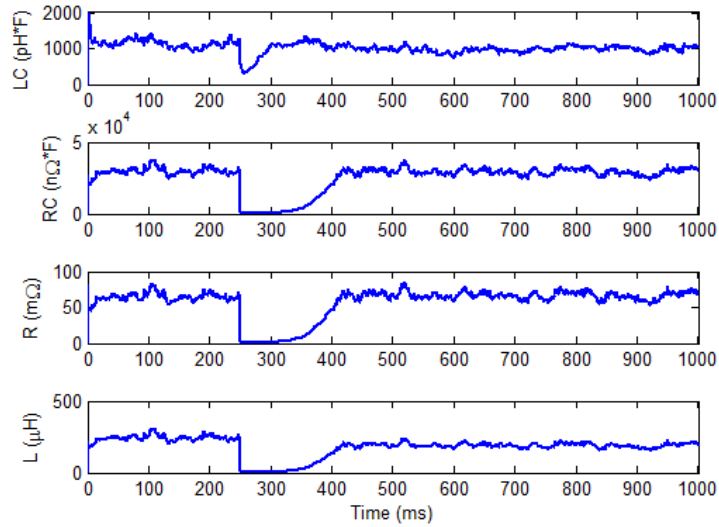


Figure 4-13. 95% Confidence Margins of Error

When RLS with directional forgetting is applied to the same data, Figure 4-14, the estimates initially converge in a similar fashion as before. However, the estimates retain their values once the transient fully decayed. Examination of Figure 4-15 indicates that these improvements are also reflected in the margins of error. The bias in the LC estimates for both the standard exponential as well as the directional forgetting evaluations is attributed to non-white noise in the residuals. The autocorrelation of the last five hundred prediction errors, shown in Figure 4-16, falls outside of the 95% confidence intervals. Therefore, the white noise hypothesis is rejected with 95% confidence. During the creation of the test data, the ideal sampling and operation of the test system results in repeated errors which appear as correlated white noise in the residuals and prediction error. The lack of sufficient past information and the relatively small value of LC made these estimates more sensitive to the bias than the others.

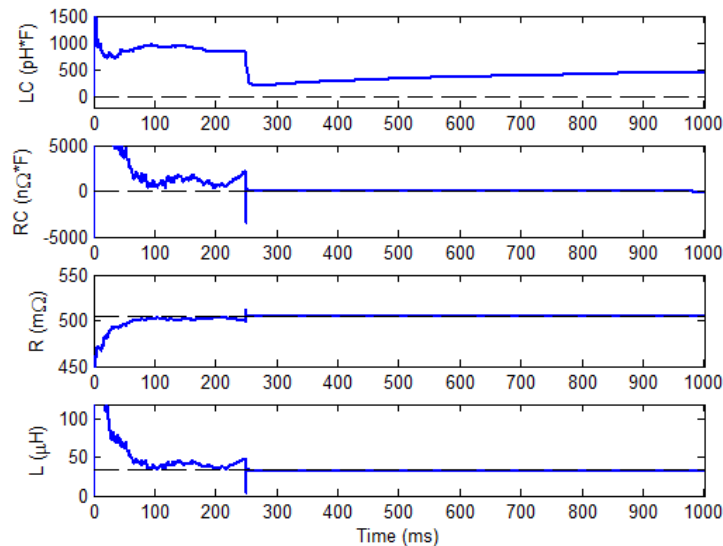


Figure 4-14. MISO Model Parameter Estimates using RLS/DF

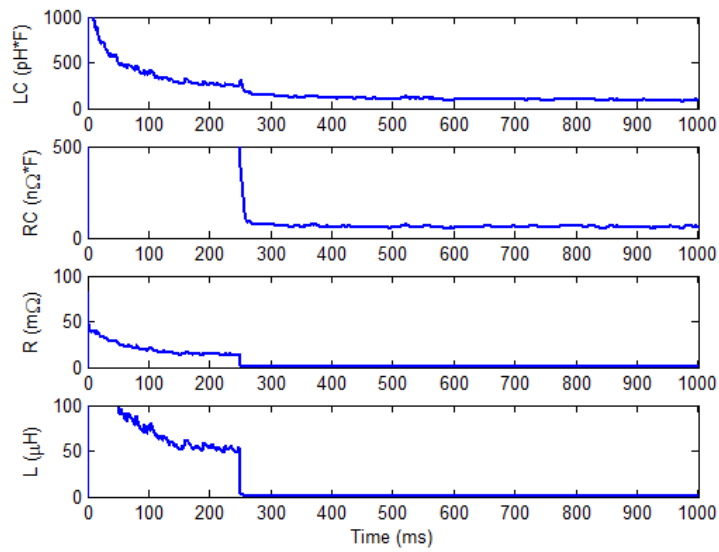


Figure 4-15. 95% Confidence Margins of Error

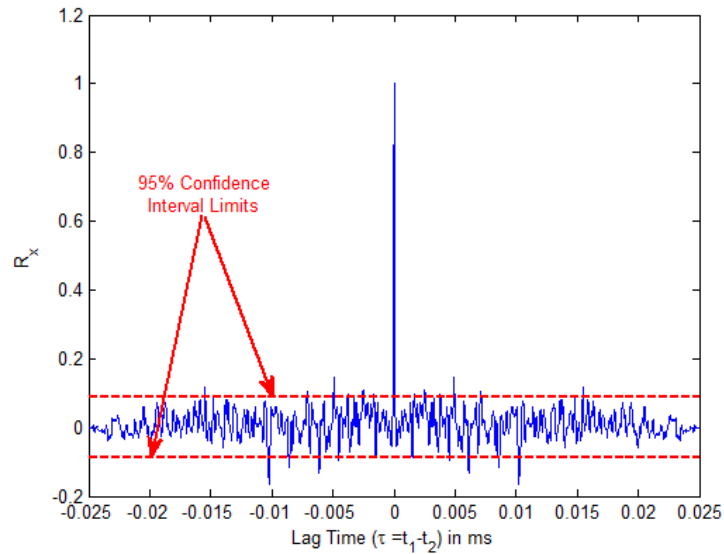


Figure 4-16. Prediction Error Autocorrelation

The information contained in the switching transient increases the excitation of the dynamics well beyond the 4th order excitation required by the MISO model. In order to show that accurate parameter estimates can be made given the minimum required excitation, the next example used a 5th harmonic current injection to temporarily increase the excitation to 4th order. The harmonic is injected at the load starting at 250 ms and for a period of 500 ms. No other system or load changes occur during this time. Voltage and current waveforms before and after the start of the harmonic injection are shown in Figure 4-17 to illustrate the change in the measured waveforms. As shown in Figure 4-18, the RLS solution quickly converged during the harmonic injection due to the increased excitation. However, the estimates again drift once the additional excitation is removed. In contrast, the RLS with directional forgetting shows no signs of drifting estimates as seen in Figure 4-19. It is also interesting to note that information observed during the harmonic injection results in the estimate of LC being less sensitive to bias than in Figure 4-14.

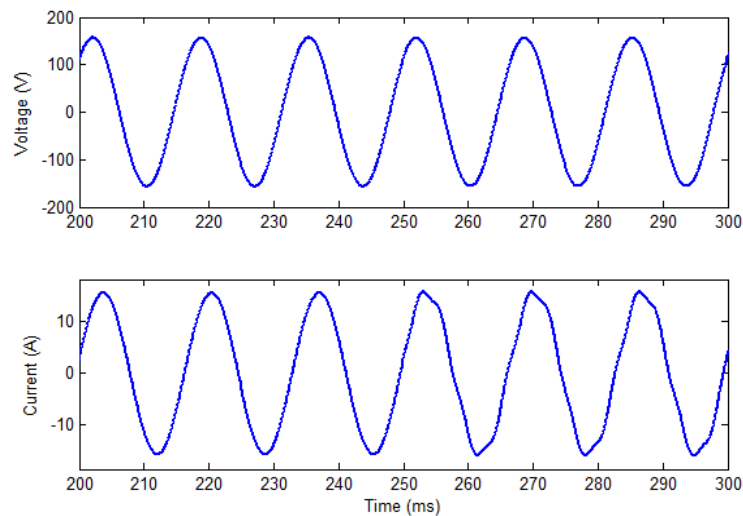


Figure 4-17. Sending End Voltage and Current Waveforms

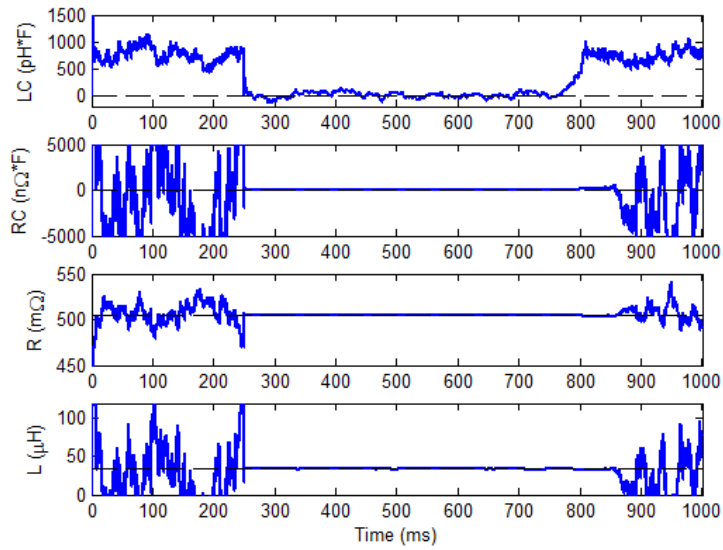


Figure 4-18. Parameter Estimates using RLS

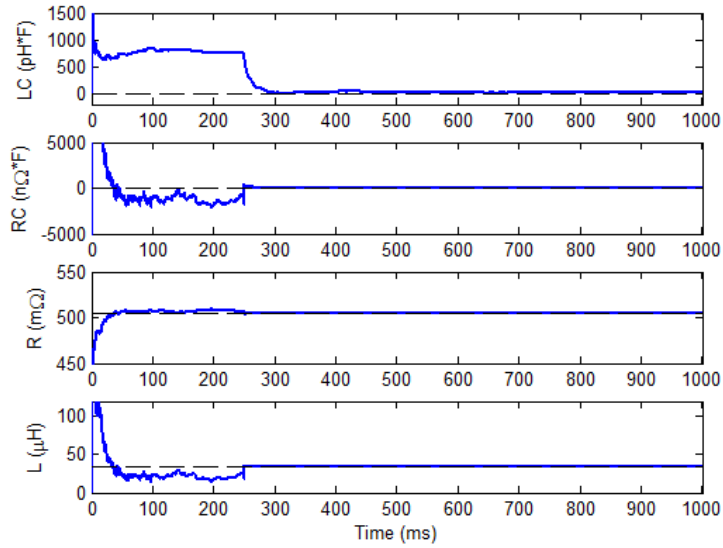


Figure 4-19. Parameter Estimates using RLS/DF

As past data is discounted by the directional forgetting method only as newer information becomes available, it is still capable of tracking parameter changes. The tracking response of the RLS/DF for a step change in resistance is illustrated in Figure 4-20. The order of excitation was increased to the required level by the injection of the 5th harmonic current over the duration of the observations. Note that the estimates were not governed by the forgetting time constant. Given that the directional forgetting method only discounts past data as newer data becomes available, slower tracking rates result when information concerning the parameter is not available in each sample. Additionally, even though the step change only occurred in R and RC , L and LC diverge from their converged solutions. However, the bias in the other estimates is reduced as R converges to the new solution. Additionally, the more information observed about an unknown parameter before an abrupt change, the smaller the deviations. This is demonstrated through the small deviations in L .

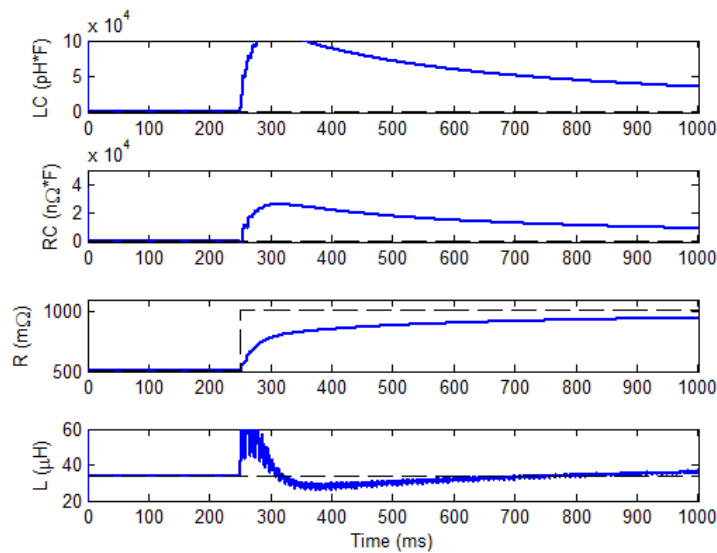


Figure 4-20. Parameter Estimates using RLS/DF

The parameter estimates using RLS with standard forgetting for the same dataset is provided in Figure 4-21. Note that similar deviations in the parameters estimated occurred using this method as well. Obviously, tracking the parameter changes using directional forgetting takes considerably longer when compared to the standard method of discounting. Nevertheless, in situations where the excitation is intermittent in nature the prevention of parameter drift greatly outweighs a faster tracking ability. Still, for certain applications it may be sufficient to estimate the parameters with RLS and then only retain estimates whose margins of error satisfy predetermined tolerances.

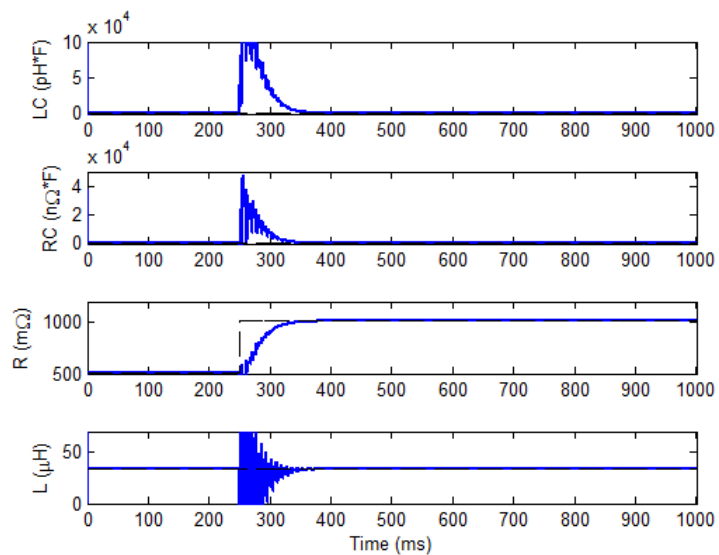


Figure 4-21. Parameter Estimates using RLS

The tracking response of the directional forgetting method to the abrupt change might be improved by varying λ in response to the prediction error. The results when variable directional forgetting, as discussed in section 3.2.2, was applied to the dataset are

shown in Figure 4-22. As λ is no longer constant it is also provided in Figure 4-22. As shown, dynamically altering the memory size allowed the solution to more quickly track the parameter changes. Notice the variance of L is also significantly larger than in Figure 4-20 due to the increased discounting of information relevant to this parameter.

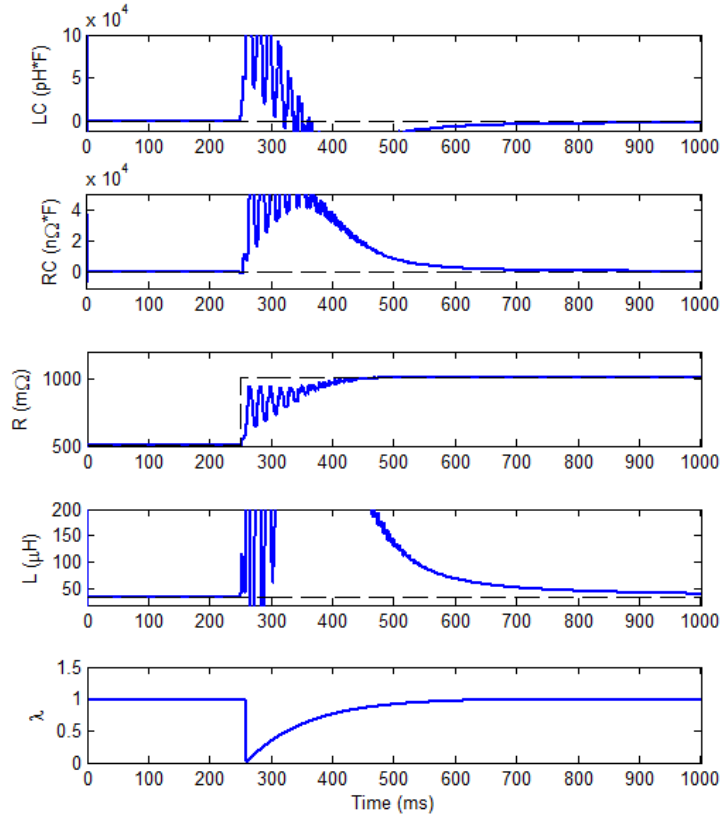


Figure 4-22. Parameter Estimates using RLS/VDF

Model selection should consider many factors such as the necessary parameters for accurate condition monitoring and the expected parameter magnitudes relative to the noise levels and/or measurement accuracy. The capacitance associated with short spans of wire is particularly difficult to estimate due to its relatively small value. This was seen

not only in the SISO/MISO model combination, but also in the MISO results which indicate the estimates of RC and LC are far from ideal.

If the estimation of a particular parameter is unnecessary, or unfeasible, one option is to reduce the model order by discarding the parameter. Removing the variable from the model not only reduces the required level of excitation but also reduces variance in the parameter estimates due to parsimony. On the other hand, this does not mean that just any parameter can be removed from the model without consequence. In fact, any unmodeled content will end up in the residuals of the least-squares solution violating the assumption that the residuals consist of white noise. The non-white signals in the residuals will in turn result in biased parameter estimates as well as inaccurate variance estimates.

Multiple models could be estimated in parallel if different models are expected to offer better estimations during varying conditions. A comparison of the 95% confidence intervals for three model types is given in Table 4-2; the SISO/MISO model combination, the MISO model alone, and the short transmission line model (RL). Each model's parameters were estimated using one second of data containing the fundamental and 5th harmonic waveforms. While the results in Table 4-2 are not meant to be statistically conclusive, the results do support earlier conclusions. For example, the SISO model (which has the benefit of the additional information from the 2nd current measurement) provides the most accurate means to estimate the capacitance. Obviously the wide variances associated with the estimates of RC and LC will result in a low level of confidence if either is used to approximate C . Moreover, the confidence intervals for both RC and LC cross zero which indicates that these parameters can potentially be removed

from the model. Another interpretation would be that the margin of error is larger than the estimate itself. Actually, the margins of error for these parameters are nearly twice the estimates. Consequently, very little if any bias is present when the capacitance terms are removed as seen by the results for the short transmission line model (RL) model. However, the estimates of RC and LC are not without merit as the capacitance could increase over time to a level where its dynamic contributions were no longer negligible. If this were the case, it would be very important to have the capacitance modeled as not to introduce bias into the estimations. Including the capacitance did not show signs of significantly increasing the other parameter variances.

Table 4-2. 95% Univariate Confidence Intervals

	R (mΩ)		L (μH)		C (nF)		RC (nΩF)		LC (pHF)	
	Low	High	Low	High	Low	High	Low	High	Low	High
SISO/MISO	504.99	505.01	33.47	33.48	0.790	1.085	NA	NA	NA	NA
MISO	504.90	505.00	33.42	33.59	NA	NA	-5.983	13.320	-11.84	39.32
RL	504.94	505.03	33.40	33.63	NA	NA	NA	NA	NA	NA

The techniques are also applicable to DC networks. While constant DC values only provide a 1st order excitation, i.e. sufficient excitation to estimate the line resistance, transient events increase the excitation to sufficient levels to estimate other model parameters. If we assume that these events will not occur with any predictable regularity, directional forgetting should provide better estimates than standard directional forgetting. In order to examine how well the directional forgetting algorithm handles periods of low

excitation between short bursts of high excitation, a case consisting of a periodically switched RL load connected to a 24 V DC system is evaluated. The observed voltage and currents at both ends of the line are presented in Figure 4-23 and the same example line of the previous simulations is assumed to connect the load to the 24 V source. During the estimations, base values of $V_{\text{base}} = 24$ V, $I_{\text{base}} = 10$ A, and $T_{\text{base}} = 10$ μs were used to normalize the measurements. The values were again heuristically chosen in an attempt to provide regressors whose magnitudes would be within the same general range.

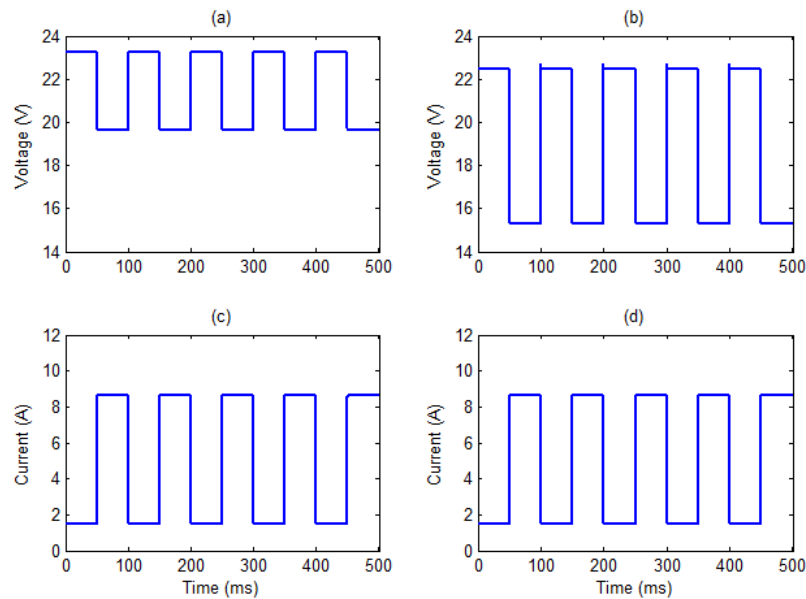


Figure 4-23. DC Signals for a Switching DC Load
(a) Sending End and (b) Receiving End

For this example, the sampling period was increased to 10 μs in order to better observe the faster dynamics of the transient while the forgetting factor was left at $\lambda = 0.99$. While the switching transients increase the excitation, they also contain frequencies

higher than the Nyquist frequency. For that reason, anti-aliasing filters were introduced during the generation of the test data. Identical second order low-pass filters with 5 kHz cutoff frequencies were used as the anti-aliasing filters for each measurement. The high sampling frequency also results in five thousand samples being observed between each switching transient. Even though the transients occur at fixed intervals, the resulting excitation can still be considered intermittent in nature.

The parameter estimations for the short transmission line model using the RLS/DF algorithm are given in Figure 4-24. As expected, during the steady-state periods only information concerning the resistance is available and this parameter quickly converges to its “true” value. However, during the transient periods the dynamics associated with the inductor are excited and the estimate begins to approach a converged solution. While the switching transients in the example are equally spaced this is not a requirement as the directional forgetting algorithm clearly shows no signs of estimate drift during the low excitation periods.

In contrast, the solution using standard discounting, as shown in Figure 4-25, clearly drifts during each period of low excitation. The estimates using directional forgetting also show indications of improving over time. This improvement can be attributed to the retention of the relevant information during each event whereas the standard method steadily discounts information as time progresses. For instance, based on the time constant approximation of (3.35) and the selected forgetting factor, the information gained during the transient is completely discounted after 500 samples. Given that there is an order of magnitude more samples between the transients, there is ample time for the

information to be completely discounted before the next transient. Although it is not shown in Figure 4-25, the loss of information is reflected in the estimates as they eventually drift back to zero in between switching transients.

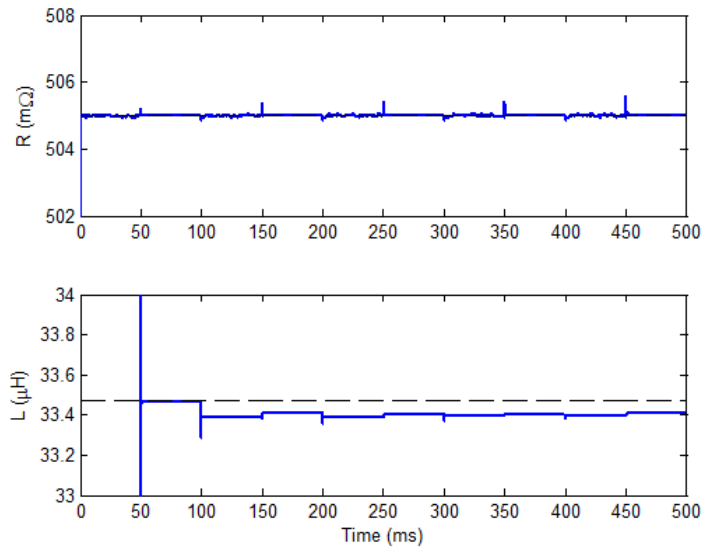


Figure 4-24. Parameter Estimates using RLS/DF

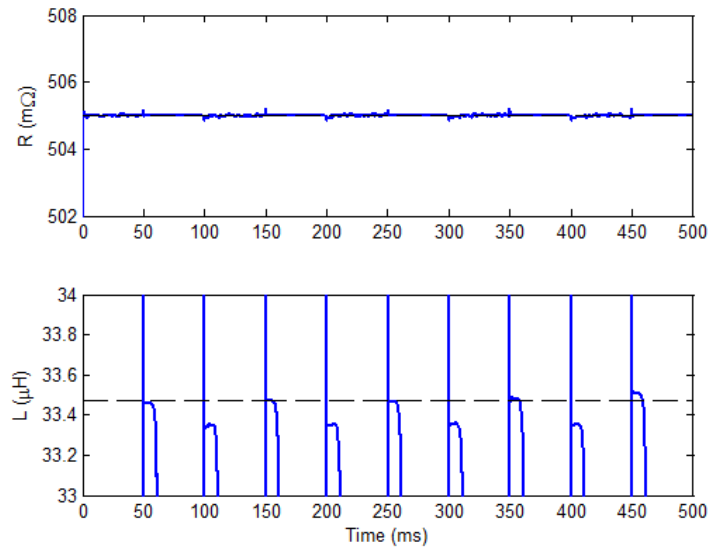


Figure 4-25. Parameter Estimates using RLS

4.4. SUMMARY

In cases where the excitation is intermittently sufficient, directional forgetting is clearly a better alternative to standard exponential discounting. The method has been shown to provide accurate solutions of two-conductor wiring physical-based parameters under intermittent conditions while retaining the ability to track parameter changes. Accuracy of the physically-based parameter estimates was also shown to be dependent upon the measurement type, measurement noise, as well as the model formulation. The level of accuracy was gauged by recursively calculated margins of error which are not only easily calculated but necessary to interface the estimates with stochastic prognosis techniques. The same techniques as applied to multiple conductor models are examined in the next chapter. While the multiple conductor models are innately more complex, the conclusions derived in this chapter concerning the effectiveness of the parameter estimation techniques still hold true.

CHAPTER 5

MULTIPLE CONDUCTOR MODELS

In this chapter the identifiability requirements of multiple conductor network elements are examined. The presented models are based on general assumptions concerning conductor characteristics and the availability of time-domain measurements. Due to the additional interactions that exist between conductors in close proximity, the models and identifiability requirements in this chapter represent an increased complexity compared to the models of the previous chapter. The identifiability requirements are examined under the assumption of intermittent excitation, as the identifiability requirements are intended to facilitate the monitoring method described in Chapter 1.

Lines with more than two conductors can be approached in a similar fashion as two-conductor lines except for the obvious increase to the number of required measurements and unknown parameters. A multiple conductor model including mutual coupling and capacitance between conductors 1 through n is shown in Figure 5-1. It is assumed that the n^{th} conductor models the return path, whether it is a neutral conductor, shield, vehicle hull, or combination of the three. Given voltage measurements at both ends of the conductors and currents at only one side, the relationships between the measured values and the unknown parameters values can be described by (5.1) and (5.2). In the matrix of

(5.1) the diagonals represent the total capacitance connected to the node (i.e., $C_{11} = C_{12} + C_{1n} + \dots$, $C_{22} = C_{12} + C_{2n} + \dots$, etc.). However, measurement using the equipotential reference depicted in Figure 5-1 is not practical in many applications. It is also beneficial to reduce the number of unknown parameters by lumping the neutral's parameters in with the other conductors.

$$\begin{bmatrix} i_1^* \\ i_2^* \\ \vdots \\ i_n^* \end{bmatrix} = \begin{bmatrix} i_{1,1} \\ i_{2,1} \\ \vdots \\ i_{n,1} \end{bmatrix} - \begin{bmatrix} C_{11} & -C_{12} & \cdots & -C_{1n} \\ -C_{12} & C_{22} & & -C_{2n} \\ \vdots & & \ddots & \\ -C_{1n} & -C_{2n} & & C_{nn} \end{bmatrix} \frac{d}{dt} \begin{bmatrix} v_{1,1} \\ v_{2,1} \\ \vdots \\ v_{n,1} \end{bmatrix} \quad (5.1)$$

$$\begin{bmatrix} v_{1,1} - v_{1,2} \\ v_{2,1} - v_{2,2} \\ \vdots \\ v_{n,1} - v_{n,2} \end{bmatrix} = \begin{bmatrix} R_{11} & & & \\ & R_{22} & & \\ & & \ddots & \\ & & & R_{nn} \end{bmatrix} \begin{bmatrix} i_1^* \\ i_2^* \\ \vdots \\ i_n^* \end{bmatrix} + \begin{bmatrix} L_{11} & L_{12} & \cdots & L_{1n} \\ L_{12} & L_{22} & & L_{2n} \\ \vdots & & \ddots & \vdots \\ L_{1n} & L_{2n} & \cdots & L_{nn} \end{bmatrix} \frac{d}{dt} \begin{bmatrix} i_1^* \\ i_2^* \\ \vdots \\ i_n^* \end{bmatrix} \quad (5.2)$$

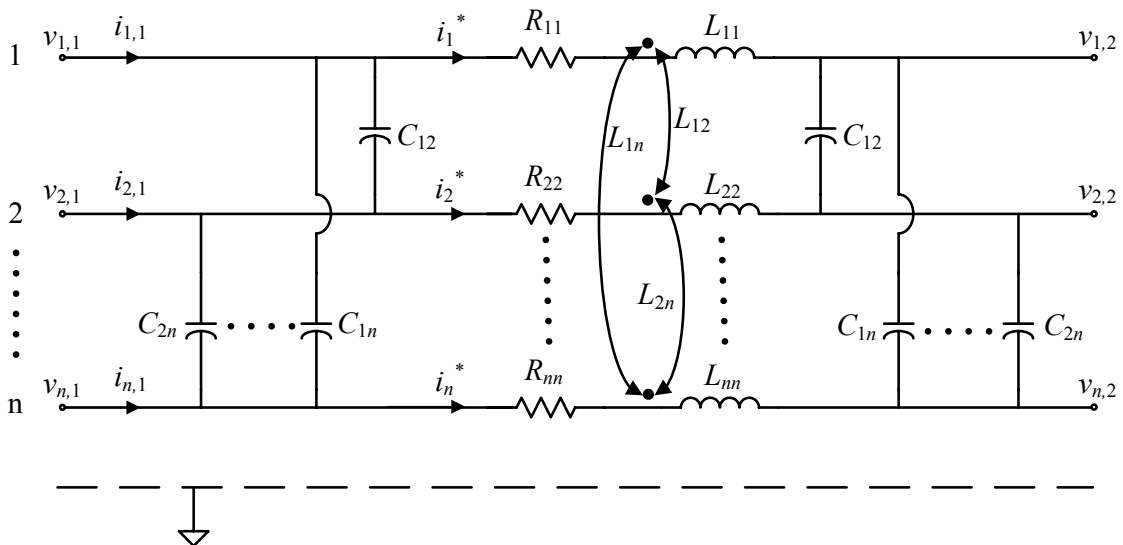


Figure 5-1. Multiple Conductor Line Model

By subtracting the last equation in (5.2) from the rest of the rows, the voltages are redefined as between the individual phases and the neutral, as shown in (5.3), eliminating the need for the equipotential plane shown in Figure 5-1.

$$\begin{bmatrix} v_{1n,1} - v_{1n,2} \\ v_{2n,1} - v_{2n,2} \\ \vdots \\ 0 \end{bmatrix} = \begin{bmatrix} R_{11} & & & \\ & R_{22} & & \\ & & \ddots & \\ 0 & 0 & \cdots & 0 \end{bmatrix} \begin{bmatrix} i_1^* \\ i_2^* \\ \vdots \\ i_n^* \end{bmatrix} + \begin{bmatrix} L_{11} - L_{1n} & L_{12} - L_{2n} & \cdots & L_{1n} - L_{nn} \\ L_{12} - L_{1n} & L_{22} - L_{2n} & & L_{2n} - L_{nn} \\ \vdots & & \ddots & \vdots \\ 0 & 0 & \cdots & 0 \end{bmatrix} \frac{d}{dt} \begin{bmatrix} i_1^* \\ i_2^* \\ \vdots \\ i_n^* \end{bmatrix} \quad (5.3)$$

Kirchhoff's current law states that at every instant in time the sum of the currents across any cut-set equals zero. Hence, the currents (and their derivatives) sum to zero and the bottom row of (5.4) can be set to one.

$$\begin{bmatrix} v_{1n,1} - v_{1n,2} \\ v_{2n,1} - v_{2n,2} \\ \vdots \\ 0 \end{bmatrix} = \begin{bmatrix} R_{11} & & & \\ & R_{22} & & \\ & & \ddots & \\ 1 & 1 & \cdots & 1 \end{bmatrix} \begin{bmatrix} i_1^* \\ i_2^* \\ \vdots \\ i_n^* \end{bmatrix} + \begin{bmatrix} L_{11} - L_{1n} & L_{12} - L_{2n} & \cdots & L_{1n} - L_{nn} \\ L_{12} - L_{1n} & L_{22} - L_{2n} & & L_{2n} - L_{nn} \\ \vdots & & \ddots & \vdots \\ 1 & 1 & \cdots & 1 \end{bmatrix} \frac{d}{dt} \begin{bmatrix} i_1^* \\ i_2^* \\ \vdots \\ i_n^* \end{bmatrix} \quad (5.4)$$

Finally, through matrix and vector manipulations, it can be shown that (5.4) reduces to (5.5).

$$\begin{bmatrix} v_{1n,1} - v_{1n,2} \\ v_{2n,1} - v_{2n,2} \\ \vdots \\ v_{Nn,1} - v_{Nn,2} \end{bmatrix} = \begin{bmatrix} R_{11} + R_{nn} & R_{nn} & \cdots & R_{nn} \\ R_{nn} & R_{22} + R_{nn} & & R_{nn} \\ \vdots & & \ddots & \vdots \\ R_{nn} & R_{nn} & \cdots & R_{NN} + R_{nn} \end{bmatrix} \begin{bmatrix} i_1^* \\ i_2^* \\ \vdots \\ i_N^* \end{bmatrix} + \begin{bmatrix} L_{11} + L_{nn} - 2L_{1n} & L_{12} + L_{nn} - L_{1n} - L_{2n} & \cdots & L_{1N} + L_{nn} - L_{1n} - L_{Nn} \\ L_{12} + L_{nn} - L_{1n} - L_{2n} & L_{22} + L_{nn} - 2L_{2n} & & L_{2N} + L_{nn} - L_{2n} - L_{Nn} \\ \vdots & \vdots & \ddots & \vdots \\ L_{1N} + L_{nn} - L_{1n} - L_{Nn} & L_{2N} + L_{nn} - L_{2n} - L_{Nn} & \cdots & L_{NN} + L_{nn} - 2L_{Nn} \end{bmatrix} \frac{d}{dt} \begin{bmatrix} i_1^* \\ i_2^* \\ \vdots \\ i_N^* \end{bmatrix} \quad (5.5)$$

As shown in (5.6), the inductances can be defined by equivalent lumped values and alphabetical subscripts introduced in order to simplify the notation. The neutral's resistance, R_{nn} , is also factored out from the matrix of resistances to reduce the number of unknown parameters.

$$\begin{aligned}
 \begin{bmatrix} v_{an,1} - v_{an,2} \\ v_{bn,1} - v_{bn,2} \\ \vdots \\ v_{Nn,1} - v_{Nn,2} \end{bmatrix} &= \begin{bmatrix} R_{aa} & 0 & \cdots & 0 \\ 0 & R_{bb} & & 0 \\ \vdots & & \ddots & \vdots \\ 0 & 0 & \cdots & R_{NN} \end{bmatrix} \begin{bmatrix} i_a^* \\ i_b^* \\ \vdots \\ i_N^* \end{bmatrix} + R_{nn} \begin{bmatrix} 1 & 1 & \cdots & 1 \\ 1 & 1 & & 1 \\ \vdots & & \ddots & \vdots \\ 1 & 1 & \cdots & 1 \end{bmatrix} \begin{bmatrix} i_a^* \\ i_b^* \\ \vdots \\ i_N^* \end{bmatrix} \\
 &+ \begin{bmatrix} L_{aa} & L_{ab} & \cdots & L_{aN} \\ L_{ab} & L_{bb} & & L_{bN} \\ \vdots & & \ddots & \vdots \\ L_{aN} & L_{bN} & \cdots & L_{NN} \end{bmatrix} \frac{d}{dt} \begin{bmatrix} i_a^* \\ i_b^* \\ \vdots \\ i_N^* \end{bmatrix}
 \end{aligned} \tag{5.6}$$

Recognizing the neutral as the new reference, (5.1) can be restated in the form shown in (5.7). In (5.7), the matrix diagonals still represent the total capacitance connected to that node (i.e. $C_{aa}=C_{ab}+C_{an}+\dots$). Finally, if desired, an additional equation relating the current outputs could be found as provided in (5.8).

$$\begin{bmatrix} i_a^* \\ i_b^* \\ \vdots \\ i_N^* \end{bmatrix} = \begin{bmatrix} i_{a,1} \\ i_{b,1} \\ \vdots \\ i_{N,1} \end{bmatrix} - \begin{bmatrix} C_{aa} & -C_{ab} & \cdots & -C_{aN} \\ -C_{ab} & C_{bb} & & -C_{bN} \\ \vdots & & \ddots & \vdots \\ -C_{aN} & -C_{bN} & \cdots & C_{NN} \end{bmatrix} \frac{d}{dt} \begin{bmatrix} v_{an,1} \\ v_{bn,1} \\ \vdots \\ v_{Nn,1} \end{bmatrix} \tag{5.7}$$

$$\begin{bmatrix} i_{a,2} \\ i_{b,2} \\ \vdots \\ i_{N,2} \end{bmatrix} = \begin{bmatrix} i_a^* \\ i_b^* \\ \vdots \\ i_N^* \end{bmatrix} - \begin{bmatrix} C_{aa} & -C_{ab} & \cdots & -C_{aN} \\ -C_{ab} & C_{bb} & & -C_{bN} \\ \vdots & & \ddots & \vdots \\ -C_{aN} & -C_{bN} & \cdots & C_{NN} \end{bmatrix} \frac{d}{dt} \begin{bmatrix} v_{an,2} \\ v_{bn,2} \\ \vdots \\ v_{Nn,2} \end{bmatrix} \quad (5.8)$$

Substituting (5.7) into (5.6) and collecting like regressors, the linear regression model for the multiple conductor line can be written as (5.9).

$$\begin{aligned} \begin{bmatrix} v_{an,1} - v_{an,2} \\ v_{bn,1} - v_{bn,2} \\ \vdots \\ v_{Nn,1} - v_{Nn,2} \end{bmatrix} &= \begin{bmatrix} R_{aa} & 0 & \cdots & 0 \\ 0 & R_{bb} & & 0 \\ \vdots & & \ddots & \vdots \\ 0 & 0 & \cdots & R_{NN} \end{bmatrix} \begin{bmatrix} i_{a,1} \\ i_{b,1} \\ \vdots \\ i_{N,1} \end{bmatrix} + R_{nn} \begin{bmatrix} 1 & 1 & \cdots & 1 \\ 1 & 1 & & 1 \\ \vdots & & \ddots & \vdots \\ 1 & 1 & \cdots & 1 \end{bmatrix} \begin{bmatrix} i_{a,1} \\ i_{b,1} \\ \vdots \\ i_{N,1} \end{bmatrix} \\ &+ \begin{bmatrix} L_{aa} & L_{ab} & \cdots & L_{aN} \\ L_{ab} & L_{bb} & & L_{bN} \\ \vdots & & \ddots & \vdots \\ L_{aN} & L_{bN} & \cdots & L_{NN} \end{bmatrix} \frac{d}{dt} \begin{bmatrix} i_{a,1} \\ i_{b,1} \\ \vdots \\ i_{N,1} \end{bmatrix} \\ &+ \begin{bmatrix} R_{aa} + R_{nn} & R_{nn} & \cdots & R_{nn} \\ R_{nn} & R_{bb} + R_{nn} & & R_{nn} \\ \vdots & & \ddots & \vdots \\ R_{nn} & R_{nn} & \cdots & R_{NN} + R_{nn} \end{bmatrix} \frac{d}{dt} \begin{bmatrix} -C_{aa} & C_{ab} & \cdots & C_{aN} \\ C_{ab} & -C_{bb} & & C_{bN} \\ \vdots & & \ddots & \vdots \\ C_{aN} & C_{bN} & \cdots & -C_{NN} \end{bmatrix} \begin{bmatrix} v_{an,1} \\ v_{bn,1} \\ \vdots \\ v_{Nn,1} \end{bmatrix} \\ &+ \begin{bmatrix} L_{aa} & L_{ab} & \cdots & L_{aN} \\ L_{ab} & L_{bb} & & L_{bN} \\ \vdots & & \ddots & \vdots \\ L_{aN} & L_{bN} & \cdots & L_{NN} \end{bmatrix} \frac{d^2}{dt^2} \begin{bmatrix} v_{an,1} \\ v_{bn,1} \\ \vdots \\ v_{Nn,1} \end{bmatrix} \end{aligned} \quad (5.9)$$

As the number of conductors increase, so do the number of unknowns in each model. However, it can be shown that when modeling $N > 2$ conductors, equation (5.9) requires N less parameters than the line model of Figure 5-1.

The equivalent model for a four conductor cable is provided in Figure 5-2. Examining the equations individually, as done during the two-conductor model analyses, each phase can be evaluated using individual MISO models. Note that the individual

phase models each require the estimation of eleven parameters as shown in the a-phase conductor model provided in (5.10). To simplify (5.10), the number of dots above the regressor terms indicates that it is a 1st or 2nd order derivative. As with the two-conductor models, the capacitance cannot be directly identified and is instead accounted for by RC and LC parameters. Similar expressions to (5.10) can be derived for both b and c phases with the only common directly estimated parameters between the models being the neutral resistance and the mutual inductances. Additionally, the neutral current could be measured directly. While this constitutes an additional measurement requirement, it may reduce the variance resulting from summing the quantized currents.

$$\begin{bmatrix} v_{an,1} - v_{an,2} \end{bmatrix} = \begin{bmatrix} R_{aa} \\ R_{nn} \\ L_{aa} \\ L_{ab} \\ L_{ac} \\ R_{aa}C_{aa} + R_{nn}C_{an} \\ -R_{aa}C_{ab} + R_{nn}C_{bn} \\ -R_{aa}C_{ac} + R_{nn}C_{cn} \\ L_{aa}C_{aa} - L_{ab}C_{ab} - L_{ac}C_{ac} \\ L_{ab}C_{bb} - L_{aa}C_{ab} - L_{ac}C_{bc} \\ L_{ac}C_{cc} - L_{aa}C_{ac} - L_{ab}C_{bc} \end{bmatrix}^T * \begin{bmatrix} i_{a,1} \\ i_{a,1} + i_{b,1} + i_{c,1} \\ \bullet \\ i_{a,1} \\ \bullet \\ i_{b,1} \\ \bullet \\ i_{c,1} \\ \bullet \\ -v_{an,1} \\ \bullet \\ -v_{bn,1} \\ \bullet \\ -v_{cn,1} \\ \bullet\bullet \\ -v_{an,1} \\ \bullet\bullet \\ v_{bn,1} \\ \bullet\bullet \\ v_{cn,1} \end{bmatrix} \quad (5.10)$$

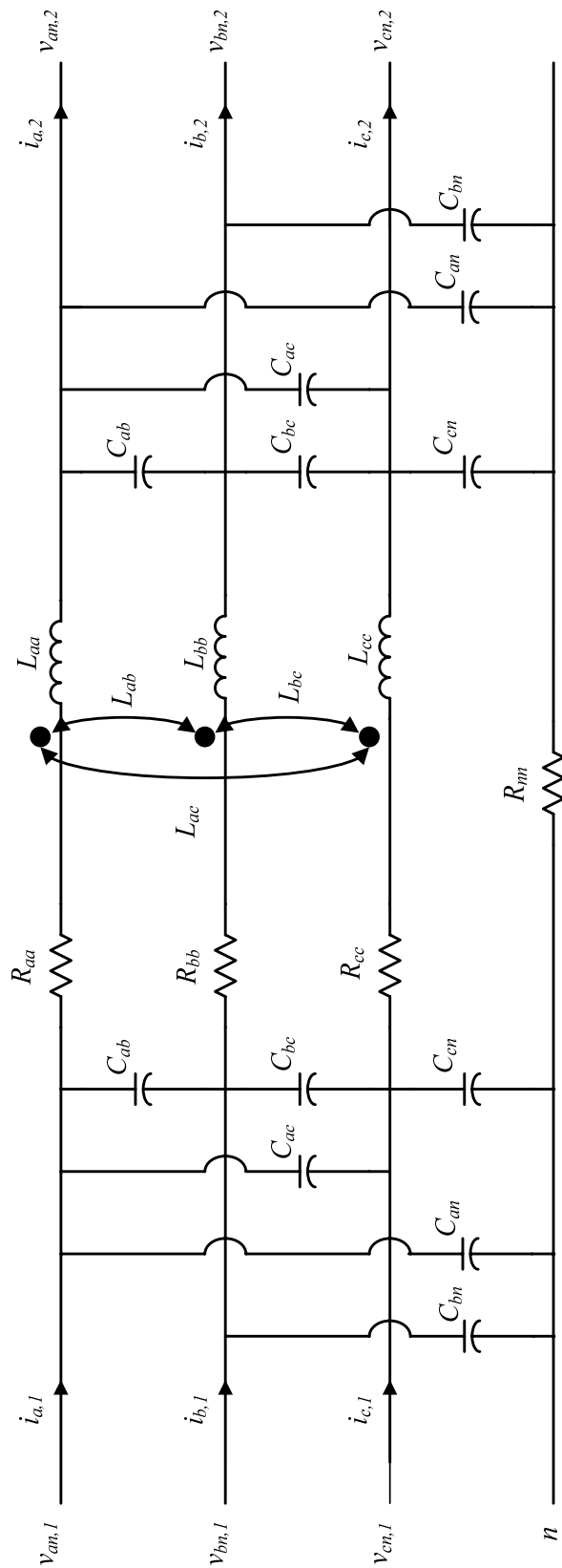


Figure 5-2. Four-Conductor Line Model

Numerous other model configurations can be derived based on various conductor configurations and characteristic assumptions. If the mutual coupling is assumed to be equal in each phase, the unknowns can be reduced by modeling the mutual coupling by a single term, L_m . Additionally, given current and voltage measurements at both ends of the conductors, the capacitances could be determined independently of the resistance and inductance terms as indicated by the three-phase model shown in (5.11). Equation (5.11) was derived using the relationships in (5.7) and (5.8).

$$\begin{bmatrix} i_{a,1} - i_{a,2} \\ i_{b,1} - i_{b,2} \\ i_{c,1} - i_{c,2} \end{bmatrix} = \begin{bmatrix} C_{aa} & -C_{ab} & -C_{ac} \\ -C_{ab} & C_{bb} & -C_{bc} \\ -C_{ac} & -C_{bc} & C_{cc} \end{bmatrix} \frac{d}{dt} \begin{bmatrix} v_{an,1} + v_{an,2} \\ v_{bn,1} + v_{bn,2} \\ v_{cn,1} + v_{cn,2} \end{bmatrix} \quad (5.11)$$

While the multi-conductor models are considerably more complex, the estimation algorithms remain unchanged. The same generalized conclusions concerning convergence, estimator drift, and parameter tracking equally apply to the multi-conductor models as to the two-conductor models. However, interactions between the conductors results in linearly dependent regressors for most system conditions. Hence, identification of the modeled parameters requires more than sufficient harmonic content. It should also be noted that additional models could be produced as long as the derived models are linear.

5.1. IDENTIFIABILITY

The excitation requirements of the multiple conductor models are not only complicated by the number of parameters, but the interactions between the measurements as well. More specifically, when these inputs operate in balanced conditions, they mask interactions that are necessary to estimate the parameters. Therefore, sufficient excitation not only depends on harmonic content but unbalanced operation as well. Analysis of the multi-conductor models' identifiability requirements first requires reexamination of the persistence of excitation introduced in Chapter 3.

The persistence of excitation is inherently determined by the steady-state behavior of the regressors. As noted in section 3.2, a periodic signal of k sinusoids provides a $2k$ order excitation. Therefore, the level of excitation during the steady-state operation of the branch can be evaluated through the frequency domain phasor components of the model's regressors. As the multiple conductor models will contain multiple regressors of the same type (i.e. i_a , i_b , i_c , etc.) each potentially containing multiple frequencies, relationships between regressors will be easier to evaluate in the frequency domain.

The excitation requirement for a system with two unknown parameters is expressed in (5.12) by equivalent phasors for the input (\bar{y}) and regressors (\bar{u}_1 and \bar{u}_2). As long as \bar{u}_1 and \bar{u}_2 are not scalar multiples of each other, a unique solution exists between the unknown scalar parameters A and B . In fact, this relationship is commonly used to perform spectral analysis using least-squares techniques.

$$\bar{y} = A\bar{u}_1 + B\bar{u}_2 \quad (5.12)$$

Multi-phase power systems are typically operated as near to balanced conditions as possible. However, balanced operation actually limits the excitation in the measurements. Consider the estimation of three unknowns using three phasor measurements, \bar{u}_1 , \bar{u}_2 , and \bar{u}_3 . If only a single frequency is considered, only two equations – the real and imaginary portions of (5.13) – can be written relating these three parameters. As an infinite number of regressor vector combinations will provide the predicted output vector, a unique solution cannot be determined.

$$\bar{y} = A\bar{u}_1 + B\bar{u}_2 + C\bar{u}_3 \quad (5.13)$$

If an additional sinusoid is included, the number of equations appears to increase to a sufficient level as indicated in (5.14).

$$\begin{aligned} \bar{y}_\omega &= A\bar{u}_{1,\omega} + B\bar{u}_{2,\omega} + C\bar{u}_{3,\omega} \\ y_{a\omega} &= A\bar{u}_{1,a\omega} + B\bar{u}_{2,a\omega} + C\bar{u}_{3,a\omega} \end{aligned} \quad (5.14)$$

However, if the phasors are related through a scalar, as shown in (5.15), the number of effective equations reduces to two.

$$\begin{bmatrix} \bar{y}_\omega \\ \bar{u}_{1,\omega} \\ \bar{u}_{2,\omega} \\ \bar{u}_{3,\omega} \end{bmatrix} = x^* \begin{bmatrix} \bar{y}_{a\omega} \\ \bar{u}_{1,a\omega} \\ \bar{u}_{2,a\omega} \\ \bar{u}_{3,a\omega} \end{bmatrix} \quad (5.15)$$

Consequently, balanced operation will always limit the persistence of excitation to 2nd order regardless of the number of harmonics or phases involved. The conditions under

which the excitation will increase beyond 2nd order are determined via examination of the physics-based models.

Before analyzing a full MISO model such as (5.10), a simpler model where the capacitance is assumed to be negligible is examined. This model, as shown in (5.16), requires at least a 5th order excitation. The frequency-domain regressor matrix for the minimal frequency case is given in (5.17) where the derivatives are expressed in terms of the original current phasors. During steady-state operation, the rank of (5.17) is equivalent to the rank of the time-domain regressor matrix. Hence, the operational criterion that determines if $\bar{\Phi}$ is full rank is defined by the model's identifiability requirements.

$$[v_{an,1} - v_{an,2}] = \begin{bmatrix} R_{aa} \\ R_{nn} \\ L_{aa} \\ L_{ab} \\ L_{ac} \end{bmatrix}^T * \begin{bmatrix} i_{a,1} \\ i_{a,1} + i_{b,1} + i_{c,1} \\ \vdots \\ i_{a,1} \\ \vdots \\ i_{b,1} \\ \vdots \\ i_{c,1} \end{bmatrix} \quad (5.16)$$

$$\bar{\Phi} = \begin{bmatrix} \bar{I}_{a',\omega} & \bar{I}_{n',\omega} & (\omega \angle 90^\circ) \bar{I}_{a',\omega} & (\omega \angle 90^\circ) \bar{I}_{b',\omega} & (\omega \angle 90^\circ) \bar{I}_{c',\omega} \\ \bar{I}_{a',\alpha\omega} & \bar{I}_{n',\alpha\omega} & (\alpha\omega \angle 90^\circ) \bar{I}_{a',\alpha\omega} & (\alpha\omega \angle 90^\circ) \bar{I}_{b',\alpha\omega} & (\alpha\omega \angle 90^\circ) \bar{I}_{c',\alpha\omega} \\ \bar{I}_{a',\beta\omega} & \bar{I}_{n',\beta\omega} & (\beta\omega \angle 90^\circ) \bar{I}_{a',\beta\omega} & (\beta\omega \angle 90^\circ) \bar{I}_{b',\beta\omega} & (\beta\omega \angle 90^\circ) \bar{I}_{c',\beta\omega} \end{bmatrix} \quad (5.17)$$

Unbalanced operation itself is not a sufficient condition for identifiability. The imbalance must also cause neutral current to flow. Obviously, if current is not flowing in the neutral, the R_{nn} cannot be estimated. This in itself will reduce the rank of (5.17). However if the neutral is not involved with the imbalance, the line currents must still sum

to zero. Thus, the line currents are linearly dependent by definition. The imbalance must therefore result from either a fault or load that allows current to flow into the neutral. Neutral +current alone is also not a sufficient condition either as a balanced fault only provides a 3rd order excitation.

Excitation requirements for a capacitance only model, such as (5.11), are similar in nature to that of (5.16). The voltage regressors must contain sufficient harmonic content as well linear independence in order to provide the necessary excitation. The equivalent regressor matrix for this model is shown in (5.18). Again, linear dependence between the regressors is governed by unbalanced system operation that results in current in the neutral. When no voltage drop occurs in the neutral, the voltages in (5.18) are forced to sum to zero. Consequently, (5.11) and (5.16) share the same general identifiability requirements.

$$\bar{\Phi} = \begin{bmatrix} (1 \angle 90^\circ)(\bar{V}_{an,1} - \bar{V}_{an,2})_{\omega} & (1 \angle 90^\circ)(\bar{V}_{bn,1} - \bar{V}_{bn,2})_{\omega} & (1 \angle 90^\circ)(\bar{V}_{cn,1} - \bar{V}_{cn,2})_{\omega} \\ (\alpha \angle 90^\circ)(\bar{V}_{an,1} - \bar{V}_{an,2})_{\alpha\omega} & (\alpha \angle 90^\circ)(\bar{V}_{bn,1} - \bar{V}_{bn,2})_{\alpha\omega} & (\alpha \angle 90^\circ)(\bar{V}_{cn,1} - \bar{V}_{cn,2})_{\alpha\omega} \end{bmatrix} \quad (5.18)$$

Models such as (5.10), which consider both the series and shunt terms, will obviously increase both the required harmonic content as well as the complexity of the imbalance required. Linear independence between the regressors is additionally challenging for (5.10) as some type of underlying physical relationship will potentially exist between the current and voltage based regressors. The associated regressor matrix for the full model of (5.10) is given in (5.19) through (5.23). The fundamental frequency term ω was factored out of the derivative terms in order to simplify the expressions.

$$\bar{\Phi} = [\bar{A} \mid \bar{B} \mid \bar{C} \mid \bar{D}] \quad (5.19)$$

$$\bar{A} = \begin{bmatrix} \bar{I}_{a'\omega} & \bar{I}_{n'\omega} \\ \bar{I}_{a'ao} & \bar{I}_{n'ao} \\ \bar{I}_{a'\beta\omega} & \bar{I}_{n'\beta\omega} \\ \bar{I}_{a'\delta\omega} & \bar{I}_{n'\delta\omega} \\ \bar{I}_{a'\sigma\omega} & \bar{I}_{n'\sigma\omega} \\ \bar{I}_{a'\zeta\omega} & \bar{I}_{n'\zeta\omega} \end{bmatrix} \quad (5.20)$$

$$\bar{B} = \begin{bmatrix} (1 \angle 90^\circ) \bar{I}_{a'\omega} & (1 \angle 90^\circ) \bar{I}_{b'\omega} & (1 \angle 90^\circ) \bar{I}_{c'\omega} \\ (\alpha \angle 90^\circ) \bar{I}_{a'ao} & (\alpha \angle 90^\circ) \bar{I}_{b'ao} & (\alpha \angle 90^\circ) \bar{I}_{c'ao} \\ (\beta \angle 90^\circ) \bar{I}_{a'\beta\omega} & (\beta \angle 90^\circ) \bar{I}_{b'\beta\omega} & (\beta \angle 90^\circ) \bar{I}_{c'\beta\omega} \\ (\delta \angle 90^\circ) \bar{I}_{a'\delta\omega} & (\delta \angle 90^\circ) \bar{I}_{b'\delta\omega} & (\delta \angle 90^\circ) \bar{I}_{c'\delta\omega} \\ (\sigma \angle 90^\circ) \bar{I}_{a'\sigma\omega} & (\sigma \angle 90^\circ) \bar{I}_{b'\sigma\omega} & (\sigma \angle 90^\circ) \bar{I}_{c'\sigma\omega} \\ (\zeta \angle 90^\circ) \bar{I}_{a'\zeta\omega} & (\zeta \angle 90^\circ) \bar{I}_{b'\zeta\omega} & (\zeta \angle 90^\circ) \bar{I}_{c'\zeta\omega} \end{bmatrix} \quad (5.21)$$

$$\bar{C} = \begin{bmatrix} (1 \angle 90^\circ) \bar{V}_{a'\omega} & (1 \angle 90^\circ) \bar{V}_{b'\omega} & (1 \angle 90^\circ) \bar{V}_{c'\omega} \\ (\alpha \angle 90^\circ) \bar{V}_{a'ao} & (\alpha \angle 90^\circ) \bar{V}_{b'ao} & (\alpha \angle 90^\circ) \bar{V}_{c'ao} \\ (\beta \angle 90^\circ) \bar{V}_{a'\beta\omega} & (\beta \angle 90^\circ) \bar{V}_{b'\beta\omega} & (\beta \angle 90^\circ) \bar{V}_{c'\beta\omega} \\ (\delta \angle 90^\circ) \bar{V}_{a'\delta\omega} & (\delta \angle 90^\circ) \bar{V}_{b'\delta\omega} & (\delta \angle 90^\circ) \bar{V}_{c'\delta\omega} \\ (\sigma \angle 90^\circ) \bar{V}_{a'\sigma\omega} & (\sigma \angle 90^\circ) \bar{V}_{b'\sigma\omega} & (\sigma \angle 90^\circ) \bar{V}_{c'\sigma\omega} \\ (\zeta \angle 90^\circ) \bar{V}_{a'\zeta\omega} & (\zeta \angle 90^\circ) \bar{V}_{b'\zeta\omega} & (\zeta \angle 90^\circ) \bar{V}_{c'\zeta\omega} \end{bmatrix} \quad (5.22)$$

$$\bar{D} = \begin{bmatrix} -\bar{V}_{a'\omega} & -\bar{V}_{b'\omega} & -\bar{V}_{c'\omega} \\ -\alpha^2 \bar{V}_{a'ao} & -\alpha^2 \bar{V}_{b'ao} & -\alpha^2 \bar{V}_{c'ao} \\ -\beta^2 \bar{V}_{a'\beta\omega} & -\beta^2 \bar{V}_{b'\beta\omega} & -\beta^2 \bar{V}_{c'\beta\omega} \\ -\delta^2 \bar{V}_{a'\delta\omega} & -\delta^2 \bar{V}_{b'\delta\omega} & -\delta^2 \bar{V}_{c'\delta\omega} \\ -\sigma^2 \bar{V}_{a'\sigma\omega} & -\sigma^2 \bar{V}_{b'\sigma\omega} & -\sigma^2 \bar{V}_{c'\sigma\omega} \\ -\zeta^2 \bar{V}_{a'\zeta\omega} & -\zeta^2 \bar{V}_{b'\zeta\omega} & -\zeta^2 \bar{V}_{c'\zeta\omega} \end{bmatrix} \quad (5.23)$$

Nonetheless, the excitation requirements associated with the resistive and inductive parameters of (5.10) do not differ from those of (5.16) despite the inclusion of the additional parameters. However, there is obviously more potential for rank deficiency to occur. Given imbalance and sufficient harmonic content in the currents, the order of the excitation will be at least 3rd order. But sufficient harmonics must also exist in the voltages as well or the overall excitation can be no larger than 7th order. Furthermore, a direct linear relationship cannot exist between voltages and currents. Therefore, the necessary but not sufficient conditions for determining a unique solution for (5.10) are:

- A minimum of six harmonics in the voltage and currents
- Unbalanced operation and neutral current, and
- Linear independence between the voltage and currents.

These conditions are necessary but not sufficient to guarantee sufficient excitation as other forms of linear dependence can arise given various configurations and operating conditions.

5.2. MODEL EVALUATIONS

Parameters representing 100 feet of 1 kV 6AWG belted cable [86] were selected to examine the estimation techniques' performance when estimating the three-phase line parameters in Figure 5-2. The cable is assumed to have balanced characteristics with the parameters listed in Table 5-1. PSPICE was again used to create pseudo-observation data for various system configurations and modes of operation. Samples were recorded at a

rate of 50 kHz and stored using eight significant digits. The same MATLAB codes used in the two-conductor model evaluations are used again here.

Table 5-1. Four-Conductor Example Parameters

Name	Value	Name	Value	Name	Value
R_{aa}	47.3 m Ω	L_{aa}	11.6 μ H	C_{ab}	1.21 nF
R_{bb}	47.3 m Ω	L_{bb}	11.6 μ H	C_{ac}	1.21 nF
R_{cc}	47.3 m Ω	L_{cc}	11.6 μ H	C_{bc}	1.21 nF
R_{nn}	52.0 m Ω	L_{ab}	1.97 μ H	C_{an}	4.34 nF
		L_{ac}	1.97 μ H	C_{bn}	4.34 nF
		L_{bc}	1.97 μ H	C_{cn}	4.34 nF

Per-unitization or normalization of the data is handled in exactly the same manner as outlined for the two-conductor models, except now it is necessary to account for potential use of three-phase quantities. Multi-conductor models such as (5.9) can be rewritten using line-to-line instead of line-to-neutral voltage measurements. However, no clear benefit is gained by using three-phase quantities in the derived models. As a result, all the voltage measurements here are assumed to be line-to-neutral, and the base relationships contained in Table 3-2 are directly applied. The bases were again selected to provide an acceptable scaling of the regressor values during the expected range of operation and are listed in Table 5-2.

Table 5-2. Test System Per-Unit Bases

Base	Units
V_{base}	200 (v)
I_{base}	20 (A)
t_{base}	2.653 (ms)
S_{base}	4,000 (VA)
R_{base}	10 (Ω)
L_{base}	26.53 (mH)
C_{base}	265.3 (μF)

The test system is illustrated by Figure 5-3. The three-phase source is modeled by a set of balanced three-phase voltage sources each with an internal impedance of 3 Ω connected in grounded wye. The large internal resistance was selected to insure a sufficient amount of the harmonic currents produced by the rectifier would translate into voltage harmonics. A three-phase diode bridge rectifier was selected as the load to ensure enough harmonic content was generated to achieve the necessary excitation conditions.

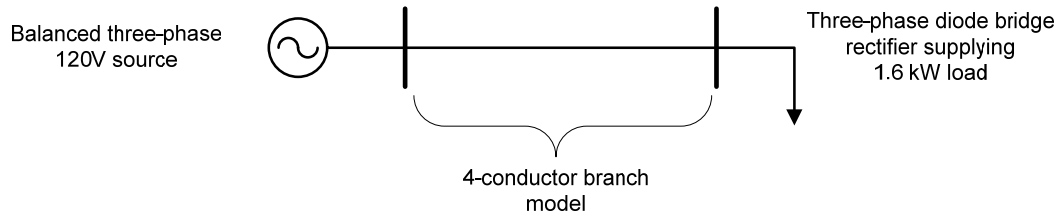


Figure 5-3. Single Line Diagram of the Three-Phase Test System

The harmonic currents produced by the rectifier during normal conditions can be approximated by dividing the fundamental rms current, \bar{I}_1 , by the harmonic number, h , as

shown in (5.24) where $h = 5, 7, 11$, etc. and the even and triplen harmonics are zero. The chosen 50 kHz sampling rate, however, has a Nyquist frequency of 25 kHz and any discernable harmonics above this frequency will cause aliasing in the sampled measurements. Given the small physical values to be estimated, any aliasing can result in significant bias in the estimations which must be avoided. For the 60 Hz system in Figure 5-3, the first harmonic produced by the rectifier beyond the Nyquist is the 421st harmonic (25.26 kHz) which is approximately $|\bar{I}_h|/421$. While the harmonics beyond the Nyquist are small in comparison to the fundamental, they must be small enough to not be detectable from the measurement noise. The quantization error, (3.59), could be used to determine whether the normally generated harmonics have a strong signal-to-noise ratio and would be expected to influence the measurements. However, this process cannot account for transients or other operating conditions which increase the harmonic magnitudes. Additionally, accurately estimating the small parameter values requires minimizing the measurement noise which increases the likelihood of detecting these higher frequencies. Therefore, when designing the monitoring device either the sampling rate must be set high enough to insure harmonics above the Nyquist frequency cannot be observed or anti-aliasing filters should be introduced to remove the higher frequency content. In this case, 2nd order low pass filters with 10 kHz corner frequencies were introduced during simulation in PSPICE to limit aliasing.

$$|\bar{I}_h| \approx \frac{|\bar{I}_1|}{h} \quad (5.24)$$

The parameter estimation techniques used are exactly the same as those applied for the two-conductor models. All the conclusions about the estimation techniques' parameter tracking abilities, convergence, and estimator windup apply to the multi-conductor models. The main concern with the multi-conductor models then is the increased difficulties with achieving sufficient excitation.

5.2.1. SERIES ELEMENT MODEL

It is convenient to begin by examining the characteristics of a simple model such as (5.16). In this case, neither the simulations nor the model included the conductor's shunt capacitances. As discussed in the previous section, excitation is limited to 2nd order during balanced three-phase conditions regardless of the harmonic content. To achieve independence between the regressors, a 1 Ω resistive fault is introduced at the load between the a-phase and neutral conductors. The voltage and current waveforms before and after the fault is introduced, at 250 ms, are given in Figure 5-4. The Fourier series rms voltages and currents before and after the fault are also provided in Table 5-3 through Table 5-6.

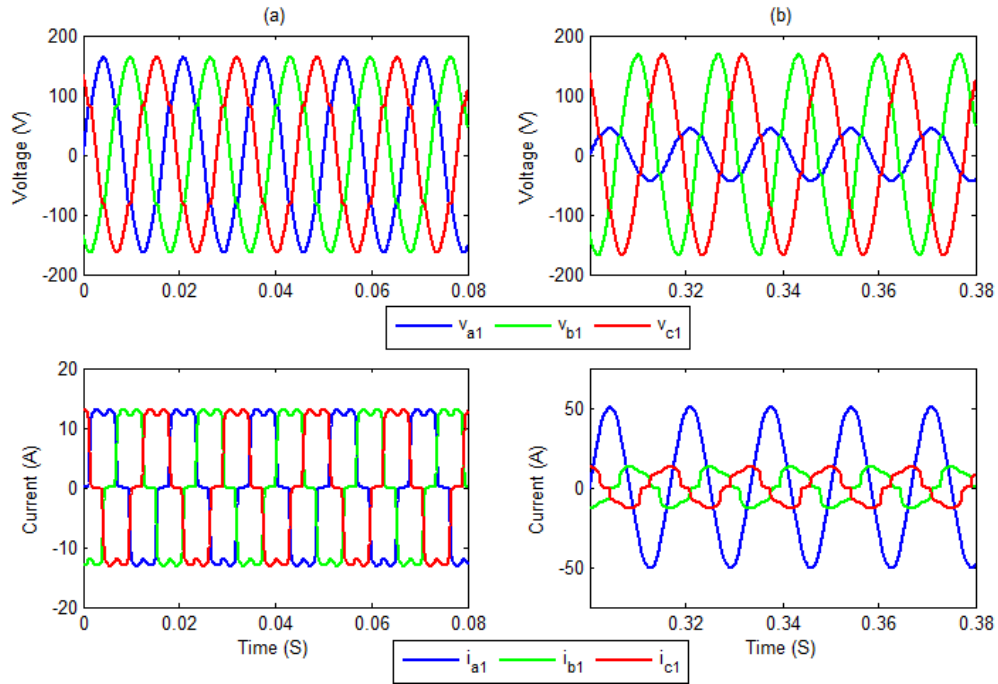


**Figure 5-4. Test System Voltage and Current Waveforms
(a) Before and (b) After the Fault**

Table 5-3. Voltage Fourier Components for Balanced Conditions

Harmonic	Phase A		Phase B		Phase C	
	Fourier Component	Phase (Deg)	Fourier Component	Phase (Deg)	Fourier Component	Phase (Deg)
1	111.51	-1.04	111.51	-121.10	111.51	119.00
5	6.29	-5.12	6.30	114.70	6.31	-125.10
7	3.13	-7.37	3.13	-127.30	3.13	112.70
11	1.97	168.60	1.97	-71.48	1.97	48.68
13	1.40	166.60	1.40	46.46	1.40	-73.41
17	0.77	-17.48	0.77	102.50	0.77	-137.40
19	0.61	-19.25	0.61	-139.50	0.61	100.70

Table 5-4. Current Fourier Components for Balanced Conditions

Harmonic	Phase A		Phase B		Phase C	
	Fourier Component	Phase (Deg)	Fourier Component	Phase (Deg)	Fourier Component	Phase (Deg)
1	9.81	-1.10	9.81	-121.10	9.81	118.90
5	2.07	174.52	2.07	-65.50	2.07	54.50
7	1.03	172.26	1.03	52.20	1.03	-67.70
11	0.65	-12.00	0.65	107.96	0.65	-132.04
13	0.46	-14.20	0.46	-134.22	0.46	105.79
17	0.25	161.54	0.25	-78.50	0.25	41.50
19	0.20	159.54	0.20	39.50	0.20	-80.46

Table 5-5. Voltage Fourier Components for Unbalanced Conditions

Harmonic	Phase A		Phase B		Phase C	
	Fourier Component	Phase (Deg)	Fourier Component	Phase (Deg)	Fourier Component	Phase (Deg)
1	30.94	-1.10	115.33	-125.00	115.33	123.00
5	1.04	-5.40	2.23	161.50	2.23	-171.50
7	0.77	172.40	3.01	-64.94	3.02	50.67
11	0.37	-12.00	0.79	175.70	0.79	162.10
13	0.23	-14.02	0.48	166.60	0.48	167.50
17	0.11	161.60	0.84	56.68	0.84	-91.17
19	0.17	-20.38	0.40	-172.20	0.40	134.30

Table 5-6. Current Fourier Components for Unbalanced Conditions

Harmonic	Phase A		Phase B		Phase C	
	Fourier Component	Phase (Deg)	Fourier Component	Phase (Deg)	Fourier Component	Phase (Deg)
1	35.72	-1.10	9.16	-107.33	9.17	105.15
5	0.36	174.36	0.72	-19.30	0.71	8.40
7	0.26	-8.00	0.98	113.83	0.98	-129.21
11	0.13	167.34	0.25	-5.30	0.25	-19.00
13	0.08	165.38	0.16	-14.80	0.15	-13.60
17	0.04	-19.20	0.27	-124.32	0.27	87.21
19	0.06	158.52	0.13	6.60	0.13	-47.80

Using RLS with directional forgetting resulted in the parameter estimations given in Figure 5-5. Before the fault is applied the excitation is insufficient to result in convergence to a unique solution. Once imbalance is introduced, however, the excitation rises to sufficient levels for the estimates to converge to their actual values. Additionally, the margins of error for the estimates, shown in Figure 5-6, indicate a strong level of confidence for the estimates. It is interesting to note that the resistance, R_{aa} , can be determined even before the imbalance is introduced. While the individual solutions for each inductance parameters cannot be determined during balanced conditions, their influence is still accounted for in the estimates. Analysis of the parameter estimates during this period confirms that estimates are approximately $L_{aa}-L_{ab} \approx L_{aa}-L_{ac} \approx 9.64 \mu\text{H}$ which is easily shown to be the equivalent positive-sequence inductance.

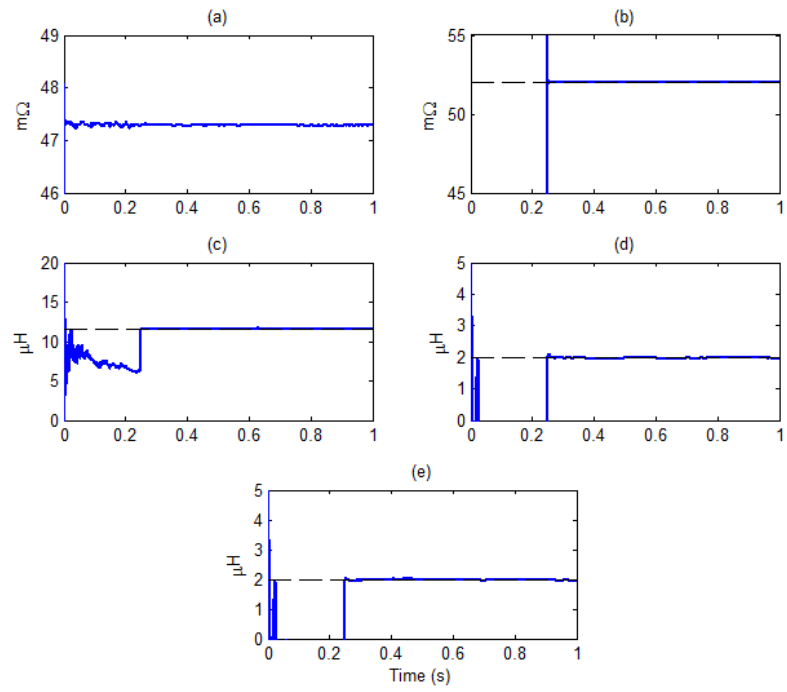


Figure 5-5. Multi-conductor Parameter Estimates
 (a) R_{aa} (b) R_{nn} (c) L_{aa} (d) L_{ab} (e) L_{ac}

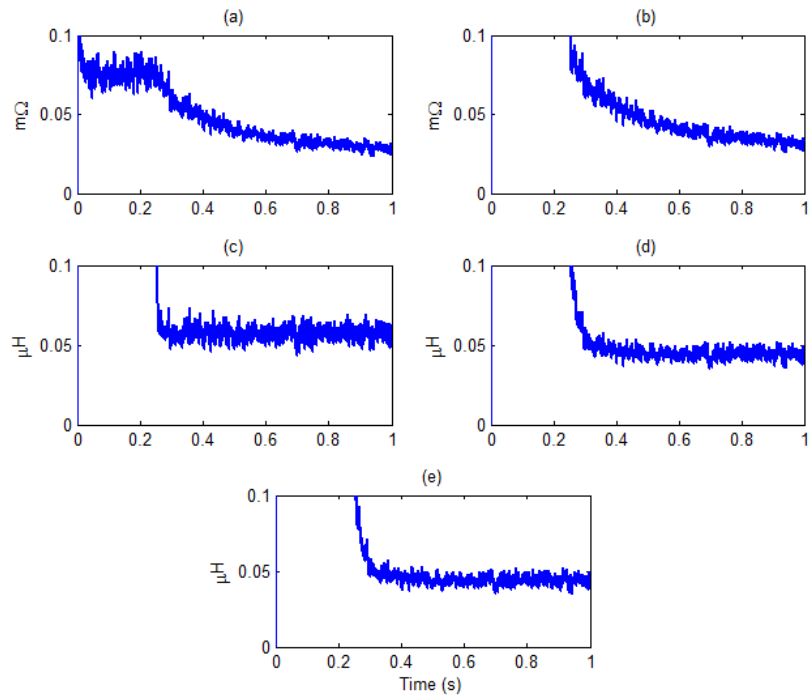


Figure 5-6. 95% Confidence Margins of Error
 (a) R_{aa} (b) R_{nn} (c) L_{aa} (d) L_{ab} (e) L_{ac}

To illustrate that improvements in the estimates are due to the introduced imbalance, the correlation matrices, before and after the fault, are depicted in Figure 5-7. These figures graphically illustrate the regressors' correlation coefficients as colors with the red and blue hues denoting positive and negative correlation, respectively. The axes of the figure denote the variables associated with each particular regressor. Before the fault, the inductance terms are strongly correlated, as seen in Figure 5-7(a), resulting in infinite solutions to the parameter estimates. In comparison, the correlation matrix after the fault is shown in Figure 5-7(b) and indicates little correlation between the regressors except for some negative correlation between the a-phase and the neutral. This correlation is somewhat expected given the nature of the applied fault. While perfectly balanced conditions may be unlikely, strong correlations between the regressors will still occur when the imbalance is small. This case is examined further in a later example.

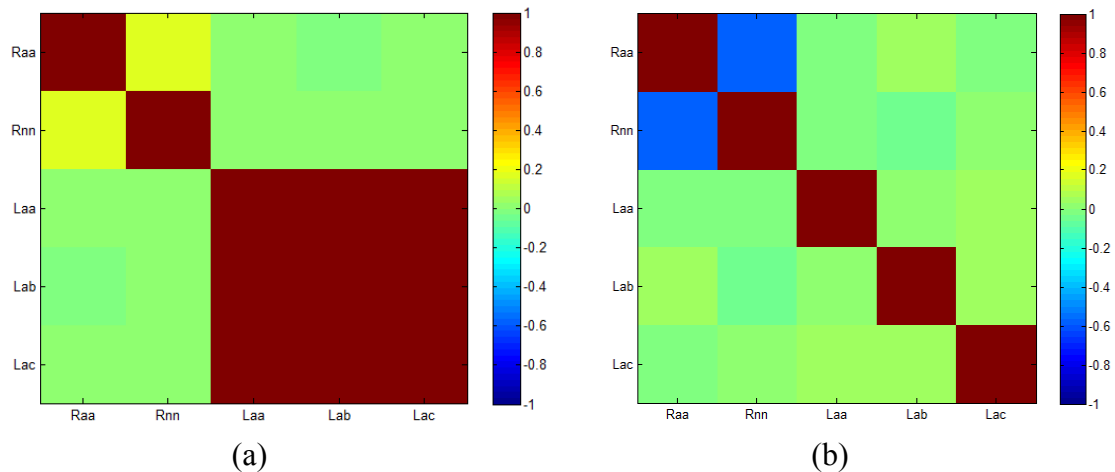


Figure 5-7. A-Phase Correlation Matrices
(a) Balanced and (b) Line to Ground Fault Conditions

As previously noted, models for both b and c phases can be written that are similar in form to (5.10) and can each be estimated using the same sampled data. To illustrate, b-phase parameter estimates, using the same data as before, are plotted in Figure 5-8. The estimation of the parameters for the b-phase models using the same data set is important as it proves the disturbance does not have to occur in a modeled phase. As expected, the correlation between the b-phase and neutral current is not significant during the fault as illustrated by the covariance matrix displayed in Figure 5-9.

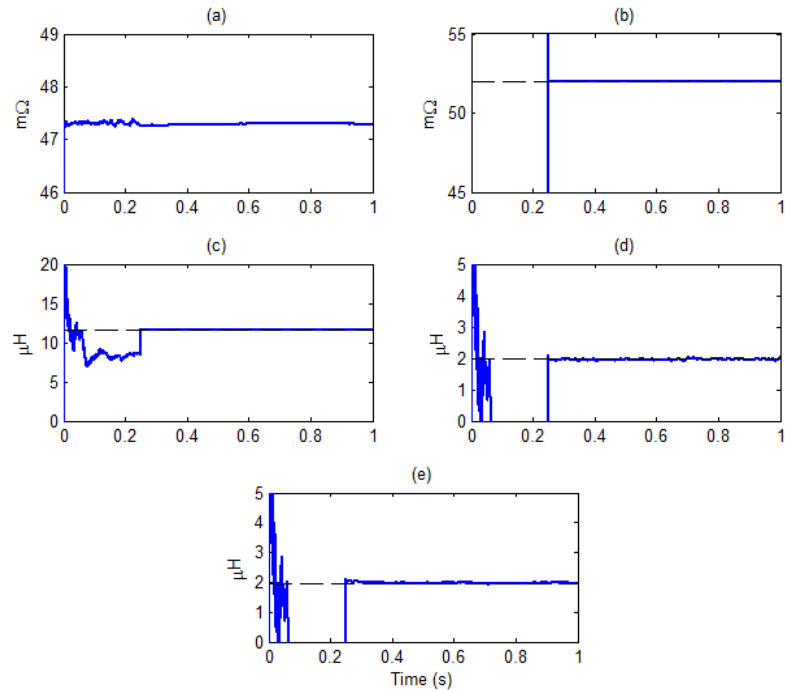


Figure 5-8. Multi-conductor Parameter Estimates
(a) R_{bb} (b) R_{nn} (c) L_{bb} (d) L_{ab} (e) L_{bc}

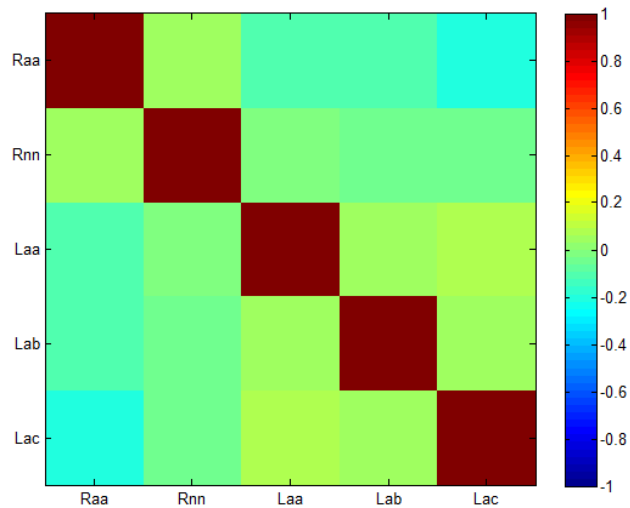


Figure 5-9. B-Phase Correlation Matrix

The parameter tracking abilities of the algorithm are unchanged by the increased model complexity as shown in Figure 5-10. In this case, the fault results in a large step change in the neutral resistance, R_{nn} . The estimates successfully track the parameter change, but the abrupt change also causes bias in the estimates. The estimated margins of error are also influenced by the abrupt change as indicated in Figure 5-11. The changing parameter estimates result in non-white content in the residual and prediction errors. Consequently, both parameter and error margin estimates are biased during this period. However, any non-white noise in the prediction error also increases the noise variance estimate and consequently the margins of error. While they are not an accurate measure of the confidence, the large margins of error are clear indicators of general inaccuracy in the estimates during this period. Once the estimates have converged to the new unique solution, the margins of error will again accurately reflect the level of confidence in the parameter estimates.

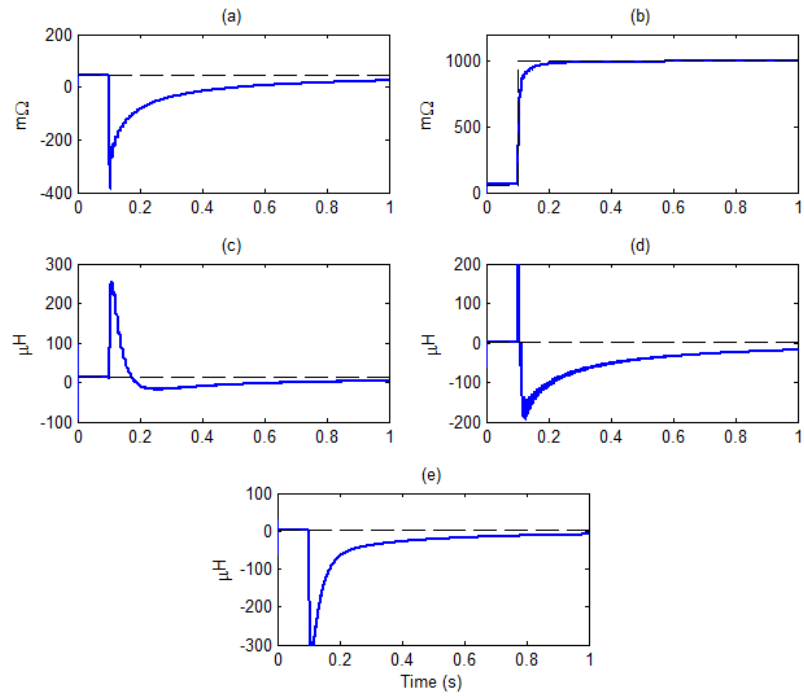


Figure 5-10. Multi-conductor Parameter Estimates
 (a) R_{bb} (b) R_{nn} (c) L_{bb} (d) L_{ab} (e) L_{bc}

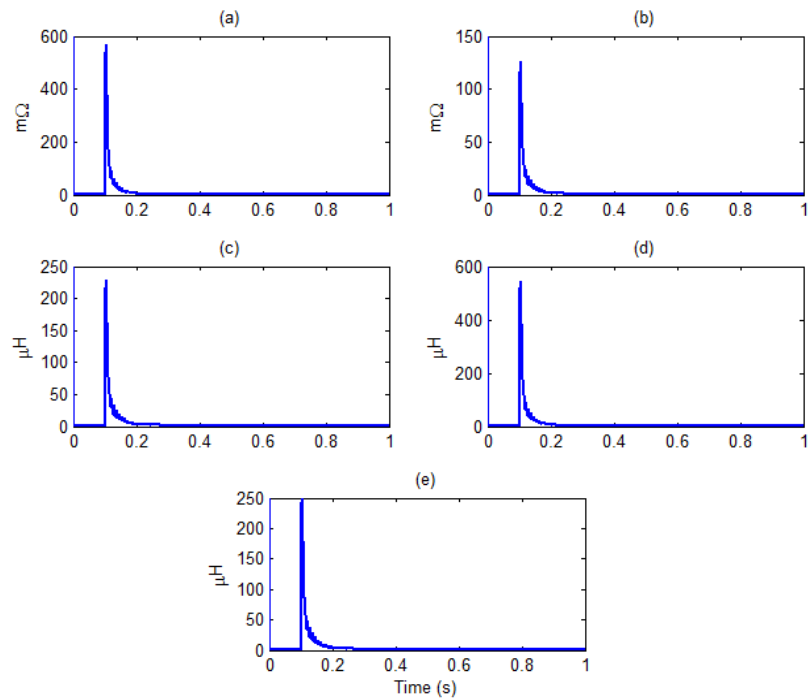


Figure 5-11. 95% Confidence Margins of Error
 (a) R_{aa} (b) R_{nn} (c) L_{aa} (d) L_{ab} (e) L_{ac}

In the next example the excitation provided from a small single phase load is examined. Instead of the 1Ω fault, a 20Ω single phase load is introduced to the a-phase terminals. Additionally, the load is already in service at the start of the observations. Therefore, the estimates do not benefit from extra excitation induced by a switching transient. The resulting parameter estimates are shown in Figure 5-12. As with the line-to-ground fault example, R_{aa} quickly converged. Yet, the level of independent excitation provided by the load is not as great as the faulted case, as shown by the correlation matrix in Figure 5-13. Consequently, the calculated estimations do not converge as quickly. The influence of multicollinearity is also seen in the margins of error, shown in Figure 5-14, which are an order of magnitude larger than those in Figure 5-6.

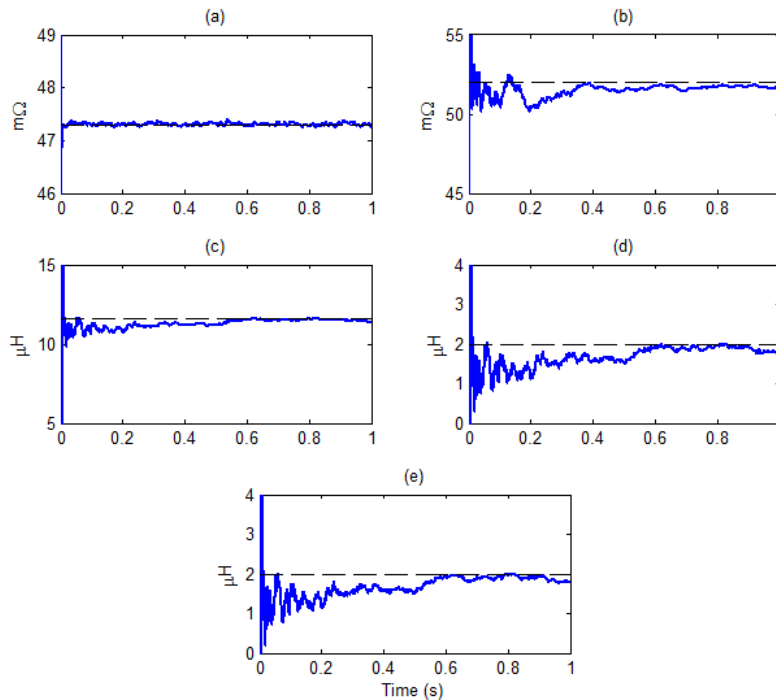


Figure 5-12. Parameter Estimates using RLS/DF
 (a) R_{cc} (b) R_{nn} (c) L_{cc} (d) L_{ac} (e) L_{bc}

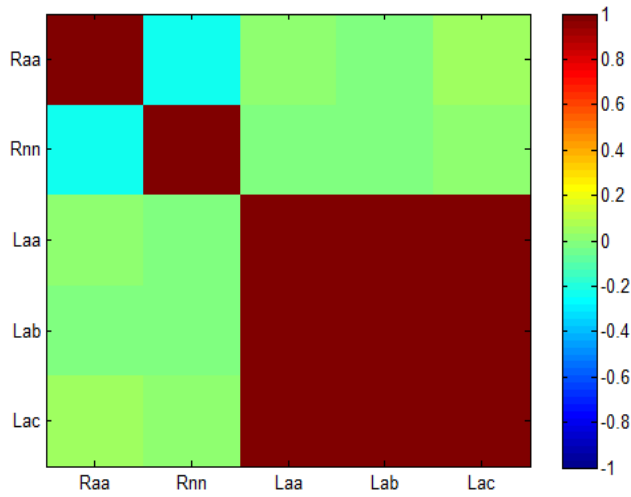


Figure 5-13. Correlation Matrix for A-phase Estimations

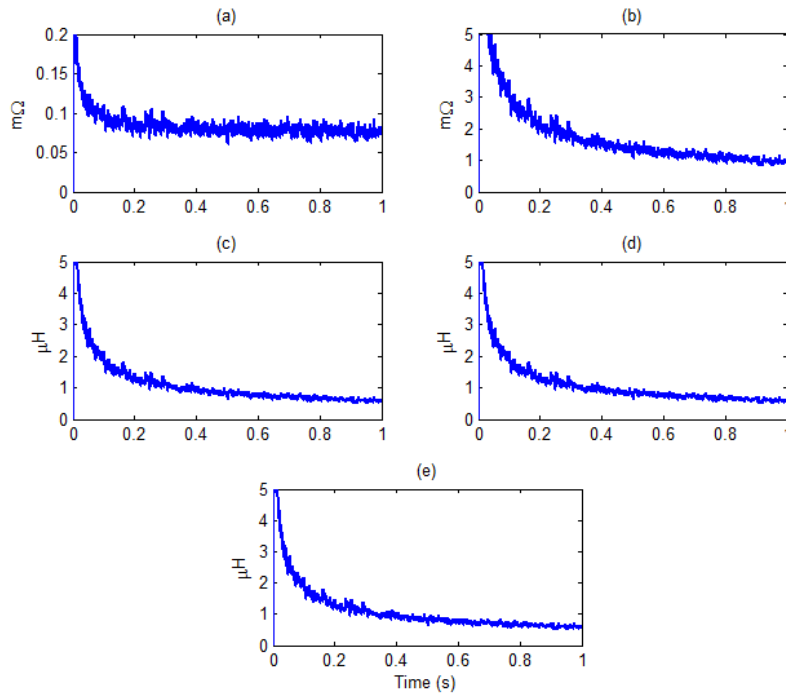


Figure 5-14. 95% Margins of Error
 (a) R_{cc} (b) R_{nn} (c) L_{cc} (d) L_{ac} (e) L_{bc}

Even though the parameter estimates shown in Figure 5-12 are far from ideal, they are better than those provided by discounting the data at a fixed rate. The estimates in Figure 5-15, for example, generated using standard exponential discounting have a much larger variance than the estimates in Figure 5-12. The large variance of the estimates when using exponential discounting indicates that the relevant excitation is not observed in each sample set. If the small influence of the single phase load is discernable only in particular points in the waveform, the resulting excitation may indeed be intermittent in nature. Directional forgetting in this case clearly makes better use of the available information.

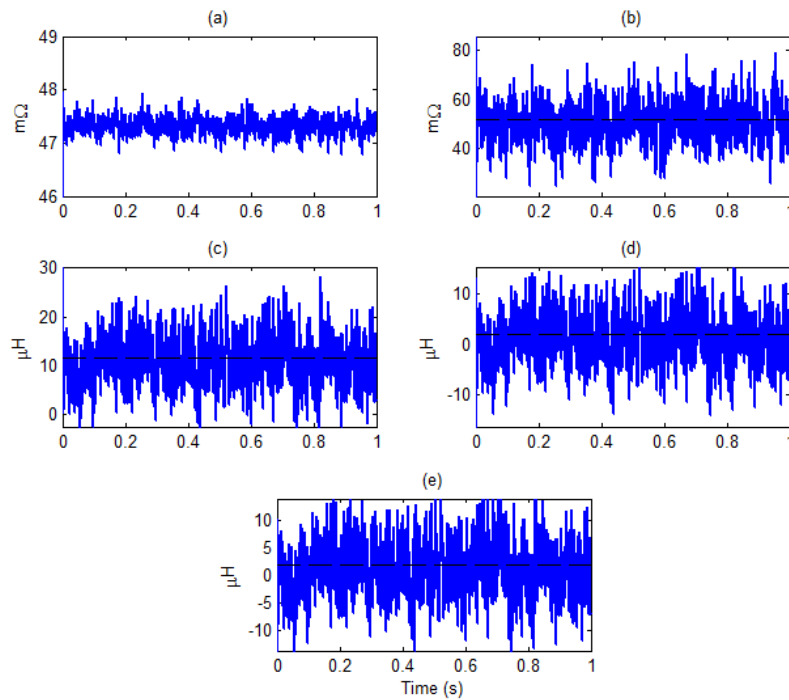


Figure 5-15. Parameter Estimates using RLS
(a) R_{cc} (b) R_{nn} (c) L_{cc} (d) L_{ac} (e) L_{bc}

5.2.2. SHUNT ELEMENT MODEL

Before returning to the complete four-conductor model of Figure 5-2, estimation of the capacitances via (5.11) is examined. Estimating capacitance in multiphase lines displays the same difficulties expressed earlier for the two-conductor models. Namely, accurate estimation of the relatively small capacitances is influenced by the accuracy of the measurements. In this example, the PSPICE model was updated to include the capacitances as well as the resistive and inductive values denoted in Table 5-2 and the test data was generated using the identical line-to-neutral fault scenario as before. The ensuing parameter estimates along with each estimated margins of error are documented in Figure 5-16. As expected, the estimates do not converge until the application of the fault. Even after the fault occurs, the margins of error do not indicate a strong degree of confidence in the estimates. In particular, the margins of error for C_{ab} and C_{ac} indicate little confidence in the estimates. Statistically, it cannot be concluded that these values are not indeed zero. In diagnostic terms, however, this could also be interpreted as negligible values. As before, improving the capacitance estimations requires either reducing the measurement noise or increasing λ .

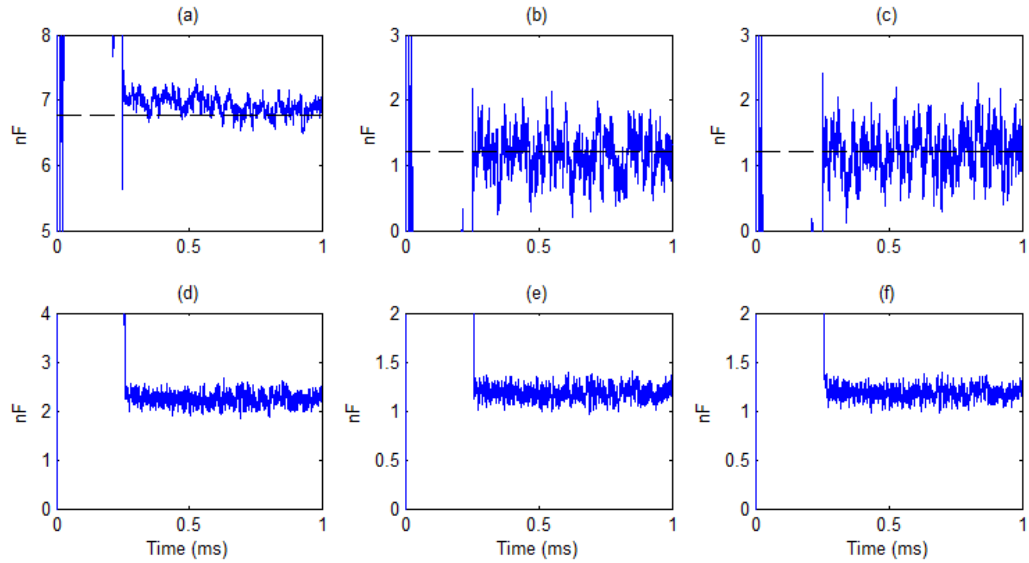


Figure 5-16. Parameter Estimates using RLS (Upper) and 95% Confidence Margins of Error (Lower) C_{aa} (a & d) C_{ab} (b & e) and C_{ac} (c & f)

5.2.3. FULL PARAMETER MODEL

As previously noted, estimation of the parameters using (5.10) requires a higher degree of excitation since the overall number of parameters is significantly higher. One of the more significant difficulties will be achieving linear independence between the multiple regressor terms. Evaluation of the full model is examined by looking at the same fault scenario used in the previous model evaluations. However, a change to the system model is necessary to satisfy linear independence between the voltage and current derivatives. Specifically, the 60 Hz source impedance was changed from 3Ω to a impedance of $\bar{Z}_s = 2 + j0.377 \Omega$. The source inductance was necessary to remove the strong linear relationship between the currents and voltages caused by the source

resistance. The resulting parameters estimates are shown in Figure 5-17 and the corresponding margins of error are shown in Figure 5-18. The results demonstrate many of the expected difficulties with the model including the fact that the RC and LC terms do not converge to acceptable values. Still, once the fault occurs, the resistance and inductance estimates converge to within acceptable ranges. The large margins of error in Figure 5-18 are an indication that many of the parameters estimated by the full model may be unnecessary. Therefore, the same parameter set is used to fit the model in (5.16). As shown in Figure 5-19, the estimates using this model show little signs of bias due to minimal influence of the capacitances.

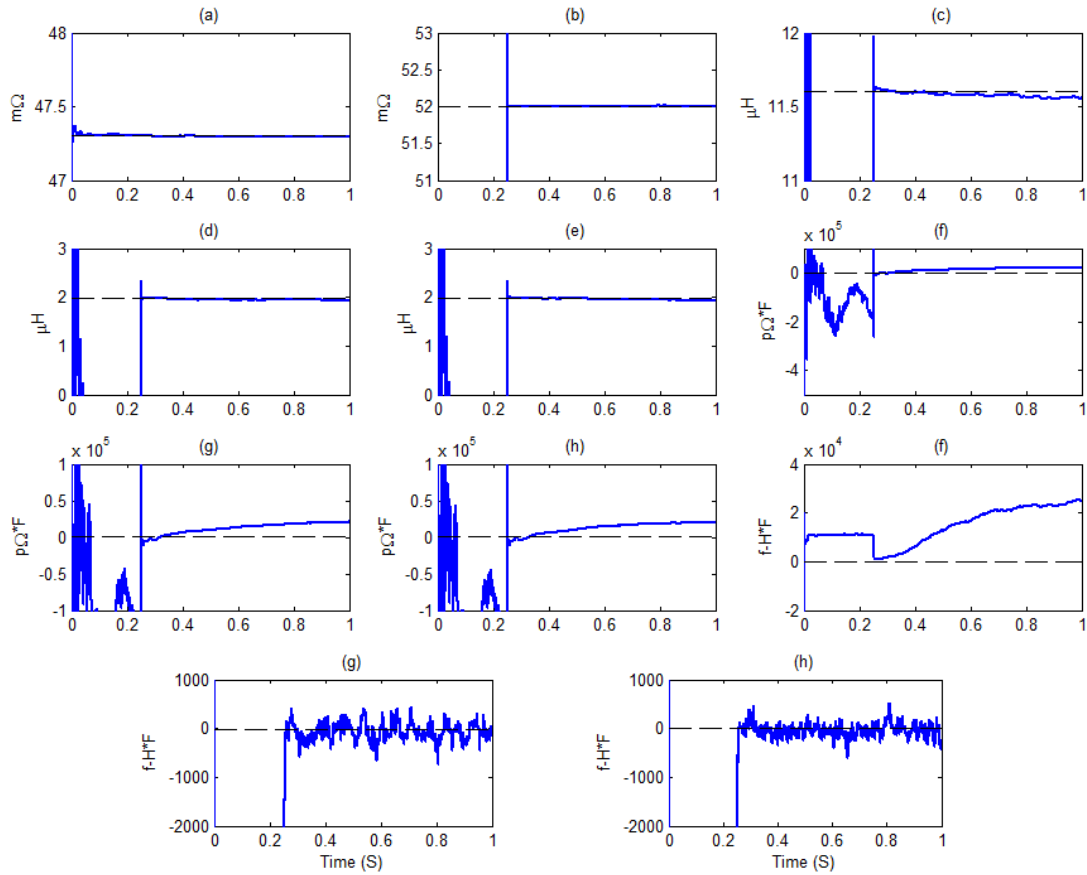


Figure 5-17. Parameter Estimates using RLS/DF
(a) R_{aa} (b) R_{nn} (c) L_{aa} (d) L_{ab} (e) L_{ac} (f) $R_{aa}C_{aa}+R_{nn}C_{nn}$ (g) $-R_{aa}C_{ab}+R_{nn}C_{bn}$
(h) $-R_{aa}C_{ac}+R_{nn}C_{cn}$ (i) $L_{aa}C_{aa}-L_{ab}C_{ab}-L_{ac}C_{ac}$ (j) $L_{ab}C_{bb}-L_{aa}C_{ab}-L_{ac}C_{bc}$
(k) $L_{ac}C_{cc}-L_{aa}C_{ac}-L_{ab}C_{bc}$

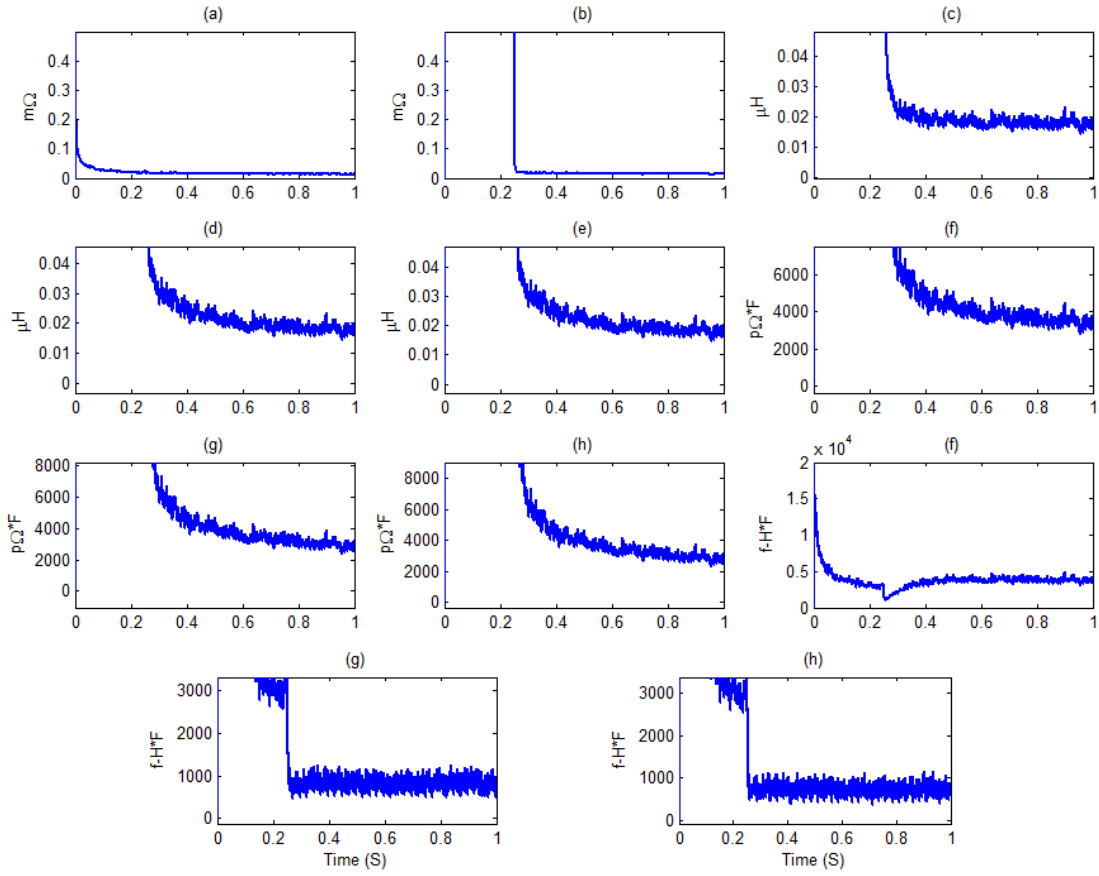


Figure 5-18. 95% Confidence Margins of Error
 (a) R_{aa} (b) R_{nn} (c) L_{aa} (d) L_{ab} (e) L_{ac} (f) $R_{aa}C_{aa}+R_{nn}C_{nn}$
 (g) $-R_{aa}C_{ab}+R_{nn}C_{bn}$ (h) $-R_{aa}C_{ac}+R_{nn}C_{cn}$ (i) $L_{aa}C_{aa}-L_{ab}C_{ab}-L_{ac}C_{ac}$ (j) $L_{ab}C_{bb}-$
 $L_{aa}C_{ab}-L_{ac}C_{bc}$ (k) $L_{ac}C_{cc}-L_{aa}C_{ac}-L_{ab}C_{bc}$

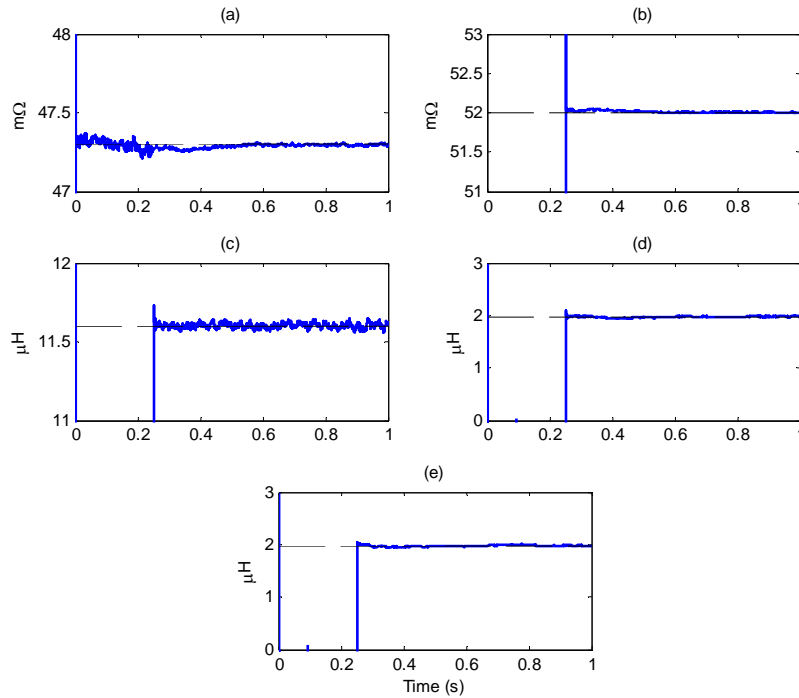


Figure 5-19. Parameter Estimates using RLS/DF
(a) R_{cc} (b) R_{nn} (c) L_{cc} (d) L_{ac} (e) L_{bc}

5.3. SUMMARY

As demonstrated, recursive least-squares with directional forgetting is applicable to multiple conductor models as well as two-conductor models. However, the increased complexity of the multiple conductor models does change the conditions under which sufficient excitation is achieved. Specifically, accurate estimation of the physical parameters describing the interactions between the cables requires unbalanced conditions, current in the neutral conductor, linear dependence between the voltages and currents, as well as sufficient dynamic content. Once these conditions were satisfied, directional forgetting was shown to provide good parameter estimates and tracking capabilities.

Directional forgetting was also shown to provide good estimates when the intermittency is increased by strong correlations between the measurements, as evidenced in Figure 4-12. The proposed methods show good results using time-domain measurements and models of both two and multiple conductor models. Estimation of network parameter using frequency-domain measurements and models is examined in Chapter 6.

CHAPTER 6

FREQUENCY-DOMAIN MODELS

The estimation and tracking techniques utilized in the time domain models are equally applicable to frequency-domain models. In fact, sufficient excitation can be more difficult to achieve in the steady-state frequency domain as the excitation cannot be increased through additional harmonic content. Consequently, excitation can only occur through changes in the phasor values over time. While the nature of the excitation is different between time-domain and frequency domain, the requirements of the estimation methods are unchanged. In this chapter, estimation of network characteristics using frequency-domain measurements is examined. While the line parameters can be identified using frequency-domain measurements, estimation and tracking of the Thevenin equivalent provides the most benefit by allowing monitoring of network characteristics even with limited measurements.

6.1. LINE MODELS

An equivalent frequency domain model can be derived for all of the time-domain models presented in Chapters 4 and 5. The two-conductor MISO model equivalent is provided in (6.1) - (6.4). There are still four unknown parameters, the real and imaginary

parts of each unknown, which require a minimum 4th order excitation. However, as previously stated, the excitation can no longer be increased through additional harmonic content. Sufficient excitation must then arise from changes in the steady-state measurements over time. Recognizing that a particular operating point essentially provides two equations, the minimum excitation will be satisfied when at least two different operating points are observed. Thus, each different operating point increases the order of excitation by two. Additional operating points will increase the order of excitation and also improve the estimates by accounting for measurement errors. Given that frequency-domain models are solely reliant upon changes in the time-domain to supply the necessary excitation, it is more convenient to describe the excitation requirements by the number of different operating points required.

$$\bar{y}(k) = \tilde{\varphi}(k)^T \tilde{\theta}(k) \quad (6.1)$$

$$\bar{y}(k) = \bar{V}_R(k) - \bar{V}_S(k) \quad (6.2)$$

$$\tilde{\varphi}(k)^T = [\bar{V}_S(k) \quad \bar{I}_S(k)] \quad (6.3)$$

$$\tilde{\theta}(k) = \begin{bmatrix} (-\omega^2 RC) + j(\omega LC) \\ R + jX \end{bmatrix} \quad (6.4)$$

In general, estimation of line models using frequency domain data is well understood with recent literature taking advantage of new phasor synchronization techniques [52, 53]. The method proposed in [53] is especially interesting as it uses online phasor

measurements to determine both the positive and zero sequence impedances. Furthermore, the excitation requirements mirror those determined for the multi-conductor models. Specifically, synchronized phasor measurements obtained during ground faults were needed to estimate the zero sequence impedance and mutual coupling terms.

Estimation of the models in [53] was performed using least-squares, (3.5), and a minimal number of measurements. Tracking capabilities could be added by using RLS with some form of discounting as the estimation method. Recalling that parameter drift (estimator windup) is a function of solution method and not the data type, retention of sufficiently exciting information is still an important issue. This is especially true for line models at frequencies other than the fundamental where the excitation is dependent on factors such as harmonic injections and system configuration. As repeated measurement of the same operating conditions does not provide additional information at any frequency, intermittency can occur even at the fundamental frequency. In general, directional forgetting RLS is beneficial to any online automated application where the excitation is potentially intermittent.

6.2. THEVENIN EQUIVALENT

Measurements at both terminals of a branch in the network are not always possible; however, some form of evaluating the network health is still desirable. In these cases, tracking the Thevenin equivalent provides potentially useful information about the network or device. Before examining steady-state approaches using frequency domain

measurements it is enlightening to first examine estimation of the Thevenin equivalent in the time domain.

6.2.1. TIME-DOMAIN

Time-domain information can be used to estimate the Thevenin equivalent at each frequency, but the estimates are interdependent on the selected impedance model. For example, assume that the time-domain model in (6.5) is used to model the fundamental frequency Thevenin equivalent using time-domain voltage and current measurements (v and i). In this case, it is assumed that the R and L components are adequate to represent the Thevenin impedances over all observed frequencies. Additionally, a and b parameters are introduced to estimate the real and imaginary parts of the open-circuit voltage through the inclusion of the $\cos(\omega t)$ and $\sin(\omega t)$ regressors where ω is the radian frequency for the modeled voltage source. In this formulation the reference angle is defined by $\cos(\omega t)$ and the phase angle of the terminal voltage can be found by estimating the terminal voltage phasor using (6.6).

$$v = [R \quad L \quad a \quad b]^* [i \quad \dot{i} \quad \cos(\omega t) \quad \sin(\omega t)]^T \quad (6.5)$$

$$v = [V_R \quad V_I]^* [\cos(\omega t) \quad \sin(\omega t)]^T \quad (6.6)$$

When a constant fundamental frequency current and voltage are observed, the excitation is insufficient to provide a converged solution. If the excitation is increased by a transient or harmonic, the Thevenin equivalent can be estimated. However, if the

Thevenin impedance model inaccurately represents the impedance of the additional harmonic content, the voltage source estimate will be biased. Therefore, selection of an impedance model that is accurate over all the observed frequencies is critical.

Time-domain estimation of the network impedance model has been examined before using high order transfer functions [87, 88]. In this case, the Thevenin impedances are represented by an n^{th} order discrete transfer function shown in (6.7). Modeling the Thevenin impedances in this manner not only increases the minimum excitation by $2n$, but also removes the direct correlation between estimates and known physical quantities. Nonetheless, impedance for each frequency can easily be extrapolated from the transfer function estimate. Furthermore, each harmonic source in the modeled portion of the network must be represented by an additional open-circuit voltage model. Otherwise, the unmodeled information will introduce bias in the estimates.

$$H(k) = \frac{1 + c_1 y(k-1) + \dots + c_n y(k-n)}{d_0 + d_1 u(k-1) + \dots + d_n u(k-n)} \quad (6.7)$$

It should be noted that the application of directional forgetting could allow for better estimation and tracking of the transfer impedance using high order transfer functions. As the transfer function's order increases so does the number of parameters; the excitation requirements for these models will require significant harmonic content to estimate each parameter. Recalling that directional forgetting only replaces information as newer information becomes available, the transfer function poles and zeros would not drift during periods of insufficient excitation. This allows for an accurate estimation of the

transfer impedance even when the chosen model is over-parameterized. Thus, higher order models could be used to improve the results in [87]. However, it is unclear how the past information might bias the general shape of the transfer impedance when network changes occur and an incomplete harmonic spectrum is available.

Unmodeled frequencies could be filtered from the observations to eliminate the influence of the transfer impedance model. For instance, all but the fundamental frequency could theoretically be removed from the data used to fit the model in (6.5). In this case, sufficient excitation is only achieved by changes in the fundamental frequency content. Note that there are four unknown parameters but two are associated with regressors representing steady-state values. At least one outside change in the current regressor terms is required for sufficient excitation. This formulation is analogous to a frequency domain approach.

6.2.2. FREQUENCY-DOMAIN

While estimation of the Thevenin equivalent is possible in the time domain, there are several reasons why it may be an unattractive approach:

- Difficulties in defining an accurate model,
- Design and implementation of multiple filters,
- Availability of time-domain measurements, and
- Measurements must be sampled at a fixed rate

An alternative is to use steady-state phasor measurements to independently estimate the Thevenin equivalent at each frequency. In this approach, methods for providing the

phasor quantities act as the filter and the Thevenin impedance models are independent. Therefore, a simple model can be used for the Thevenin impedance at each frequency. Additionally, estimating the parameters in the frequency domain eliminates the need to update the parameter estimates based on a fixed sampling rate.

Assuming phasor measurements are available, the Thevenin equivalent shown in Figure 6-1 can be fit to the measured phasor for each harmonic h . The complex-space regression model then takes the form given in (6.8) - (6.11). Estimation of the Thevenin equivalent using recursive least-squares has been recently examined in [89] with favorable results. However, the proposed recursive identification method does not implement any discounting of past data; and therefore, is not capable of tracking of the parameter changes. Nevertheless, the recursive least-squares solution methods using the various discounting methods proposed earlier are still valid in complex space; that is $\bar{y} \in \mathbb{C}$, $\tilde{\theta} \in \mathbb{C}$, and $\bar{\Phi} \in \mathbb{C}$.

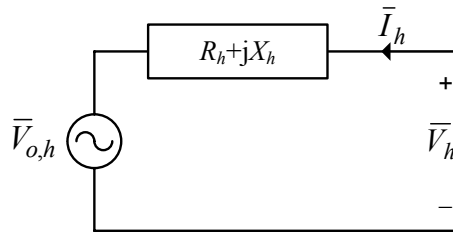


Figure 6-1. Thevenin Equivalent Circuit for h^{th} Order Harmonic Frequency

$$\bar{y}(k) = \tilde{\bar{\varphi}}(k)^T \tilde{\bar{\theta}}(k) \quad (6.8)$$

$$\bar{y}(k) = \bar{V}_h(k) \quad (6.9)$$

$$\tilde{\bar{\varphi}}(k)^T = [\bar{I}_h(k) \quad c_h] \quad (6.10)$$

$$\tilde{\bar{\theta}}(k) = \begin{bmatrix} \bar{Z}_h(k) \\ \bar{V}_{o,h}(k) \end{bmatrix} \quad (6.11)$$

When an abrupt change occurs in the modeled network, the past information will bias the estimates until this information is replaced. This was not as significant an issue when examining the time-domain models because the intermittent information was expected to come in adequately sampled bursts. In contrast, frequency-domain observations only provide a single data point for each observed change in the loading. Recognizing an abrupt change in the model network will change all of the Thevenin equivalent parameters, covariance resetting is proposed in conjunction with directional forgetting. By resetting the covariance matrix to an initial starting value, all of the past information is thrown out and a new solution is quickly determined using subsequent observations.

The proposed frequency-domain estimation procedure is shown in Figure 6-2. The methods in [52, 53] rely on phasor measurement units (PMUs) to provide synchronized phasor measurements of the fundamental frequency content. Given the small distance associated with vehicular networks, synchronization of the measurements is not a significant issue. However, any delays associated with transferring the measurements

could, for example, be accounted for by introducing delays in the model. Once the discrete sampled measurements are synchronized, multiple options exist for converting the measurements into the frequency domain including the fast Fourier transform, Kalman filtering, and least-squares spectral analysis. The fast Fourier transform was used in the following the model evaluations.

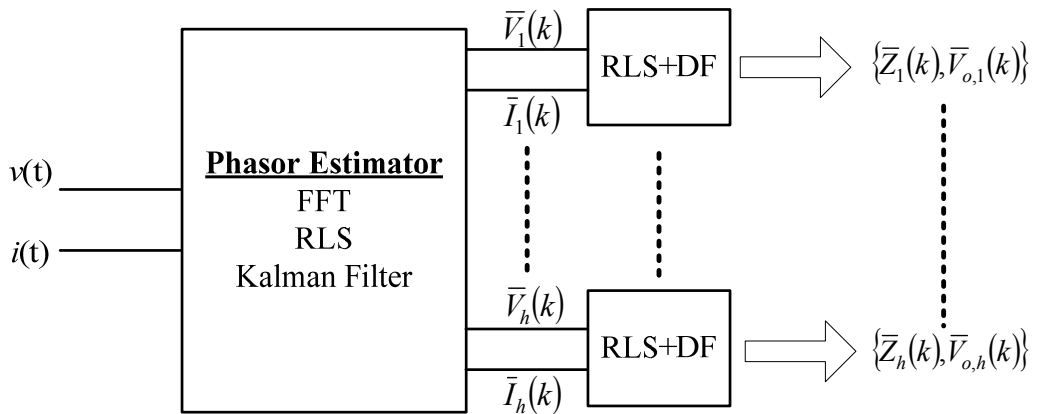


Figure 6-2. Frequency-Domain Thevenin Equivalent Estimation Method

6.3. PARAMETER ESTIMATE ACCURACY

As with the time-domain models it is desirable to statistically evaluate the accuracy of the steady-state model parameter estimates. Interpretation of the complex covariance matrix is therefore needed. The complex covariance matrix of two random variables \bar{U} and \bar{V} is defined in terms of a covariance matrix of its real and imaginary parts as shown in (6.12) and (6.13).

$$\text{cov}(\bar{U}, \bar{V}) = \text{cov}(U_R, V_R) + \text{cov}(U_I, V_I) + j(\text{cov}(U_I, V_R) + \text{cov}(U_R, V_I)) \quad (6.12)$$

$$\text{cov}(\bar{U}, \bar{V}) = \begin{bmatrix} \text{var}(U_R) + \text{var}(U_I) & \text{cov}(U_R, V_R) + \text{cov}(U_I, V_I) \\ \text{cov}(U_R, V_R) + \text{cov}(U_I, V_I) & \text{var}(V_R) + \text{var}(V_I) \end{bmatrix} + j^* \begin{bmatrix} \text{var}(U_I) - \text{var}(U_R) & \text{cov}(U_I, V_R) - \text{cov}(U_R, V_I) \\ \text{cov}(U_I, V_R) - \text{cov}(U_R, V_I) & \text{var}(V_I) - \text{var}(V_R) \end{bmatrix} \quad (6.13)$$

The least-squares matrices \mathbf{P} and \mathbf{R} are positive definite, so the diagonal terms of the covariance matrix are always positive real values. If (6.13) is also positive definite, the variance of the real and imaginary parts of the complex random variables \bar{U} and \bar{V} must be equal. The covariance matrix shown in (6.13) also demonstrates that the real diagonal entries of \mathbf{P} are indicative of the variance of only the complex random variable associated with each regressor. Additionally, it agrees with a common definition of the complex random variable variance given in (6.14). Therefore, the real numbers contained in the diagonal entries of \mathbf{P} directly indicate the variance of the phasor magnitude as defined by (6.15).

$$\text{var}(\bar{Z}) = E\left[(\bar{Z} - E[\bar{Z}])^* (\bar{Z} - E[\bar{Z}])\right] = \text{var}(z_R) + \text{var}(z_I) \quad (6.14)$$

$$\begin{aligned} \text{var}(\bar{U}) &= \text{var}(U_R)/2 = \text{var}(U_I)/2 = \sigma^2 P_{11} \\ \text{var}(\bar{V}) &= \text{var}(V_R)/2 = \text{var}(V_I)/2 = \sigma^2 P_{22} \end{aligned} \quad (6.15)$$

The prediction error is also a complex random variable. The residual variance can still be estimated using (3.52) but the variance of the real and imaginary portions of the prediction error must be determined separately as shown in (6.16) and (6.17). The

variance needed in (6.15) can then be found as the sum of these two variances using the relationship in (6.14).

$$\hat{\sigma}^2(k) = \lambda \hat{\sigma}^2(k-1) + (1-\lambda) * \left[1 - \tilde{\varphi}(k)^T \mathbf{P}(k) \tilde{\varphi}(k) \right] * \Re \left\{ y(k) - \tilde{\varphi}(k)^T \tilde{\theta}(k-1) \right\} \quad (6.16)$$

$$\hat{\sigma}^2(k) = \lambda \hat{\sigma}^2(k-1) + (1-\lambda) * \left[1 - \tilde{\varphi}(k)^T \mathbf{P}(k) \tilde{\varphi}(k) \right] * \Im \left\{ y(k) - \tilde{\varphi}(k)^T \tilde{\theta}(k-1) \right\} \quad (6.17)$$

6.4. MODEL EVALUATIONS

The test system used to evaluate the Thevenin equivalent estimations is shown in Figure 6-3. The general goal of the following example is to determine and track the Thevenin equivalent looking into the transformer at bus 3. A general description of the loads at bus 3 is provided in the figure. However, a series of step-changes will be imposed in both the impedance and rectifier loads in order to generate the needed excitation. Due to the stiffness of the source, step changes to the constant impedance load were necessary to provide sufficient changes to the fundamental observations.

PSPICE was again used to generate the discrete time data under different system configurations and successive loading conditions. The discrete measurements were recorded with a sampling frequency of 10240 Hz followed by the application of the fast Fourier transform (FFT) to determine the Fourier components. The window size of the FFT was selected as 1024 samples resulting in phasor measurements updates every 100 ms. As the frequency-domain models are independent of the time, the frequency of the updates is immaterial. However, the changes in the test system were selected to ensure at

least ten sample points of the same phasors were generated for each change in the loading. The equivalent memory size was also decreased, by fixing $\lambda = 0.9$, to sufficiently test the directional forgetting algorithm.

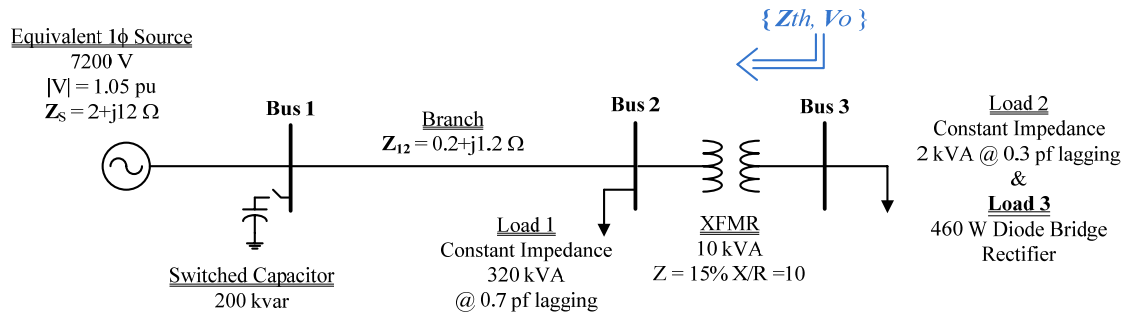


Figure 6-3. Single-Phase Test Network

Evaluation of parameter tracking ability is tested by alteration of the Thevenin equivalent via the switched capacitor located at bus 1. The capacitor is switched into service during the simulation corresponding to reactive compensation at the substation. A frequency scan of the transfer impedance looking into the network with and without the capacitor in service is shown in Figure 6-4. While the diode rectifier generates numerous odd harmonics, it is not necessary to fit a model for every harmonic. Instead, only those harmonic frequencies listed in Table 6-1, along with their relevant Thevenin equivalent values, are evaluated.

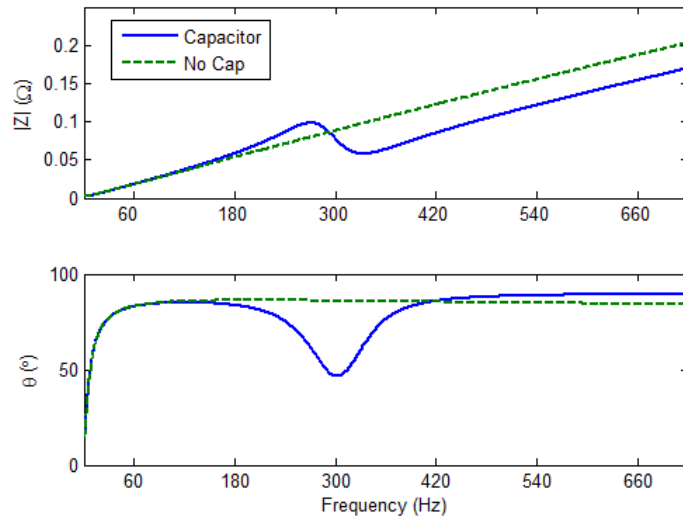


Figure 6-4. Network Transfer Impedances Seen at Bus 3

Table 6-1. Thevenin Equivalent Circuit Data

Frequency (Hz)	Capacitor			No Cap		
	$ Z $ (m Ω)	θ ($^{\circ}$)	V_o (V)	$ Z $ (m Ω)	θ ($^{\circ}$)	V_o (V)
60	17.95	82.9	122.0 \angle 2.6 $^{\circ}$	18.09	83.1	116.8 \angle 2.0 $^{\circ}$
300	78.05	46.7	0	88.18	85.9	0
420	85.05	85.8	0	122.20	85.3	0
660	153.90	89.3	0	187.20	84.3	0

During the simulation six network events are enacted. A brief description of the network events is provided in Table 6-2 along with their influence on the measured fundamental components in Figure 6-5. The phasor components plotted in Figure 6-5 are provided to illustrate the nature of the exact information provided to the recursive least-square solution method. This allows for direct correlation between changes in the excitation and changes to the parameter estimates. Given their usefulness, similar plots

will be provided for each harmonic model evaluated. The terminal voltage, \bar{V} , is used as the reference for each harmonic and therefore V_I is zero at each instant and not plotted.

Table 6-2. Test System Events

Event #	Description
1	Switching in of Load 2
2	Three successive increases to Load 3
3	Step increase in Load 2
4	Switching in of capacitor at Bus 1
5	Removal of Load 2
6	Three successive decreases to Load 3

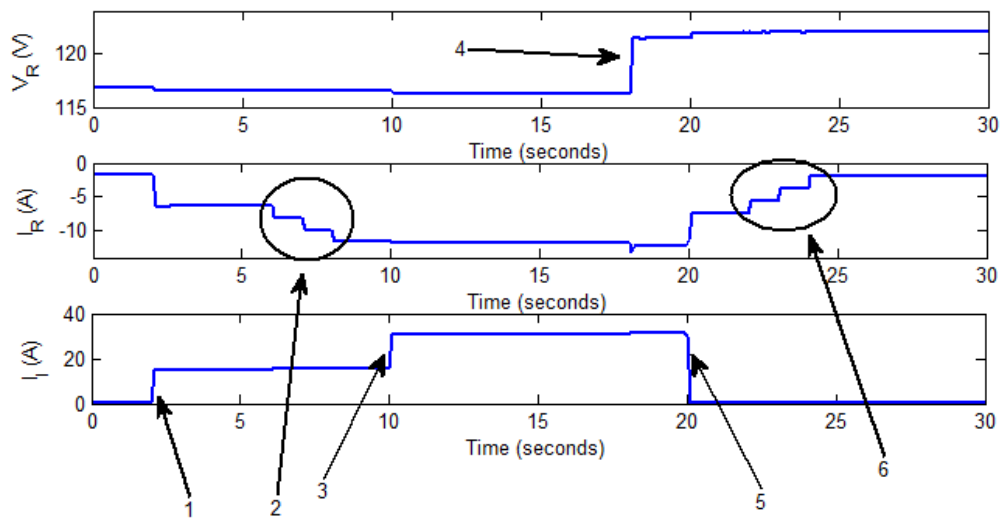


Figure 6-5. Input-Output Phasor Components at 60 Hz

Estimation of the complex space model (6.8)-(6.11) was performed using RLS with directional forgetting and covariance resetting. Resetting the covariance matrix was selected to occur whenever the prediction error was larger than 20%. Tracking small

variations in the Thevenin equivalent was provided for by selecting a value for λ of 0.99. The resulting parameter estimates are illustrated in Figure 6-6.

As expected, the estimates do not start to show signs of convergence until the second operating point. Still, the inaccuracy resulting from the flat start and the initial insufficient conditions results in a large prediction error causing the resetting of the covariance matrix as indicated in Figure 6-7. The next event to occur consists of step changes in the rectifier load which increases the real power demand of the rectifier. However, the resetting of the covariance matrix results in little confidence in the current parameter estimates at this point. Therefore, when changes occur only in I_R but not in I_L , as shown in Figure 6-5, the past excitation is insufficient to provide a good estimate of the Thevenin equivalent. Effectively, the regressor I_L is constant over all the retained observations and therefore linearly dependent with the constant voltage source regressors. Consequently, the Thevenin impedance is interpreted as being entirely real as indicated by the angle of the estimated impedance. This suggests that this method cannot be applied to estimate the Thevenin equivalent seen by a purely real or inductive load. Still when the inductive load increases during event #3, the change is observed in both phasor components. As a result, the excitation contained in all the regressors is sufficient for the solution to converge to reasonable estimates.

The estimates are accurate until the Thevenin equivalent is altered by the capacitor switching at bus 1. The abrupt change in the network model results in a large prediction error which again triggers the resetting of the covariance matrix. By discounting all of the

previous information, the process is started anew and sufficient excitation in the observed phasors must again be obtained.

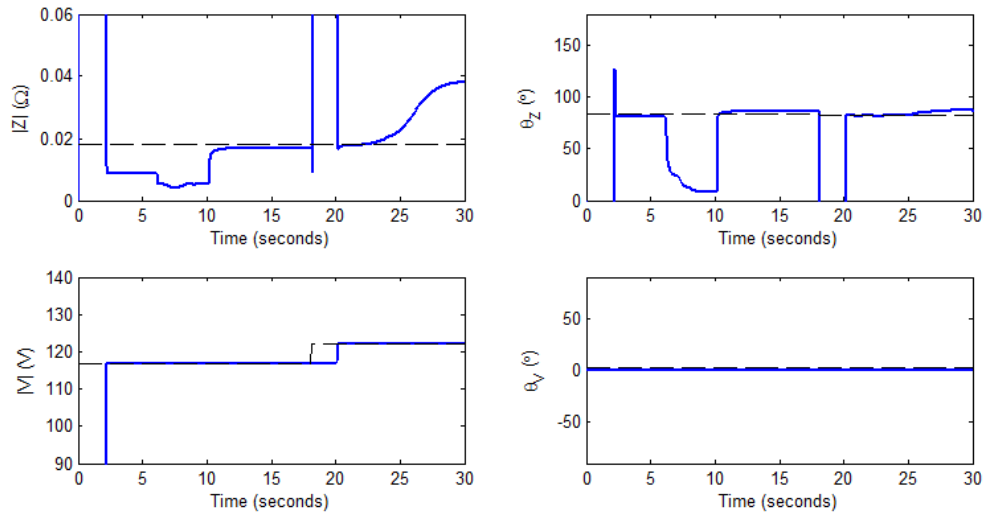


Figure 6-6. 60 Hz Thevenin Equivalent Parameter Estimates

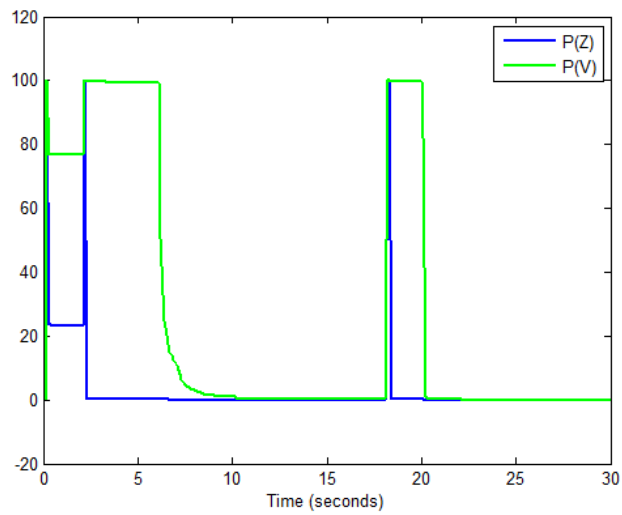


Figure 6-7. Covariance Matrix Diagonals

The same test system and procedures were applied to the 5th harmonic (300Hz) measurements shown in Figure 6-8. Examination of the phasor components at this frequency indicates that the changes in load 2 have very little influence on the 5th harmonic content. Hence, rectifier load changes are the sole source of excitation for the Thevenin equivalent model at this frequency. Nonetheless, the Thevenin equivalent estimations shown in Figure 6-9 demonstrate that the method provides good estimation and tracking properties in response to the load changes. Note that estimations accurately reflect the lack of a voltage source at this frequency in the modeled network. Similar examples can be generated for any of the harmonics observed in the network.

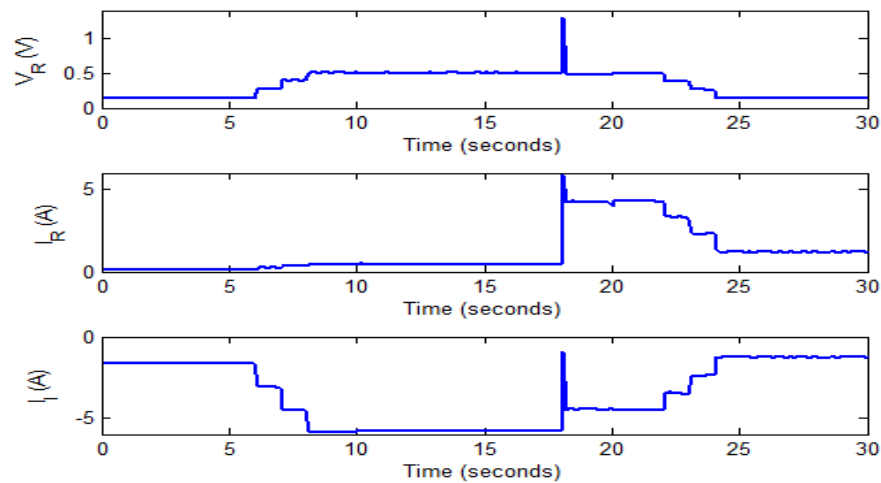


Figure 6-8. Input-Output Phasor Components at 300 Hz

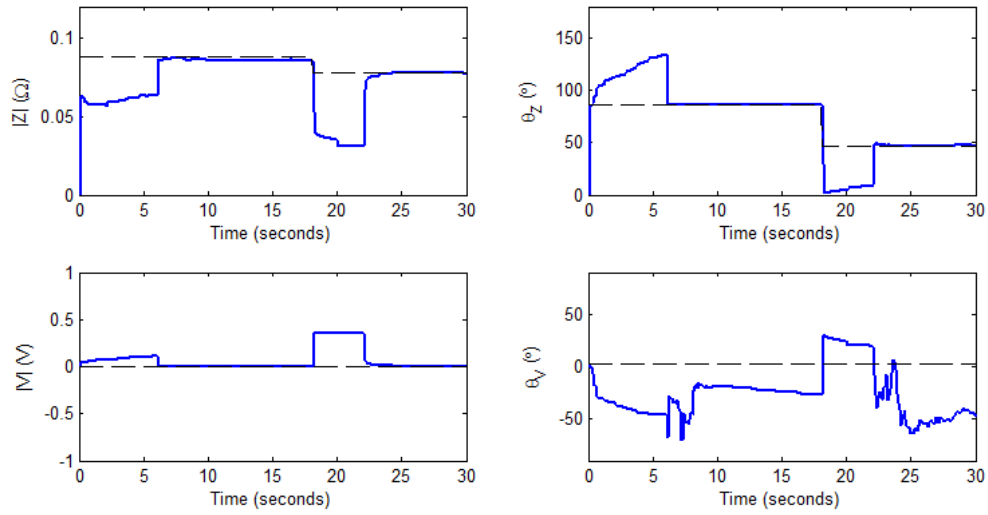


Figure 6-9. 300 Hz Thevenin Equivalent Parameter Estimates

6.5. SUMMARY

Continuous online estimation of the Thevenin equivalent provides a powerful tool from which to characterize the network and system components. This is especially true when only terminal measurements are available for some devices. The proposed frequency-domain methods have been shown to provide good parameter estimation and tracking abilities under the intermittent conditions. The parameter estimation methods given in Chapter 3 were also shown to require minimal changes when applied to complex numbers. Depending of the available measurements, the frequency-domain and time-domain parameter estimation techniques can provide sufficiently accurate estimates needed to monitor the health of not only individual devices but the overall network health as well.

CHAPTER 7

CONCLUSIONS

Parameter estimation techniques suitable to online estimation and tracking of network parameters under the assumed monitoring procedures have been presented. As the excitation is uncontrolled but must be sufficient to determine the characteristics of interest, the presented recursive least-squares methods were examined under the assumption that the excitation is intermittently spaced over time. These techniques have shown good estimation and tracking properties under the assumed conditions and will serve as the foundation for subsequent development of online model-based condition monitors. As the nature of the intermittency is also intrinsically linked to the chosen model, the techniques were evaluated and shown to be effective for multiple models in both the time and frequency domains.

7.1. SUMMARY

The recursive least-squares techniques were presented and examined in detail in Chapter 3. In order to follow time-varying parameters, the estimation method must discount past data in favor of more recently sampled information. The recursive least-squares method augmented with directional forgetting was proposed to provide better

retention of the intermittent information while still providing tracking capabilities. Variable directional forgetting and covariance resetting were also introduced to increase tracking capabilities of the method when large abrupt parameter changes occur.

As sufficient excitation cannot be guaranteed by the monitoring method, statistical measures in the form of confidence intervals, multicollinearity tests, and residual analysis were introduced to gauge the accuracy of the estimates. Additionally, the online statistical measures were designed to require minimal additional computation effort. The accuracy of the estimation is also intrinsically tied to the accuracy of the sample data. Design criteria for the filtering and the A/D conversion process governing the accuracy of the estimation algorithms were also documented.

Identifiability of the modeled parameters is not only determined by the solution method and the observed sample measurements but by the model as well. The identifiability requirements of two-conductor lines were examined in Chapter 4. Standard models representing different assumptions about the line and available measurements were developed in forms allowing for direct and accurate approximation of the desired physics-based parameters. The proposed identification algorithms and models were evaluated through MATLAB calculations using test data generated in PSPICE. The algorithms were shown to be effective in estimating and tracking the physics-based parameters even under intermittent conditions.

The ability to estimate and track physics-based parameters of multiple conductor network elements was evaluated in Chapter 5. It was shown that the interaction between the multiple conductors could result in strong multicollinearity. The additional excitation

criteria required to overcome these linear dependencies was also identified and documented. The parameter estimation algorithms were shown to provide accurate estimation and tracking characteristics for the developed multi-conductor models. In addition, directional forgetting was shown to provide better estimates than traditional discounting methods when strong multicollinearity existed between the regressors.

The parameter estimation algorithms were also applicable to frequency-domain models as demonstrated in Chapter 6. As excitation in the frequency-domain is dependent upon external changes to the system, intermittency will arise whenever these changes do not occur frequently with respect to the sampling rate. It was shown that the proposed methods again provided the desired characteristics by estimating and tracking Thevenin equivalent parameters using steady-state phasor measurements.

7.2. FUTURE WORK

The parameter estimation and statistical techniques presented here represent the initial investigations into a model-based monitoring method. The next steps will be to develop and identify performance metrics from which to base the diagnoses and prognoses. These performance metrics can be developed by integrating the physical models with stochastic modeling techniques [5]. Incorporation of the model-based techniques will also be necessary to provide a complete health monitoring device. Additionally, future work could examine extending the developed techniques to nonlinear devices.

Another area of consideration is applying the benefits of directional forgetting to applications where more accurate models are needed. For instance, errors in the network model of power system state-estimators are known to influence the state estimations, as examined in [90]. A real-time recursive parameter estimation technique to improve the network estimates was proposed in [91]. This method used Kalman filters to estimate and track changes in the network impedances over time. Future work could investigate whether recursive least-squares with directional forgetting provides a better alternative than Kalman filtering.

BIBLIOGRAPHY

- [1] R. Bartnikas and K. D. Srivastava, *Power and Communication Cables : Theory and Applications*. New York: IEEE Press : McGraw-Hill, 2000.
- [2] J. Gertler, *Fault Detection and Diagnosis in Engineering Systems*. New York: Marcel Dekker, 1998.
- [3] S. Simani, C. Fantuzzi, and R. Patton, *Model-Based Fault Diagnosis in Dynamic Systems using Identification Techniques*. London; New York: Springer, 2003.
- [4] I. Rolf, "Fault diagnosis of machines via parameter estimation and knowledge processing: tutorial paper," *Automatica*, vol. 29, no.4, pp. 815-835, 1993.
- [5] G. J. Vachtsevanos, *Intelligent Fault Diagnosis and Prognosis for Engineering Systems*. Hoboken, N.J.: Wiley, 2006.
- [6] M. E. H. Benbouzid, "Bibliography on induction motors faults detection and diagnosis," *IEEE Trans. Energy Convers.*, vol. 14, no.4, pp. 1065-1074, 1999.
- [7] M. Benbouzid, "A review of induction motors signature analysis as a medium for faults detection," *IEEE Trans. Ind. Electron.*, vol. 47, no.5, pp. 984-993, 2000.
- [8] R. Isermann, "Fault diagnosis of machines via parameter estimation and knowledge processing: tutorial paper," *Automatica*, vol. 29, no.4, pp. 815-835, 1993.
- [9] P. Vas, *Parameter Estimation, Condition Monitoring, and Diagnosis of Electrical Machines*. Oxford; New York: Clarendon Press ; Oxford University Press, 1993.
- [10] P. P. Harihara, K. Kyusung, and A. G. Parlos, "Signal-based versus model-based fault diagnosis-a trade-off in complexity and performance," in *4th IEEE Int. Symp. Diagnostics for Elect. Mach., Power Electron., and Drives*, 2003, pp. 277-282.

- [11] A. Nasiri, J. Poshtan, M. H. Kahaei, and F. Taringoo, "A new scheme in model-based fault detection in three-phase induction motors," in *Proc. IEEE Int. Conf. on Mechatronics*, 2004, pp. 19-24.
- [12] R. Dixon and A. W. Pike, "Application of condition monitoring to an electromechanical actuator: a parameter estimation based approach," *Computing & Control Engineering Journal*, vol. 13, no.2, pp. 71-81, 2002.
- [13] M. A. Awadallah and M. M. Morcos, "Stator-winding fault diagnosis of PM brushless DC motor drives," in *Large Eng. Syst. Conf. on Power Eng.*, 2002, pp. 147-152.
- [14] R. Malewski and B. Poulin, "Impulse testing of power transformers using the transfer function method," *IEEE Trans. Power Del.*, vol. 3, no.2, pp. 476-489, 1988.
- [15] L. Satish and S. K. Sahoo, "An effort to understand what factors affect the transfer function of a two-winding transformer," *IEEE Trans. Power Del.*, vol. 20, no.2, pp. 1430-1440, 2005.
- [16] T. Leibfried and K. Feser, "Monitoring of power transformers using the transfer function method," *IEEE Trans. Power Del.*, vol. 14, no.4, pp. 1333-1341, 1999.
- [17] R. Wimmer and K. Feser, "Calculation of the transfer function of a power transformer with online measuring data," in *2nd Int. Conf. on Advances in Processing, Testing, and Application of Dielectric Materials*, Wroclaw, Poland 2004.
- [18] S. D. Mikkelsen, J. Bak-Jensen, and J. T. Sorensen, "Sensitivity of identified transfer functions in transformer diagnosis," in *Proc. Electrical Electronics Insulation Conf. and Electrical Manufacturing & Coil Winding Conf.*, Chicago, 1993, pp. 533-537.
- [19] E. Rahimpour, J. Christian, K. Feser, and H. Mohseni, "Transfer function method to diagnose axial displacement and radial deformation of transformer windings," *IEEE Trans. Power Del.*, vol. 18, no.2, pp. 493-505, 2003.
- [20] L. A. Kojovic and C. W. Williams, Jr., "Sub-cycle detection of incipient cable splice faults to prevent cable damage," in *IEEE Power Eng. Soc. Summer Meeting*, 2000, pp. 1175-1180 vol. 2.
- [21] C. Furse, Y. Chung Chung, R. Dangol, M. Nielsen, G. Mabey, and R. Woodward, "Frequency-domain reflectometry for on-board testing of aging aircraft wiring," *IEEE Trans. Electromagn. Compat.*, vol. 45, no.2, pp. 306-315, 2003.

- [22] C. Furse, P. Smith, M. Safavi, and C. Lo, "Feasibility of spread spectrum sensors for location of arcs on live wires," *IEEE Sensors J.*, vol. 5, no.6, pp. 1445-1450, 2005.
- [23] P. Smith, C. Furse, and J. Gunther, "Analysis of spread spectrum time domain reflectometry for wire fault location," *IEEE Sensors J.*, vol. 5, no.6, pp. 1469-1478, 2005.
- [24] V. Taylor and M. Faulkner, "Line monitoring and fault location using spread spectrum on power line carrier," *IEEE Proc. Generation, Transmission and Distribution*, vol. 143, no.5, pp. 427-434, 1996.
- [25] P. Tsai, L. Chet, Y. Chung, and C. Furse, "Mixed-signal reflectometer for location of faults on aging wiring," *IEEE Sensors J.*, vol. 5, no.6, pp. 1479-1482, 2005.
- [26] S. L. Horton and N. G. Luijk, "Low Voltage Fault Detection and Localisation Using Topas 1000 Disturbance Recorder," *Electric Power Quality and Utilization*, vol. II, no.1, pp. 27-32, 2006.
- [27] C. M. Walton, "Incipient fault detection and management of underground LV networks," in *16th Int. Conf. and Exhibition Electricity Distribution*, 2001, p. 5 pp. vol.3.
- [28] "IEEE standard for qualifying class 1E electric cables and field splices for nuclear power generating stations," *IEEE Standard 383-2003*, 2004.
- [29] M. Subudhi, "Literature review of environmental qualification of safety-related electric cables: Summary of past work. Volume 1," Nuclear Regulatory Commission, Washington, DC, NUREG/CR-6384-Vol.1, Apr. 1996.
- [30] Y. Takezawa, J. Katagiri, and H. Shoji, "Application of optical diagnosis to aged low-voltage cable insulation in nuclear plants," in *Conf. on Electrical Insulation and Dielectric Phenomena Annu. Report 2004*, pp. 290-293.
- [31] C. Cornelissen and A. Schnettler, "Non-destructive diagnostic facilities for cable systems," in *Proc. IEEE Int. Symp. on Elect. Insulation*, 2002, pp. 557-560.
- [32] E. Watanabe, T. Moriya, and M. Yoshizawa, "Ultrasonic visualization method of electrical trees formed in organic insulating materials," *IEEE Trans. Dielectr. Electr. Insul.*, vol. 5, no.5, pp. 767-773, 1998.
- [33] Y. Sun, S. Luo, K. Watkins, and C. P. Wong, "Electrical approach to monitor the thermal oxidation aging of carbon black filled ethylene propylene rubber," *Polymer Degradation and Stability*, vol. 86, no.2, pp. 209-215, 2004.

- [34] Y. T. Hsu, K. S. Chang-Liao, T. K. Wang, and C. T. Kuo, "Monitoring the moisture-related degradation of ethylene propylene rubber cable by electrical and SEM methods," *Polymer Degradation and Stability*, vol. 91, no.10, pp. 2357-2364, 2006.
- [35] E. A. Vendrusculo and J. A. Pomilio, "Power cable parameters estimation in long distance driving of electrical machines," in *Int. Conf. Elect. Mach. and Drives*, 1999, pp. 410-412.
- [36] N. Ahmed and N. Srinivas, "The noise effect in conducting on-line partial discharge testing in distribution-class cables," in *Conf. Elect. Insulation and Dielectric Phenomena Annu. Report*, 1998, pp. 319-322 vol. 1.
- [37] N. H. Ahmed and N. N. Srinivas, "On-line partial discharge detection in cables," *IEEE Trans. Dielectr. Electr. Insul.*, vol. 5, no.2, pp. 181-188, 1998.
- [38] E. Gulski, B. R. Hamerling, F. J. Wester, J. J. Smit, E. A. Groot, and P. Schikarski, "Insulation condition assessment of medium voltage power cables using on-site pd detection and analysis techniques," in *16th Int. Conf. and Exhibition Electricity Distribution*, 2001, pp. 84-84.
- [39] B. R. Hamerling, F. J. Wester, E. Gulski, J. J. Smit, and E. R. S. Groot, "Fundamental aspects of on-line PD measurements on distribution power cables," in *Proc. IEEE 7th Int. Conf. on Solid Dielectrics*, 2001, pp. 408-411.
- [40] N. Srinivas, N. Ahmed, and G. Raju, "On line measurement of partial discharges," in *Conf. on Electrical Insulation and Dielectric Phenomena Annu. Report 2000*, pp. 678-681 vol.2.
- [41] W. Wang, S. Zhao, B. Cang, and L. En-Heng, "The study of on-line PD detector in power cable," in *Proc. 6th Int. Conf. on Properties and Applications of Dielectric Materials*, 2000, pp. 177-180 vol.1.
- [42] N. Ahmed and N. Srinivas, "On-line versus off-line partial discharge testing in power cables," in *Proc. Transmission and Distribution Conf. and Expo.*, 2001, pp. 865-870 vol.2.
- [43] N. Ahmed and N. Srinivas, "Can the operating conditions of the cable system effect the data of the field PD testing?," in *Conf. Elect. Insulation and Dielectric Phenomena*, 2001, pp. 311-314.
- [44] H. E. Orton, "Diagnostic testing of in-situ power cables: an overview," in *Transmission and Distribution Conf. and Exhibition*, 2002, pp. 1420-1425 vol.2.

- [45] G. J. Paoletti and A. Golubev, "Partial discharge theory and technologies related to medium-voltage electrical equipment," *IEEE Trans. Ind. Appl.*, vol. 37, no.1, pp. 90-103, 2001.
- [46] Q. Su and K. Sack, "New techniques for on-line partial discharge measurements," in *Proc. IEEE Int. Multi-Topic Conf.*, 2001, pp. 49-53.
- [47] J. P. Steiner and F. D. Martzloff, "Partial discharges in low-voltage cables," in *Conf. Rec. of IEEE Int. Symp. on Electrical Insulation*, 1990, pp. 149-152.
- [48] W. Pfeiffer, "Partial-discharge testing of components for low-voltage equipment," *IEEE Trans. Elect. Insul.*, vol. 26, no.2, pp. 247-257, 1991.
- [49] D. Bogh, J. Coffee, G. Stone, and J. Custodio, "Partial-discharge-inception testing on low-voltage motors," *IEEE Trans. Ind. Appl.*, vol. 42, no.1, pp. 148-154, 2006.
- [50] S. Yu, W. Li, B. Zhang, J. He, and Y. Huang, "Analysis of cable parameters on the real chassis by measurement," in *17th Int. Zurich Symp. Electromagnetic Compatibility*, 2006, pp. 73-76.
- [51] N. Damir, V. Khoi, C. Virgilio, S. Srdjan, and B. Miroslav, "Benefits of synchronized-measurement technology for power-grid applications," in *40th Annual Hawaii Int. Conf. Syst. Sciences*, Hawaii, 2007, pp. 118-118.
- [52] R. E. Wilson, G. A. Zevenbergen, D. L. Mah, and A. J. Murphy, "Calculation of transmission line parameters from synchronized measurements," *Electric Power Components and Systems*, vol. 27, no.12, pp. 1269-1278, 1999.
- [53] I. Kim and R. K. Aggarwal, "A study on the on-line measurement of transmission line impedances for improved relaying protection," *Int. J. Elect. Power & Energy Syst.*, vol. 28, no.6, p. 359, 2006.
- [54] Y. Du and J. Burnett, "Experimental investigation into harmonic impedance of low-voltage cables," *IEE Proc. Generation, Transmission and Distribution*, vol. 147, no.6, pp. 322-328, 2000.
- [55] L. Ljung, *System Identification: Theory for the User*. Upper Saddle River, NJ: Prentice Hall PTR, 1999.
- [56] K. J. Åström and B. Wittenmark, *Adaptive Control*. Reading, Mass.: Addison-Wesley, 1995.
- [57] G. A. Sullivan, "Adaptive control with an expert system based supervisory level," NASA, Washington, DC, NAS 1.26:192742; NASA-CR-192742; RPI-CIRSSE-115, Aug. 1991.

- [58] B. Porat, "Second-order equivalence of rectangular and exponential windows in least-squares estimation of Gaussian autoregressive processes," *IEEE Trans. Acoust., Speech, Signal Process.*, vol. 33, no.5, pp. 1209-1212, 1985.
- [59] T. R. Fortescue, L. S. Kershenbaum, and B. E. Ydstie, "Implementation of self-tuning regulators with variable forgetting factors," *Automatica*, vol. 17, no.6, pp. 831-835, 1981.
- [60] M. E. Salgado, G. C. Goodwin, and R. H. Middleton, "Modified least squares algorithm incorporating exponential resetting and forgetting," *Int. J. Control*, vol. 47, no.2, pp. 477-491, 1988.
- [61] T. Hägglund, "Recursive estimation of slowly time-varying parameters," in *IFAC Symp. Identification and Sys. Parameter Identification*, York, 1985, pp. 1137-1142.
- [62] R. Kulhavy, "Restricted exponential forgetting in real-time identification," *Automatica*, vol. 23, no.5, pp. 589-600, 1987.
- [63] S. Bittanti, P. Bolzern, and M. Campi, "Adaptive identification via prediction-error directional forgetting factor: convergence analysis," *Int. J. Control*, vol. 50, no.6, pp. 2407-2421, 1989.
- [64] S. Bittanti, P. Bolzern, and M. Campi, "Convergence and exponential convergence of identification algorithms with directional forgetting factor," *Automatica*, vol. 26, no.5, pp. 929-932, 1990.
- [65] R. Kulhavy and M. B. Zarrop, "On a general concept of forgetting," *Int. J. Control*, vol. 58, no.4, pp. 905-924, 1993.
- [66] J. E. Parkum, N. K. Poulsen, and J. Holst, "Recursive forgetting algorithms," *Int. J. Control*, vol. 55, no.1, pp. 109-128, 1992.
- [67] A. Vahidi, A. Stefanopoulou, and H. Peng, "Recursive least squares with forgetting for online estimation of vehicle mass and road grade: theory and experiments," *Vehicle System Dynamics*, vol. 43, no.1, pp. 31 - 55, 2005.
- [68] L. Cao and H. Schwartz, "A directional forgetting algorithm based on the decomposition of the information matrix," *Automatica*, vol. 36, pp. 1725-1731, 2000.
- [69] L. Cao and H. M. Schwartz, "A decomposition method for positive semidefinite matrices and its application to recursive parameter estimation," *SIAM J. on Matrix Analysis and Applications*, vol. 22, no.4, pp. 1095-1111, 2001.

- [70] L. Ljung and T. Söderström, *Theory and Practice of Recursive Identification*. Cambridge, Mass.: MIT Press, 1983.
- [71] G. Avanzolini, P. Barbini, and G. Cevenini, "Two new algorithms for tracking arterial parameters in nonstationary noise conditions," *IEEE Trans. Biomed. Eng.*, vol. 42, no.3, pp. 313-317, 1995.
- [72] V. Krishnan, *Probability and Random Processes*. Hoboken, N.J.: Wiley-Interscience, 2006.
- [73] E. Kyriakides and G. T. Heydt, "Calculating confidence intervals in parameter estimation: a case study," *IEEE Trans. Power Del.*, vol. 21, no.1, pp. 508-509, 2006.
- [74] J. Fox and G. Monette, "Generalized Collinearity Diagnostics," *J. of the American Statistical Association*, vol. 87, no.417, pp. 178-183, 1992.
- [75] P. M. Anderson, A. A. Fouad, and E. Institute of Electrical and Electronics, *Power System Control and Stability*. Piscataway, N.J.: IEEE Press; Wiley-Interscience, 2003.
- [76] IEEE Standard 399-1997 - IEEE recommended practice for industrial and commercial power systems analysis, 1998
- [77] C. A. Gross, *Power System Analysis*. New York: Wiley, 1986.
- [78] ANSI/IEEE Standard 575-1988, IEEE guide for the application of sheath-bonding methods for single-conductor cables and the calculation of induced voltages and currents in cable sheaths, 1987
- [79] IEC Standard 60287 - Electric cables - calculation of the current rating, I. E. Commission, 1994
- [80] IEEE Standard 1143-1994 - IEEE guide on shielding practice for low voltage cables, 1995
- [81] G. J. Anders, *Rating of Electric Power Cables : Ampacity Computations for Transmission, Distribution, and Industrial Applications*. New York: Institute of Electrical and Electronics Engineers, 1997.
- [82] O. I. Gilbertson, *Electrical Cables for Power and Signal Transmission*. New York: John Wiley, 2000.
- [83] IEEE Standard 835-1994 - IEEE Standard Power Cable Ampacity Tables, 1994

- [84] G. J. Anders, *Rating of Electric Power Cables in Unfavorable Thermal Environment*. Hoboken, N.J.: Wiley, 2005.
- [85] W. A. Thue, *Electrical Power Cable Engineering*. New York: Marcel Dekker, 1999.
- [86] A. B. B. E. S. T. Institute, *Electrical Transmission and Distribution Reference Book*. Raleigh, N.C.: ABB Electric Systems Technology Institute, 1997.
- [87] A. A. Girgis, J. Qiu, and R. B. McManis, "A time-domain approach for distribution and transmission network modeling," *IEEE Trans. Power Del.*, no.1, pp. 365-371, 1990.
- [88] A. A. Girgis, W. H. Quaintance, III, J. Qiu, and E. B. Makram, "A time-domain three-phase power system impedance modeling approach for harmonic filter analysis," *IEEE Trans. Power Del.*, vol. 8, no.2, pp. 504-510, 1993.
- [89] S. Cobreces, P. Rodriguez, D. Pizarro, F. J. Rodriguez, and E. J. Bueno, "Complex-space recursive least squares power system identification," in *IEEE Power Electron. Specialists Conf.*, 2007, pp. 2478-2484.
- [90] P. Zarco and A. G. Exposito, "Power system parameter estimation: a survey," *IEEE Trans. Power Syst.*, vol. 15, no.1, pp. 216-222, 2000.
- [91] I. W. Slutsker, S. Mokhtari, and K. A. Clements, "Real time recursive parameter estimation in energy management systems," *IEEE Trans. Power Syst.*, vol. 11, no.3, pp. 1393-1399, 1996.